Experimental and Numerical Simulation Studies of the Zwitterionic Polymer for Enhanced Oil Recovery

by

Damir Karimov

Submitted in partial fulfillment of the requirement of Nazarbayev University
for the degree of
Doctor of Philosophy in Chemical Engineering

School of Engineering and Digital Sciences
Nazarbayev University

Supervised by
Dr. Nurxat Nuraje
Dr. Peyman Pourafshary
Dr. Muhammad Hashmet

2025

Declaration

I, Damir Karimov, hereby declare that this submission is my own work and to the best of my knowledge it contains no materials previously published or written by another person, or substantial proportions of material which have been accepted for the award of any other degree or diploma at Nazarbayev University or any other educational institution, except where due acknowledgment is made in the thesis.

Any contribution made to the research by others, with whom I have worked at NU or elsewhere, is explicitly acknowledged in the thesis.

I also declare that the intellectual content of this thesis is the product of my own work, except to the extent that assistance from others in the project's design and conception or in style, presentation, and linguistic expression is acknowledged.

.

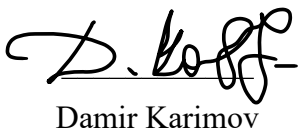

Damir Karimov

Date:

ABSTRACT

This study presents a comprehensive investigation into the synthesis, characterization, and performance evaluation of zwitterionic polymers for enhanced oil recovery (EOR) applications. Three zwitterionic copolymers, which contains positively and negatively charged groups, designated as zPAM 1, zPAM 2, and zPAM 3, were synthesized and subjected to a series of analytical techniques to validate their successful synthesis and assess their properties. Fourier-transform infrared (FTIR) spectroscopy confirmed successful synthesis through characteristic peaks of N–H (3319–3338 cm^{-1}), C=O (1639–1662 cm^{-1}), and sulfonate groups (1113–1189 cm^{-1}). Proton nuclear magnetic resonance (1H NMR) spectra further verified the incorporation of zwitterionic units into the polymer backbone. Dynamic light scattering (DLS) revealed high molecular weights ranging from 598 to 734 kDa, confirming their suitability for EOR applications. Scanning electron microscopy (SEM) showed distinct morphologies, with zPAM 1 and zPAM 2 exhibiting highly ordered network structures conducive to enhanced stability and mechanical integrity. Rheological experiments demonstrated typical shear-thinning behavior across all copolymers. Among them, zPAM 1 exhibited the highest viscosity values, with a 30 % viscosity increase as salinity rose from 100,000 to 200,000 ppm and a 60% viscosity loss as temperature increased from 25 °C to 60 °C. Coreflooding experiments, conducted at 63 °C and 200,000 ppm salinity using a polymer concentration of 1000 ppm, revealed that zPAM 1 achieved a total oil recovery factor of 56.5%, compared to 52.3% for commercial hydrolyzed polyacrylamide (HPAM). The higher pressure drop observed during postflush indicated stronger mobility control for zPAM 1. The superior EOR performance of zPAM 1 is attributed to its optimized molecular architecture, enhanced salinity tolerance, and favorable viscoelastic behavior arising from its DMAPMAPS-based zwitterionic structure. These findings underscore the importance of molecular design and structural composition in influencing the rheological behavior and performance of zwitterionic polymers in EOR applications. The insights gained from this study contribute to a deeper understanding of zwitterionic polymers' potential for enhancing oil recovery efficiency and sustainability, discovering new ways for further research and optimization in this field.

ACKNOWLEDGEMENT

I express my heartfelt gratitude to my main supervisor, Nurxat Nuraje, for their exceptional mentorship, profound expertise, and steadfast encouragement throughout the journey of this thesis. Their insightful feedback, careful attention to details, and ability to inspire critical thinking not only refined the scope and quality of my research but also motivated me to pursue excellence in every aspect of my work. I am also thankful to my supervisor, Peyman Pourafshary, whose thoughtful and constructive comments provided clarity and direction during essential moments of this project. His expertise in identifying key areas for improvement and offering practical recommendations greatly enhanced the depth of my research. My sincere appreciation also goes to my co-supervisor, Muhammad Rehan Hashmet, for his support and motivational guidance. His encouragement during challenging phases of the research process was instrumental in sustaining my drive, and his belief in my potential gave me the confidence to continue.

I am immensely grateful to my research team, whose collaborative efforts, diverse perspectives, and shared commitment to excellence created an inspiring and productive environment. Their willingness to engage in in-depth discussions, offer technical insights, and provide constructive feedback during brainstorming sessions and peer reviews significantly enhanced the outcomes of this thesis. The team's mutual encouragement, and collective problem-solving approach transformed complex challenges into opportunities for growth, making the research process both fulfilling and enjoyable.

Regular meetings with my supervisors and research team were invaluable, fostering a dynamic exchange of ideas and maintaining a high standard of accountability. These interactions consistently challenged me to improve my methodologies, enhance my analytical skills, and set ambitious goals for my research. The collective dedication, intellectual rigor, and collaborative spirit of my supervisors and team have left an eternal impact on this thesis and my development as a researcher.

This work stands as evidence to the guidance, inspiration, and teamwork provided by these remarkable individuals, whose contributions were essential to the success of this thesis.

TABLE OF CONTENTS

LIST OF TABLES

LIST OF FIGURES

LIST OF ABBREVIATIONS

API	American Petroleum Institute
AM	Acrylamide
ASP	Alkaline-surfactant-polymer
AA	Acrylic Acid
CFS	Coreflooding system
CMG	Computer modelling group
CSS	Cyclic steam stimulation
DLS	Dynamic light scattering
DMAPMAPS	Dimethyl-n-(3-methacrylamidopropyl)-n-(3-sulfopropyl) ammonium betaine
EOR	Enhanced oil recovery
FTIR	Fourier-transform infrared
HPAM	Hydrolyzed polyacrylamide
MW	Molecular weight
NMR	Nuclear magnetic resonance
OOIP	Original oil in place
PV	Pore volume
RF	Recovery factor
RFF	Residual resistance factor
SAGD	Steam-assisted gravity drainage
SBVI	Sulfobetaine vinylimidazole
SBVP	Sulfobetaine vinylpyridine
SEM	Scanning electron microscopy
SRB	Sulfate resistant bacteria
TGA	Thermogravimetric analy
zPAM	Zwitterionic polyacrylamide-based copolymers

LIST OF SYMBOLS

^{o}C	a degree Celsius
wt %	Weight percentage
K_c	Optical constant
R_θ	Rayleigh ratio
M_w	Molecular weight
C	concentration
pKa	acid dissociation constant
$P(\theta)$	angular dependence of scattering intensity
A_2	second virial coefficient
N_a	Avogadro's constant
λ_0	wavelength
n_0	solvent refractive index
Dn/dc	differential refractive index.
ppm	Parts per million
g	gram
mL	milliliters
rpm	rotations per minute
cP	Centipoise (viscosity unit)
Swi	initial water saturation
W_{dry}	dry weight of the core
W_{wet}	wet weight of the core after saturation
ρ_{FW}	density of the formation water
kDa	kiloDaltons
Tg	glass transition temperature
μ	viscosity

CHAPTER 1. INTRODUCTION

1.1 Intent of this thesis

The primary intent of this work is to advance the field of enhanced oil recovery (EOR) by designing, synthesizing, and evaluating newly synthesized zwitterionic copolymers required to overcome the limitations of conventional polymer flooding in challenging reservoir environments characterized by high salinity and high temperatures conditions. The research focuses on developing three distinct zwitterionic copolymers, zPAM 1, zPAM 2, and zPAM 3, through the copolymerization of acrylamide with the selected zwitterionic monomers: N,N-dimethyl-N-(3-methacrylamidopropyl)-N-(3-sulfopropyl) ammonium betaine (DMAPMAPS), sulfobetaine vinylimidazole (SBVI), and sulfobetaine vinylpyridine (SBVP). These monomers were chosen for their unique molecular structures and varying glass transition temperatures (Tg, ranging from 276.52°C to 313.69°C) (Amrenova et al., 2025), which are hypothesized to enhance thermal stability, salinity tolerance, and viscosity retention under harsh reservoir conditions, thereby improving oil displacement efficiency.

The thesis aims to address the limitations of hydrolyzed polyacrylamide (HPAM), a widely used polymer in EOR, which suffers from viscosity loss and thermal degradation in high-salinity and high-temperature reservoirs due to interactions with divalent ions and thermal stress (Iravani et al., 2025). By influencing the "salting-in" effect and electrostatic crosslinking characteristics to zwitterionic polymers, this study pursues to develop polymers with superior rheological properties, including shear-thinning behavior, robust viscosity retention across a wide range of salinities and enhanced thermal stability at temperatures up to 63°C, as encountered in Kazakhstani oilfield reservoirs like the Uzen oilfield.

A comprehensive characterization of the synthesized copolymers is a central objective, using advanced analytical techniques to highlight the insights in molecular structure, morphology, and functional performance. FTIR and HNMR the successful synthesis and chemical composition of the polymers, while DLS determines their molecular weights. SEM provided insights into the morphological features, such as the ordered network

structures and intermolecular crosslinking that contribute to structural integrity. Rheological experiments evaluate the polymers' viscosity behavior under varying conditions of concentration, temperature, salinity, and shear rate, with a particular focus on identifying the copolymer with optimal performance for EOR applications.

The thesis further aims to validate the practical applicability of the most promising zwitterionic copolymer, zPAM 1, through coreflooding experiments conducted under simulated reservoir conditions using Berea sandstone core samples and crude oil from the Uzen oilfield. These experiments will compare zPAM 1's oil recovery efficiency, mobility control, and pressure drop performance against a commercial HPAM polymer, with the goal of demonstrating superior sweep efficiency and higher recovery factors. The study also includes numerical simulations using Computer Modelling Group (CMG) software to validate experimental findings and assess the scalability of the proposed polymer flooding approach.

Ultimately, this PhD thesis aims to contribute to the scientific understanding of zwitterionic polymers by highlighting the critical role of molecular design, charge distribution, and structural composition in optimizing their performance for EOR. By developing robust, efficient, and sustainable polymers, the research aims to address the growing demand for advanced EOR technologies capable of maximizing oil recovery in mature and depleted reservoirs. The findings are expected to provide valuable insights into the oil and gas industry in Kazakhstan, paving the way for the design of new polymers that enhance the economic and environmental sustainability of oil recovery operations.

1.2 Problem Statement

The global demand for efficient oil recovery from mature and depleted reservoirs has intensified due to declining production rates and increasingly challenging reservoir conditions. Polymer flooding, a cornerstone of chemical enhanced oil recovery, faces significant limitations that diminish its effectiveness in harsh environments, such as high-salinity and high-temperature reservoirs. The following specific problems such as

limitations of conventional polymers in harsh conditions and underexplored potential of zwitterionic polymers for EOR applications underscore the need for advanced polymer solutions. These problems highlight the critical need for novel zwitterionic copolymers designed to overcome the limitations of HPAM by maintaining viscosity, resisting thermal degradation, and enhancing oil recovery in high-salinity, high-temperature reservoirs.

1.3 Aims of the study

Considering the above-mentioned problems, this study aims to address the challenges of polymer flooding in enhanced oil recovery under harsh reservoir conditions by developing and evaluating novel zwitterionic polymers, which include:

1) Design and synthesis of zwitterionic polymers by copolymerizing acrylamide with zwitterionic monomers, selected for their unique molecular structures and high glass transition temperature.
2) Characterization of the synthesized copolymers using advanced analytical techniques, including FTIR spectroscopy and 1H NMR to confirm chemical composition, DLS to determine molecular weights, SEM to analyze morphological features, and rheological experiments to evaluate viscosity behavior under different conditions.
3) Validation of zwitterionic polymers through Coreflooding experiments to evaluate EOR efficiency.
4) Numerical simulation and model validation to compare experimental results and validate the reliability of the developed model for predicting EOR performance.

1.4 Research Hypotheses

Hypotheses 1: Zwitterionic polymers exhibit superior rheological and thermal stability under high-salinity and high-temperature conditions due to their electrostatic crosslinking and “salting-in” behavior, enabling enhanced viscosity retention and shear-thinning performance.

Hypotheses 2: The high glass transition temperature and linear molecular architecture of zwitterionic copolymers contribute to their improved structural rigidity and thermal stability, resulting in better injectivity and sustained mobility control during polymer flooding.

Hypotheses 3: Compared to conventional HPAM, zwitterionic polymers achieve higher oil recovery and improved sweep efficiency in coreflooding experiments by providing stronger rock–fluid interaction, greater salt tolerance, and enhanced flow resistance, as evidenced by a higher pressure drop profiles.

1.5 Scientific Significance and Novelty of Study

This work holds significant scientific importance and novelty by advancing enhanced oil recovery (EOR) through the development and evaluation of newly synthesized zwitterionic copolymers tailored for high-salinity and high-temperature reservoirs, where conventional polymers such as hydrolyzed polyacrylamide often fail due to viscosity loss, salinity sensitivity, and thermal degradation. The research involves a comprehensive set of synthesis and characterization steps that provide new insights into the relationship between molecular structure, the “salting-in” effect, and polymer performance under reservoir-relevant conditions. Comprehensive synthesis and characterization of zwitterionic copolymers provide new insights into the relationship between molecular structure, "salting-in" effects, and EOR performance. By integrating advanced analytical techniques (FTIR, 1H NMR, SEM, DLS, rheological analysis), coreflooding experiments and numerical simulations with Computer Modelling Group (CMG) software, the research establishes a solid basis for validating zwitterionic polymers’ performance, outperforming conventional polymers. This work not only bridges laboratory and field applications but also offers a novelty for designing sustainable EOR solutions, enhancing recovery in oilfield reservoirs while contributing to the scientific understanding of zwitterionic polymer design for challenging environments.

1.6 Research Outputs

Journal Papers

1) Karimov, D., Imekova, G., Toktarbay, Z., & Nuraje, N. (2025). Experimental and numerical simulation studies of the zwitterionic polymers for enhanced oil recovery. *Scientific Reports*, *15*(1), 34728.
2) Karimov, D., & Toktarbay, Z. (2023). Enhanced oil recovery: techniques, strategies, and advances. *ES Materials & Manufacturing*, *23*(2), 1005.
3) Imekova, G., Karimov, D., Nuraje, N., & Toktarbay, Z. (2024). Polymerization dynamics of zwitterionic monomers with polyacrylamide for enhanced oil recovery. *Engineered Science*, *31*, 1260.

1.7 Thesis Overview

This PhD thesis is structured into eight main chapters, each designed to systematically address the research objectives in logical progression, from the synthesis and characterization of zwitterionic polymers to their performance evaluation for EOR applications in high-salinity, high-temperature reservoirs. The work includes extensive data collected over a four-year PhD study, culminating in the development and assessment of three novel zwitterionic copolymers: zPAM 1, zPAM 2, and zPAM 3.

Chapter 1 delivers the basis by providing an introduction to EOR and the challenges of polymer flooding in harsh reservoir conditions, followed by a problem statement identifying the limitations of conventional polymers, the aim of the study to develop zwitterionic copolymers with superior thermal stability and oil displacement efficiency, and the novelty of zwitterionic polymers for EOR applications.

Chapter 2 offers a comprehensive literature review, exploring the state-of-the-art in polymer flooding technologies, the role of zwitterionic polymers in high-salinity environments, and identifying research gaps that this study addresses, thereby justifying the focus on zwitterionic polymers.

Chapter 3 presents the synthesis of three zwitterionic monomers, DMAPMAPS, SBVI, and SBVP, followed by their copolymerization with acrylamide to form zwitterionic copolymers zPAM 1, zPAM 2, and zPAM 3. The selected monomers were chosen for

their high glass transition temperatures and structural stability, providing a foundation for developing thermally robust EOR polymers.

Chapter 4 presents a comprehensive characterization of the synthesized zwitterionic copolymers zPAM 1, zPAM 2, and zPAM 3 using FTIR, ^{1}H NMR, DLS, and SEM techniques. The analysis confirms the successful copolymerization and reveals key structural features, including sulfonate and quaternary ammonium groups, supporting their zwitterionic nature. Molecular weight determination and SEM imaging further demonstrated their high polymerization efficiency, thermal stability, and distinct morphological differences, all of which contribute to their potential effectiveness in high-salinity, high-temperature EOR applications.

Chapter 5 evaluates the rheological behavior of zwitterionic copolymers under varying conditions of concentration, temperature, salinity, and aging time to simulate harsh reservoir environments.

Chapter 6 presents coreflooding experiments conducted to evaluate the EOR performance of the zwitterionic copolymer zPAM 1 in comparison with conventional HPAM under simulated Uzen reservoir conditions.

Chapter 7 presents a numerical simulation study using CMG-STARS to replicate and validate the coreflooding experiments performed with the zwitterionic polymer zPAM 1.

Chapter 8 concludes the thesis by summarizing the key contributions, notably zwitterionic polymer potential as a transformative EOR solution, and offers a perspective on future research directions, including strategies to mitigate the challenges, and explore hybrid EOR approaches, opening the doors for further advancements in the field of chemical EOR.

CHAPTER 2. LITERATURE REVIEW

2.1 A comprehensive overview of enhanced oil recovery methods

Challenges related to enhanced oil recovery within the oil and gas industry have resulted in the need for advanced strategies to optimize oil production and refining processes. EOR methods have emerged as viable approaches to enhance oil recovery efficiency. According to the book *Modern Chemical Enhanced Oil Recovery: Theory and Practice,* the foundational principle of oil recovery revolves around creating a substantial differential pressure between the underground oil reservoir and the production well, facilitating the migration of hydrocarbons towards the wellbore (Sheng, 2010). This process includes primary, secondary, and tertiary stages, each addressing specific reservoir conditions and challenges.

Primary oil recovery constitutes the initial phase of production, relying primarily on the natural pressure within the reservoir to displace oil towards the wellbore. As the reservoir pressure decreases, secondary recovery techniques become necessary for achieving effective displacement. Water flooding and gas injection for the pressure maintenance, are frequently employed during this stage to increase the reservoir pressure and enhance oil recovery rates. Secondary recovery methods have the potential to recover up to 50% of the original oil in place (Alagorni et al., 2015; Malozyomov et al., 2023). Tertiary recovery methods come into play when secondary techniques prove economically insufficient. These methods include the injection of miscible gases, chemicals, or thermal energy into the reservoir, aiming to further enhance oil recovery. Notably, tertiary recovery represents a cumulative approach, capable of yielding an additional 15% of the cumulative oil recovery following the implementation of secondary recovery methods (Kalita et al., 2021). The terminology surrounding EOR requires clarification, as it is occasionally used interchangeably with Improved Oil Recovery (IOR). However, according to the society of professional oil field workers, EOR is considered a subgroup of IOR, encompassing interventions specific to reservoir operations (Sheng, 2010). EOR methods can be broadly classified into thermal and non-thermal techniques, each offering distinct mechanisms for improving oil recovery. This classification is determined by the fundamental mechanism employed to mobilize and recover residual oil that remains

trapped after the depletion of natural reservoir energy and the application of secondary recovery processes. While both categories aim to enhance hydrocarbon recovery efficiency, they differ significantly in operational principles, applicability, and environmental and economic implications.

Thermal EOR methods function by introducing heat into the reservoir environment, thereby reducing the viscosity of crude oil, expanding reservoir fluids, and increasing reservoir pressure (Seidy-Esfahlan et al., 2024). These processes collectively enhance the mobility of oil and facilitate its flow towards production wells. Thermal techniques are particularly effective in reservoirs containing heavy and extra-heavy crudes, which exhibit high viscosity under ambient conditions (Sun et al., 2024). Among the widely practiced thermal techniques are Cyclic Steam Stimulation (CSS), steam flooding, Steam-Assisted Gravity Drainage (SAGD), and in-situ combustion (Ahmed & Tunio, 2025). CSS, often referred to as "huff and puff," involves three stages: steam injection, soak, and oil production from the same well (Zhang, 2024). This method has been extensively applied in shallow heavy oil formations. Steam flooding, by contrast, entails continuous steam injection into the reservoir, which sweeps the oil towards adjacent production wells (Zhang et al., 2025). SAGD, an advanced thermal method, employs a pair of horizontal wells, the upper well for steam injection and the lower for oil production, allowing gravity to assist in oil drainage once viscosity is reduced. In-situ combustion relies on igniting a portion of the in-place oil to generate heat internally, which propagates through the reservoir and enhances oil mobility (Wu et al., 2025). More recently, electromagnetic and microwave-assisted heating have been investigated as alternatives to conventional steam-based methods, especially for deeper or heterogeneous formations, although these remain largely in the experimental stage (Yadali Jamaloei, 2022). Despite their proven effectiveness, thermal EOR methods present several challenges. High capital and operational expenditures are required for steam generation, insulation, and infrastructure (Afra et al., 2021). These methods are also energy-intensive and result in considerable greenhouse gas emissions and water consumption. Furthermore, in deeper or fractured reservoirs, heat loss to surrounding rock formations can render thermal methods inefficient or economically unfeasible (Wang et al., 2022).

In contrast, non-thermal EOR techniques enhance oil recovery through chemical, physical, or biological means, without the direct application of heat. These methods are especially advantageous in deeper reservoirs or in formations containing light to medium crude oils, where thermal losses are substantial or heat application is impractical (Ahmed & Tunio, 2025). Non-thermal EOR mechanisms operate by reducing interfacial tension between oil and water, altering rock wettability to promote water-wet conditions, improving the mobility ratio between displacing and displaced fluids, or through the production of secondary agents in situ (Borhani et al., 2025).

Chemical EOR is one of the most mature and widely applied non-thermal methods. It involves the injection of chemical agents such as polymers, surfactants, and alkalis, either singly or in combination (Jain et al., 2022). Polymer flooding increases the viscosity of the injected water, thereby improving sweep efficiency and reducing channeling. Surfactants are employed to reduce interfacial tension and mobilize trapped oil, while alkaline agents react with acidic components in the oil to form in-situ soaps. In recent years, hybrid formulations such as alkaline-surfactant-polymer (ASP) blends and nanoparticle-enhanced chemical systems have demonstrated improved performance in high-temperature and high-salinity environments (Karimov & Toktarbay, 2023).

Gas injection is another prominent non-thermal method, which may be either miscible or immiscible (Mohammadi et al., 2024). Miscible gases such as carbon dioxide or hydrocarbon-rich gases dissolve into the oil phase, causing swelling, viscosity reduction, and improved miscibility (Dai et al., 2023). Immiscible gases such as nitrogen or flue gas provide displacement pressure and enhance volumetric sweep (Tileuberdi et al., 2023). Among these, CO_2 injection has gained renewed attention for its dual role in EOR and carbon sequestration, positioning it as a critical component of environmentally conscious petroleum development.

Microbial EOR involves the injection of selected microbial cultures or nutrients into the reservoir, where they generate metabolites such as biogases, biopolymers, or

biosurfactants (Sheng, 2010). These by-products contribute to oil mobilization through wettability alteration, interfacial tension reduction, and improved sweep efficiency. MEOR is considered environmentally friendly and potentially cost-effective, but field-scale implementation remains limited due to challenges in maintaining microbial viability, ensuring even distribution, and managing reservoir compatibility.

Another emerging technique is smart water flooding, also referred to as low-salinity water injection. This method modifies the ionic composition of injected water to influence rock-fluid interactions, particularly in carbonate reservoirs. Changes in brine chemistry can lead to a favorable shift in wettability and increase oil recovery (Behera et al., 2024). The performance of smart water flooding, however, is highly dependent on reservoir mineralogy and oil composition.

Extensive research conducted by Mohsenatabar Firozjaii & Saghafi, (2020) supports the significance of chemical EOR as a critical aspect of EOR. Their findings reveal that approximately 11% of all EOR mechanisms fall within the chemical EOR domain, with polymer flooding constituting 77% of these methods. The remaining 23% comprises a combination of polymer flooding with surfactants. These insights underscore the prominent role of chemical flooding, particularly polymer-based techniques, in optimizing oil recovery strategies.

The classification of EOR methods encompasses thermal recovery, miscible flooding, chemical flooding, and microbial approaches and the main EOR techniques are illustrated in Figure 1. These methods can be employed independently or in combination to maximize oil recovery rates. Chemical flooding, notably polymer flooding, has emerged as a cornerstone of EOR, playing a critical role in enhancing oil recovery efficiency.

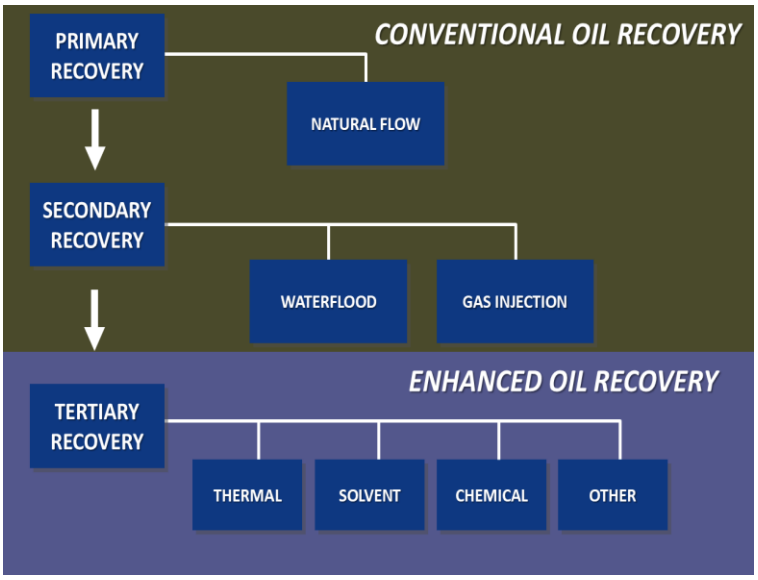

Figure 1. Overview of primary, secondary and tertiary recovery methods

2.2 Principles and Mechanisms of Polymer Flooding

According to Mohsenatabar Firozjaii and Saghafi (2020), the technique known as polymer flooding involves the addition of polymers to water in order to increase its viscosity, resulting in the transformation of water into a polymer solution. This process effectively controls the mobility of fluids within porous media by introducing a more viscous solution for injection. As a consequence, the sweep efficiency of the system is improved, leading to enhanced oil recovery. Ragab and Mansour (2021) mentioned an equation, for calculating the mobility ratio of water in polymer flooding, which compares the mobility of the displacing fluid (water) to that of the displaced fluid (oil):

$$M = \frac{\frac{k_{rw}}{\mu_w}}{\frac{k_{ro}}{\mu_o}}$$

where, k_{rw} – mobility of water

k_{ro} – mobility of oil

μ_w – viscosity of water

μ_o – viscosity of oil

This equation is primarily employed to control the viscosity of the displacing fluid, considering that the properties of the reservoir fluid can vary depending on factors such as the type of oil and porous media (Alsawafi, 2015). As for the types of polymers, the most fairly common polymers used for polymer flooding are Xanthan Gum and hydrolyzed polyacrylamides. They are widely recognized due to their favorable chemical properties, relatively low cost, and desirable viscosity characteristics (Chen et al., 2015). The chemical structures of these polymers are illustrated in Figure 2.

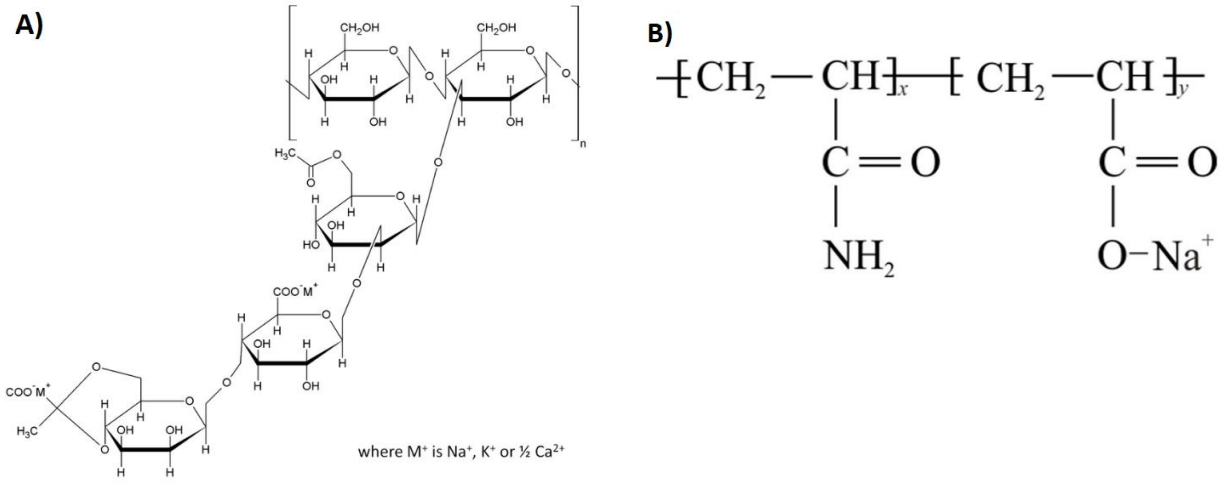

Figure 2. Chemical structure of a) Xantham gum; b) HPAM (Chen et al., 2015)

Xanthan Gum, classified as a biopolymer, is derived from natural sources, such as fermentation processes. It belongs to the polysaccharide class and possesses a powdery consistency that facilitates convenient commercial utilization (Perry, 1972). According to Chatterji & Borchardt (1981), the high viscosity of Xanthan Gum polymer solutions can be attributed to the structure of its polymer chains, characterized by double- and triple-helix formations and extended polar side chains that promote multiple ionic bonds.

Despite the relatively high viscosity and cost-effectiveness of biopolymers, they are surpassed by synthetic polymers in terms of properties required for effective polymer flooding implementation. Das et al. (2014) argue that synthetic polymers exhibit superior shear stability due to their wide molecular weight distribution. One widely employed synthetic polymer is the copolymer KYPAM, which has been extensively used in polymer flooding. Gao et al., (2014) suggest an initial concentration of 1800 ppm for KYPAM,

followed by a concentration drop to 1400-1000 ppm during the final stages of flooding to maximize oil production. The powdered form of KYPAM has been successfully employed in the Shengli oil field in North China, resulting in daily production volumes ranging from 20 to 70 tons of heavy oil. Field studies indicate that achieving efficient oil production through KYPAM-assisted polymer flooding requires an initial concentration of 1500 to 2000 ppm (Gao et al., 2014).

HPAM, a synthetic polymer comprising acrylic acid and acrylamide monomers, demonstrates high molecular weight and chain expansion due to the repulsion among negatively charged ionic groups along the polymer chain. This expansion leads to thickening of the polymer solution and an increase in viscosity. The repulsive forces generated by the carboxylic groups in the HPAM structure contribute to chain elongation, and the number of acrylic acid monomers within the polymer chain influences the polymer viscosity. HPAM injection under typical reservoir conditions is relatively straightforward and can significantly enhance the rate of oil recovery, which has been demonstrated through its application in various oilfields.

The rheological behavior of HPAM is particularly favorable for EOR applications. HPAM solutions exhibit non-Newtonian shear-thinning characteristics. It maintains high viscosity under low shear rates within the reservoir while exhibiting reduced viscosity under high shear during the injection. Additionally, HPAM is characterized by high molecular weights, typically between 5 to 20 million Daltons, which enable it to selectively plug high-permeability zones and divert injected fluids into lower permeability zones. This mechanism is critical in improving the areal and vertical sweep efficiency of polymer flooding processes (Wever et al., 2011; Mohamed & Mohyaldinn, 2025).

Despite its broad applicability, HPAM has some limitations. HPAM performance is sensitive to several reservoir conditions, notably temperature, salinity, mechanical stress, and oxygen presence (Shakeel et al., 2022). At elevated temperatures above 90°C, HPAM may undergo further hydrolysis, which increases the polymer's charge density, promotes

backbone scission, and ultimately results in viscosity loss. This thermal degradation is worsened in alkaline environments or in reservoirs with a high pH (Taylor & Nasr-El-Din, 1998). Salinity, particularly the presence of divalent cations such as calcium and magnesium, can also significantly affect HPAM performance (Seright et al., 2025). These ions neutralize the negative charges on the polymer backbone, reducing chain expansion and consequently lowering the solution's viscosity.

Mechanical degradation of HPAM is another operational concern, especially during injection through narrow tubing or tight formations where high shear rates can physically break polymer chains (Al Shakry, 2021). This results in a permanent reduction of molecular weight and viscosity, ultimately compromising the polymer's performance. Moreover, HPAM is vulnerable to microbial degradation, especially in anaerobic reservoirs, where sulfate-reducing bacteria may metabolize the polymer and produce hydrogen sulfide, contributing to reservoir souring and equipment corrosion (Al-Kindi et al., 2022). To counter these limitations, operational strategies such as oxygen scavengers, biocides, and deoxygenated water systems are typically employed in the field.

Polymer retention through adsorption onto reservoir rock surfaces is also a significant consideration for HPAM performance. HPAM molecules can interact with clay minerals and rock surfaces, particularly in sandstones, leading to polymer loss and reduced effective concentration within the reservoir. This retention is influenced by salinity, rock surface charge, polymer concentration, and degree of hydrolysis. While some degree of adsorption is inevitable, excessive retention necessitates higher polymer dosages and increases the overall cost of the flooding (Mohamed & Mohyaldinn, 2025).

Despite these limitations, HPAM has proven highly successful in numerous field-scale applications. One of the most notable example is the Daqing Oilfield in northeast China, where HPAM polymer flooding has been deployed since the 1990s. The Daqing project is widely recognized as the largest and most comprehensive polymer EOR operation globally. With reservoir temperatures ranging from 45–60°C and relatively low salinity, HPAM was ideally suited for the conditions. The large-scale deployment involved over

500 injection wells, and polymer flooding resulted in an incremental oil recovery of approximately 12% beyond conventional waterflooding. This success established polymer flooding as a mature and economically viable EOR technique (Song et al., 2022).

Similarly, in the Shengli Oilfield, also in China, HPAM polymer flooding was applied in heavy oil zones with promising results. Guo et al. (2021) report that powdered HPAM was injected at concentrations of approximately 1800 ppm, later reduced to 1000–1400 ppm during the chase water stage. The polymer program achieved sustained oil production rates ranging from 20 to 70 tons/day in individual zones. Importantly, the use of high-molecular-weight HPAM facilitated effective mobility control without significant injectivity issues, highlighting the importance of viscosity optimization and inline quality control.

Field applications outside China have also validated the efficiency of HPAM. In the Tambaredjo Field in Suriname, a polymer flooding project using HPAM was initiated in moderately permeable sandstone reservoirs with reservoir temperatures of ~36°C. The operation demonstrated significant reduction in water cut and an increase in oil recovery. The comfortable reservoir conditions allowed HPAM to maintain stability and performance throughout the injection cycle (Delamaide et al., 2016).

In North America, HPAM has been employed in the Pelican Lake Field in Canada for EOR in heavy oil reservoirs. Here, the pseudo-plastic nature of HPAM solutions facilitated cold production of high-viscosity oils in unconsolidated formations. Although thermal methods were also deployed in the field, HPAM proved useful in enhancing production in marginal zones where thermal injection was economically unfeasible (Ezeh et al., 2021).

Pilot studies in Latin America and the Middle East have further confirmed HPAM's field performance, with recovery factors improving by 6–13% and favorable project economics observed under moderate oil price scenarios. These projects emphasize the importance of polymer screening and pre-injection laboratory tests to adapt HPAM

formulations to local reservoir geochemistry, pressure, and temperature (Gutierrez et al., 2024; Al Lawati et al., 2025).

Overall, HPAM remains the industry-standard polymer for EOR applications due to its combination of performance, cost-effectiveness, and established field experience. The continued evolution of HPAM formulations, combined with improved understanding of reservoir-polymer interactions, suggests that HPAM-based flooding will remain a key strategy in the global EOR portfolio for decades to come. Therefore, before selecting the appropriate polymer for polymer flooding, several screening parameters need to be investigated under laboratory conditions. These parameters encompass rheology, thermal stability, mechanical degradation, retention, salinity, the presence of divalent ions such as Ca^{2+} and Mg^{2+}, microbial degradation, effects on molecular weight, as well as sensitivity to oxygen and pH (Abbas et al., 2013).

2.3 Polymer flooding results for Kazakhstani field

Polymer flooding has emerged as a promising EOR method for mature sandstone reservoirs in Kazakhstan, where high water cuts and significant residual oil saturations are persistent challenges. In one study, Yerniyazov et al. (2023) conducted a comprehensive polymer screening for a sandstone field in Kazakhstan to identify the most suitable HPAM polymer under high-salinity (120,000 ppm) and moderate-temperature (63 °C) reservoir conditions. Four HPAM polymers were tested in terms of rheological behavior, thermal and oxidative stability, microbial resistance, and static adsorption. One polymer was identified as optimal due to its superior viscosity (above 5 cp at reservoir conditions), low adsorption (13–14% lower than other candidates), and minimal thermal degradation over extended testing. Following this screening, coreflood experiments confirmed that conventional polymer injection in Field A resulted in an incremental oil recovery of approximately 48% over waterflooding, indicating the high applicability of the selected polymer under Kazakhstan's geological and fluid conditions (Sagandykova et al., 2024).

To further improve oil recovery and reduce water production, a hybrid approach combining polymer flooding with thermal EOR was tested. In this method, polymer solutions were preheated to 85 °C before injection. Although the viscosity of the polymer solution slightly decreased at higher temperatures, the hot polymer flooding achieved an oil recovery exceeding 52%, which is 4% higher than the conventional polymer flood. This enhanced performance was attributed to increased oil mobility, lowered viscosity, and reduced interfacial tension (IFT), all contributing to improved sweep efficiency in previously unswept zones (Sagandykova et al., 2024). The thermal activation also allowed for the use of lower polymer concentrations, which could significantly reduce chemical costs. Building on this, Sagandykova et al. (2025) investigated two polymer injection optimization techniques—slug-wise and tapered polymer flooding—to address the high chemical demand of continuous injection methods. Slug-wise injection, involving alternating polymer and water slugs, achieved a 16-fold increase in oil-to-polymer ratio compared to conventional flooding, while tapered flooding, which gradually reduced polymer concentration during the flood, provided a 38% OOIP recovery with 81% less polymer usage. Both methods maintained high recovery performance while minimizing operational costs, offering scalable, cost-efficient solutions for Kazakhstan's aging reservoirs (Sagandykova et al., 2025).

On a broader field scale, the historical and ongoing implementation of polymer flooding in the Kalamkas field provides valuable insights into practical deployment strategies. Sahuc et al. (2024) report that polymer flooding in Kalamkas began as early as the 1980s, with 2,450 tons of polymer injected, yielding an additional 270,000 tons of oil—an efficiency of 110 tons of oil per ton of polymer. More recently, two pilot strategies have been compared: the distributed pilot strategy, which injects polymers across several geological horizons to test varying conditions, and the single-horizon strategy, which concentrates efforts in one formation layer for more cost-effective deployment. While the distributed strategy provides broader reservoir understanding, the single-horizon approach simplifies operations and reduces infrastructure costs, making it more suitable for early-stage field applications in Kazakhstan (Sahuc et al., 2024). Collectively, these studies highlight that polymer flooding, particularly when coupled with thermal

enhancement and injection optimization, is a technically and economically feasible EOR strategy for Kazakhstan’s mature oilfields, capable of increasing oil recovery and mitigating excessive water production.

2.4 Polymer selection parameters

2.4.1 Rheology

As previously indicated, the rheological characteristics of polymer solutions play a critical role in the context of polymer flooding, as they directly influence the application methodology of this technique (Kaminsky et al., 2007; Navaie et al., 2022). The review on polymer flooding by Hassan et al., (2022) highlights several justifications for rejecting polymer flooding only on the basis of rheology. Firstly, the injection of polymer solutions can be economically and practically unfeasible for reservoirs containing heavy oil. Secondly, the injection of highly viscous fluids, such as polymer solutions, poses challenges due to their slow flow dynamics, resulting in prolonged injection times required to adequately displace inside the reservoir. Lastly, polymer solutions with elevated viscosity values may encounter difficulties passing through narrow gaps in the reservoir, causing retention and decreasing further movement (Kamal et al., 2015; Salam et al., 2024).

HPAM is the most discussed and analyzed polymer in scientific publications, particularly in relation to the most commonly employed polymer for polymer flooding (Cancela et al., 2022). Lewandowska (2007) and Karimov (2020) investigated the rheology concerns associated with HPAM. The studies emphasize the analysis of shear-thickening phenomena in relation to critical shear rates, with temperature, molar mass, concentration, and hydrolysis level serving as pivotal variables impacting the rheology. Notably, investigations into HPAM's molecular mass reveal that higher molecular-weight polymers exhibit lower viscosities during post-shearing when compared to their lower molecular-weight counterparts (Zaitoun et al., 2012). Additionally, Yang et al., (2024) found out that HPAM may not be optimally suited for oil reservoirs characterized by low permeability due to its high molar mass.

2.4.2 Thermal stability

The preservation of thermal stability within the reservoir plays a pivotal role in ensuring the effective execution of polymer flooding. According to Kamal et al., (2015), this stability should be maintained for up to several months, during which polymer flooding occurs. The application of polymers at elevated temperatures poses a significant risk within the boundaries of the oil reservoir. Consequently, the degradation of polymers in the solution results in reduced viscosity, having a detrimental impact on the mobility ratio of the polymer solution and oil. Han et al. (2014) provides a more detailed and field-oriented set of performance requirements for polymers designed for high-temperature reservoirs. Their screening criteria specify that suitable polymers must withstand 95–100 °C for at least six months while retaining more than 50% of their initial viscosity, ensuring functional long-term injectivity and mobility control.

Although polymers can be used at elevated temperatures, their stability is governed by their intrinsic chemical structure, molecular weight, degree of hydrolysis, and ionic composition, all of which influence how the polymer responds to thermal stress. For example, classical studies by Chang (1978) and Mirzaie Yegane et al., (2022) demonstrated that polyacrylamides possess relatively high thermal tolerance due to their carbon–carbon backbone and stable amide functionalities, allowing them to remain effective at temperatures up to approximately 121 °C before significant hydrolysis and chain scission occur. In contrast, biopolymers such as Xanthan Gum contain thermally labile glycosidic linkages, limiting their maximum operating temperature to around 71 °C, beyond which rapid degradation and viscosity loss become unavoidable. Despite such intrinsic thermal tolerances, practical field experience indicates that polymer flooding should generally be restricted to reservoirs with temperatures below 90 °C to prevent accelerated degradation. (Bourdarot and Ghedan, 2011; Hassan et al., 2022). This limitation arises because real reservoir brines often contain oxygen, transition-metal ions, and divalent cations (Ca^{2+}, Mg^{2+}), all of which catalyze oxidative and hydrolytic degradation, causing molecular weight reduction and loss of viscosity. Therefore, maintaining thermal stability is essential for preserving the mobility control required

during flooding, and screening must account for both the polymer's inherent structural stability and the chemical reactivity inside the reservoir environment.

2.4.3 Mechanical degradation

Mechanical degradation refers to the breakdown of polymer molecules caused by excessive mechanical stress during flow, particularly in regions near the wellbore where flow velocities and shear forces are highest. Such stresses can stretch, deform, and ultimately rupture polymer chains, leading to a reduction in molecular weight and a corresponding loss in solution viscosity (Sorbie, 1991; Stavland et al., 2021) . This effect is especially pronounced for high–molecular weight polymers, which are more susceptible to chain scission under shear. Puls et al. (2016) further demonstrated that mechanical forces can progressively fragment polymer chains into lower molecular weight fractions, thereby altering the overall molecular weight distribution of the polymer solution. This change in molecular architecture represents a key consequence of mechanical stress and has significant implications for polymer performance during flooding operations, as reduced molecular weight directly compromises the polymer's ability to provide effective mobility control. In contrast, Cao et al., (2023) argue that mechanical degradation relates to the irreversible decline in viscosity and resistance factors when fluid stresses reach a threshold that causes the fragmentation of polymer molecules. Such fragmentation occurs when a polymer solution rapidly crosses narrow barriers or flows into a porous media. Comparing the viscosity of the polymer solution before and after a forced flow is the most straightforward technique to measure mechanical degradation. Although viscosity loss is generally associated with chain degradation, rheological behavior must be carefully interpreted to distinguish between reversible and irreversible effects. Polymer solutions exhibit shear-thinning behavior due to the alignment and disentanglement of polymer coils under shear, which lowers viscosity but fully recovers once flow ceases. In contrast, true mechanical degradation is irreversible; viscosity does not return to its original value because the polymer chains have been physically cleaved. Two fundamental techniques employed for this purpose are the capillary tube flow and porous media flow methods (Cao et al., 2023). The capillary tube procedure encompasses the generation of an extensional laminar flow by

injecting polymers into a tube with resistant capillary geometry (Dupas et al., 2012; Stavland et al., 2021). Porous media flow methods involve studying the flow behavior of a polymer through a porous medium, such as a packed bed or a porous membrane.

Polymer solutions exhibit thickening behavior as they experience shearing from moderate to high flow rates while passing through porous media. (Seright et al., 2011; Daripa & Mishra, 2023). Nevertheless, polymer degradation is apparent at elevated flow rates of the polymer solution. Seright et al., (2011) and Gbadamosi et al., (2022) mentioned, in their study on the injectivity characteristics of EOR polymers that a pressure drop occurs at the inlet when the polymer solution crosses the sand surface, particularly during high rate flows through the cores. Primarily, mechanical degradation of the polymer occurs in the inlet region. Hassan et al., (2024) conducted investigations on polymer degradation in carbonate formations and observed a greater incidence of mechanical degradation in cores characterized by low permeability. The heterogeneous structure of carbonate cores poses challenges in the accurate prediction of polymer mechanical degradation.

Overall, mechanical degradation represents a critical factor governing polymer performance in EOR applications, as it leads to permanent molecular damage that compromises viscosity, elasticity, resistance factors, and ultimately the polymer's capacity to improve mobility control and sweep efficiency.

2.4.4 Retention

According to Manichand & Seright (2014) and Song et al., (2022), the transport of polymers through a porous medium is affected by the polymer retention. Consequently, in processes such as polymer flooding and other techniques employed in enhanced oil recovery, significant effect of polymer retention may have a substantial decelerating effect on oil injection and subsequent recovery. Today, various methodologies, including static, injection, and mass balance techniques, have been developed to measure polymer retention. For instance, Chiappa et al., (1999) and Salam et al., (2024) propose static methods for quantifying polymer retention, which involve evaluating the polymer concentration before and after contact with sand. By dividing the mass loss from the

solution by the weight of the exposed sand, the extent of polymer adsorption can be determined. However, this method possesses certain limitations due to its oversight of potential errors.

Polymer retention plays a dual role in EOR, with both beneficial and detrimental effects, depending on its magnitude. Moderate levels of retention can be advantageous by restricting polymer mobility, thereby slowing polymer propagation and delaying polymer breakthrough at the production well (Unsal et al., 2018; Sebastian, 2023). As polymer molecules adsorb onto mineral surfaces or become mechanically entrapped, the effective polymer concentration in the displacing fluid decreases, which slows the polymer front and maintains a high-viscosity bank in the near-injection region for a longer duration. This delay stabilizes the displacement front, reduces viscous fingering, and enhances sweeping efficiency by forcing injected water into unswept or low-permeability zones (Ganat & Ali, 2024). In this context, a controlled level of retention can improve mobility control and overall displacement behavior.

However, excessive polymer retention is undesirable . High retention significantly delays polymer arrival at deeper regions of the reservoir, leading to uneven polymer propagation, poor volumetric sweep, and reduced displacement efficiency (Zhang & Seright, 2014; Ilyasov et al. 2021). Excessive retention also increases chemical costs because a larger injected mass of polymer is required to achieve the target in-situ concentration. Studies such as Unsal et al. (2018) further show that retention is strongly influenced by salinity: low-salinity polymers exhibited substantially lower retention levels than high-salinity formulations at 58 °C. Lower retention is also associated with improved economic performance because less polymer mass is lost to the rock matrix.

Given its pronounced impact on polymer transport, sweep efficiency, and project economics, accurately determining polymer retention is critical during laboratory polymer screening and prior to field-scale deployment (B. Choi et al., 2016; Ilyasov et al., 2021). Optimal EOR performance requires a balance: sufficient retention to stabilize the displacement front, but low enough to avoid excessive polymer loss and delayed

propagation. Zwitterionic polymers, with their reduced adsorption tendency and electrostatic shielding behavior, have shown promise in minimizing detrimental retention while maintaining effective mobility control, which motivates their further investigation.

2.4.5 Salinity

Numerous studies are currently related to investigating the influence of salinity on the quality and economic efficiency of polymer flooding. Notably, Khorsandi et al., (2017) and Musa et al., (2023), emphasize the importance of salinity as a primary factor of polymer flooding efficiency. Their study provides an extensive examination of the effectiveness of employing low-salinity polymers for flooding, accompanied by compelling illustrations of low-salinity brine application in diverse oil well scenarios. The authors recognize that the use of low-salinity polymers for polymer flooding depends on factors such as the oil reservoir's composition, the type of reservoir constituents, and the solution's solidity level.

Polymer flooding employing low-salinity polymers is mainly applied in sandy-rocky oil formations, thereby designating low-salinity polymers as the preferred agents for polymer flooding (Kozaki, 2012; Song et al., 2024). Morrow & Buckley (2011) and Nascimento et al., (2023), argue that low-salinity polymers enhance local displacement efficiency by altering the wettability of the reservoir rock from oil-wet to a more water-wet state. This process involves implementing techniques such as manipulating the rock surface's potential within the formation, executing multicomponent ion exchange, and raising dissolution effects.

Comparative investigations examining the performance of high salinity and low salinity polymers in polymer flooding clearly indicate a superior economic advantage associated with the low salinity polymers. As posited by Khorsandi et al., (2017) and Mahajan et al., (2021), high salt retention in polymers comes at a sharp price increase and proves economically inefficient, apart the enhanced solution stability achieved through such retention.

2.4.6 Divalent ion tolerance

The ionic composition of water plays a critical role in determining the stability and flow behavior of polymer solution. These effects significantly reduce the viscosity of polymer solutions during transport through porous media, thereby affecting mobility control. For this reason, the pretreatment of produced or recycled water becomes essential to ensure polymer integrity and maintain the rheological properties required for efficient displacement performance. Sosa-Fernandez et al. (2019) reported that water required from polymer-based EOR systems requires partial desalination and targeted purification to remove multivalent ions before it can be reused. Notably, divalent cations, comprising less than 10% of total cations in the examined polymer solution, exhibit the most pronounced impact on viscosity reduction in flowing polymer solutions. This study also demonstrated the successful application of electrodialysis in selectively extracting divalent cations, particularly at elevated temperatures (40 °C) and moderate current densities. In parallel, the removal of divalent anions such as sulfate is accelerated under these specified conditions.

Given its prevalence, the concentration of HPAM, a widely employed polymer, can employ a noticeable influence on the effective diffusion rate of ions, particularly those carrying positive charges. Charged particles associated with anionic polyelectrolytes can interact with diffusing ions, leading to a partial decrease in the diffusion potential. Furthermore, investigations by Yuan et al., (2013) have examined the interaction between Ca^{2+} , Mg^{2+}, and the acrylic anion within polyacrylamide derivatives, as well as the attractive forces between calcium, magnesium, and HPAM (R. Zhang et al., 2015). In this context, the retention of these ionic compounds within the solvent is prolonged when they remain bound to the polymer, decreasing their free flow within the solution.

These observations have important implications for polymer selection in EOR. Polymers used in high-salinity or divalent-rich reservoirs must maintain structural integrity and viscosity despite the presence of Ca^{2+} and Mg^{2+}. Consequently, understanding the interactions between divalent ions and polymer functional groups is essential for selecting

polymers capable of sustaining viscosity and mobility control under harsh reservoir conditions.

2.4.7 Effects on molecular weight

Polymerization processes are subject to well-established reactions that dictate the incorporation of monomeric units into polymer molecules. Consequently, the resulting polymer exhibits non-uniform molecular characteristics across its entirety. Polymer properties are intricately linked to their molecular characteristics, with molecular weight playing a pivotal role. Understanding the effect of molecular weight on polymers properties is crucial for tailoring their properties to meet specific application requirements. Generally, as the molecular weight increases, the polymer tends to have higher melting and boiling points, greater viscosity, and increased mechanical strength. These effects arise because longer polymer chains have greater possibilities for intermolecular interactions and physical entanglements, which strengthen the cohesive forces within the polymer solution. Consequently, polymers with higher molecular weight often exhibit superior mobility control in porous media due to their ability to generate higher solution viscosities and stronger flow resistance.

However, increased chain length decreases solubility and slows dissolution kinetics, making highly entangled polymers more difficult to hydrate and more susceptible to incomplete dissolution or “fish-eye” formation. High molecular weight polymers are also more prone to mechanical degradation when subjected to high shear, as longer chains are more easily stretched and broken. Thus, while high molecular weight is beneficial for viscosity enhancement, it must be balanced against injectivity and stability constraints during field deployment.

It is important to note that the molecular weight distribution, which describes the range of molecular weights present in a polymer sample, also influences the overall behavior and properties. According to Rogosic et al., (1996) and Da Tan et al., (2022), variations in different attributes were represented in alterations in the shape and length of the

molecular weight distribution. Consequently, establishing the molecular weight distribution should be the starting point for the polymer's assessment.

2.4.8 Oxygen and pH sensitivity

Over the years, polymers have been used in the EOR concept to control the movement of injected fluids (Mahajan et al., 2021) . During polymer flooding, the uneven distribution of polymer reduces the efficiency of oil recovery. This leads to increased costs by making the displacing stage more difficult and reducing the viscosity of the water, or by redirecting the injected water from high-permeability regions to low-permeability regions of the oil reservoirs. Recently, different techniques for polymer flooding are employed to address this issue and improve mobility.

A pH-sensitive polymer has been developed and extensively studied as a chemical agent for regulating mobility or profile control in EOR applications (S. K. Choi et al., 2009; Liu et al., 2025). Generally, as pH of the polymer solution decreases, the viscosity decreases respectively (Shakeel et al., 2022). At low pH, carboxylic groups remain predominantly in the protonated –COOH state, which reduces electrostatic repulsion and permits close packing of polymer chains. As the pH increases within the acidic domain, partial deprotonation occurs, increasing the number of $–COO^-$ groups and allowing for stronger intermolecular interactions. These interactions promote chain expansion, hydrogen bonding, and the formation of transient microgel-like networks, all of which contribute to a steep rise in viscosity. To introduce a pH-sensitive polymer into a reservoir for adherence tracking, the pH of the aqueous phase through which the polymer flows must be sufficiently low to prevent microgels from expanding prematurely before reaching the desired region (Benson et al., 2007). Since polymer viscosity is highly dependent on pH and water chemistry, accurate estimation of pH and ion concentration distribution in the reservoir during injection is crucial. This prediction serves as a crucial step for industry professionals in evaluating the effectiveness of polymers in enhancing oil recovery.

To ensure the injected fluid has the appropriate viscosity, Romero-Zeron, (2016) suggests implementing an integrated viscometer and regular measurements at the well. This design

for fluid sampling must be carefully followed to ensure that the observed viscosity corresponds to the actual solution and not degraded polymer material. Incorrect measurement processes can lead to the entrance of oxygen into the material, leading to biochemical interactions between oxygen and potential reducers such as iron and H_2S. This results in the production of free radicals, which chemically degrade the polymers and cause an immediate decrease in viscosity (Romero-Zeron, 2016). However, this issue is more pronounced in the laboratory, where viscosity studies in the presence of contaminants need to be conducted within an inert environment, such as a nitrogen-blanketed glove container.

According to Romero-Zeron (2016), dissolved oxygen in the water is introduced into the reservoir during polymer flooding. This oxygen is rapidly consumed in the lower region through bacterial degradation of remaining oil, activating anaerobic microorganisms, particularly methanogens, in the oxygen-free zone of the reservoir. While the population of aerobic oxidizing and oligocarbophilic microorganisms increases less, the production of anaerobic metabolic products in the oil production solutions exponentially rises.

2.5 Application of zwitterionic polymers in polymer flooding

2.5.1 Brief overview and structure of zwitterionic polymers

Zwitterionic polymers have a 1:1 molar number of homogeneous dispersion of anionic and cationic units throughout their polymer matrix (Banerjee et al., 2011; Li et al., 2022). The structure is composed of the main polymer backbone and side chains with positively and negatively charged ions. This arrangement of positively and negatively charged molecules provides ultra-hydrophilicity on the polymers while retaining a general charge balance. These architectures of zwitterions polymers allow them to electrostatically absorb and neutralize salt counterions, which is called the “salting-in” effect. Because the oppositely charged groups are positioned along the same side chain or backbone segment, they experience strong intramolecular electrostatic attractions in salt-free water, causing the polymer to adopt a relatively compact conformation. When salt is added to the solution, this internal ion pairing becomes partially disrupted due to charge screening by

external ions. As monovalent and divalent ions surround the zwitterionic groups, the strength of the internal electrostatic interactions decreases, allowing the polymer chains to expand. This increase in chain extension enhances the hydrodynamic radius and leads to higher viscosity and improved solubility at elevated salinity levels (Lu et al., 2021). Consequently, this effect allows to have a greater solubility in salt solution than in pure water. As a result, these polymers possess outstanding viscoelastic properties due to their ability to withstand high salinity, and high temperature conditions. From an engineering standpoint, zwitterionic polymers are typically considered as a non-fouling replacement to the commonly used polyethylene glycol polymers for avoiding accidental protein binding and minimizing microbial or mammal cell attraction (Kirschner & Brenna, 2012).

The comparison of polyethylene glycol and zwitterionic polymers might be unreliable since all polyethylene glycol polymers fundamentally have identical cyclic components, whereas zwitterionic materials comprise a wide range of polymers with diverse monomeric compositions. Among the most important features are 1) the ionic groups to be incorporated into the polymer structure, such as carboxylate (Chen et al., 2023), sulfonate (Brown et al., 2022), or phosphate (Hou et al., 2025) as oppositely charged groups, and quaternary ammonium (Zhu et al., 2021), phosphonium (Brown et al., 2021), pyridinium (Hou et al., 2025) or imidazolium (He et al., 2020) as positively charged groups); 2) the physical distribution of charged groups - the closeness of negative and positive charges inside the identical monomeric component (Chen, 2022) or the complete isolation of oppositely charged functional groups onto distinct polymer side groups (Li et al., 2022); 3) different zwitterionic polymers that could make both shifts between zwitterionic and non-zwitterionic states (B. Cao et al., 2013) or transport a charged biologically active chemical as a zwitterionic polymer (Mi & Jiang, 2012).

Synthesis of zwitterionic polymers includes different strategies as there are many pathways to implement the arrangement of ionic groups. Laschewsky (2014) and Chang (2022) explained all possible zwitterionic polymer architectures which are illustrated in Figure 3. These architectures broadly differ in how the positively and negatively charged groups are positioned, whether they are located within the same group, placed on separate

side chains, or integrated directly into the polymer backbone. When both charges are located on a single side chain, the polymer forms a classic internal zwitterion, where intramolecular electrostatic pairing governs hydration and solubility. In contrast, when the charged groups reside on different side chains or at different positions relative to the backbone, the polymer displays greater freedom for intermolecular interactions and enhanced responsiveness to external ions in solution. Overall, the figure highlights how variations in charge placement, spacing, and connectivity produce zwitterionic polymers with distinct hydration behavior, solubility, and rheological properties that directly influence their suitability for EOR applications.

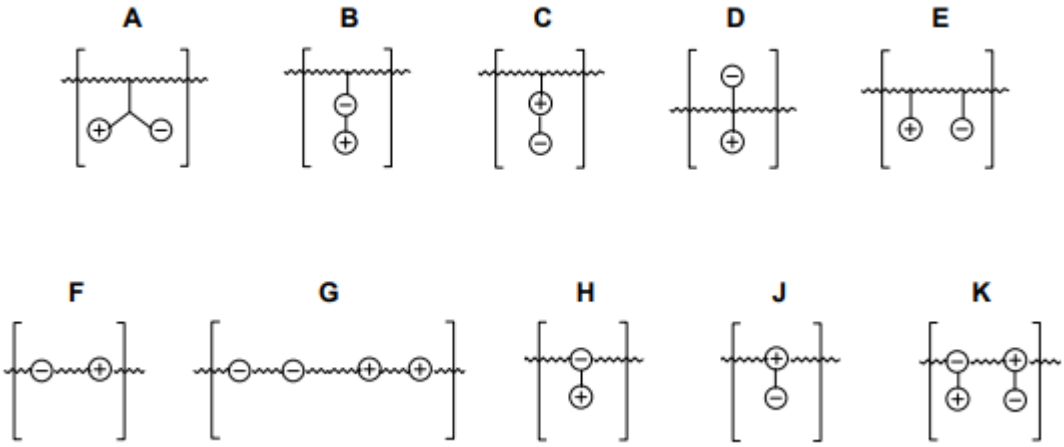

Figure 3. Possible arrangement of the ionic group in zwitterionic polymers. (Laschewsky, 2014).

The variety of zwitteronic polymers depends on the nature of ionic groups. Within the zwitterionic structure, anionic groups containing phosphates, sulfonates, and carboxylates are mostly employed for research purposes. Sulfuric acids and phosphinic acids are characterized by typically low pKa values, which allow them to stay deprotonated over a wide range of pH values. In contrast, the acidity of carboxylates is controlled by the distance between the cationic site and the negatively charge carboxylic group. Overall, the hydrophilicity of the anionic group decreases with the increase in acidity in order: $-COO^-$ > $(RO)_2^-P(=O)O^-$ > $-SO_3^-$ > - $O-SO_3^-$. As a result, sulfonates, being the most acidic and least hydrophilic group, show the lowest solubility in water compared to other anionic groups.

Nitrogen, in form of a quaternized ammonium group, is the most widely used cationic group in the zwitterionic polymer chain. The presence of an ammonium group within a structure allows it to operate and satisfy the conditions over a wide pH window.

2.5.2 Synthesis of zwitterionic polymers

The synthesis of zwitterionic polymers is commonly performed by free radical polymerization using zwitterionic monomers. This type of polymerization offers exceptional compatibility with the ionic and highly polar functional groups present in zwitterionic monomers. The technique also allows broad control over molecular weight, facilitates copolymerization with acrylamide and other vinyl monomers. The most common zwitterionic polymers synthesized via free radical polymerizations are related to sulfobetaine and carboxybetaine constituents. Zwitterionic monomers bearing sulfobetaine or carboxybetaine sites provide favorable hydrophilic-hydrophobic balance to maintain the solubility control in many solvents. In addition, due to the strong adsorption at the oil/water barrier, these zwitterionic monomers, namely alkyl carboxyl betaines and alkyl sulfobetaine, outperform nonpolar conventional monomers in lowering raw oil/water interfacial tension (Cui et al., 2012). Methods for synthesizing and refining carboxylic betaine monomer into granules are described in detail in US Patent Application Publication by Li et al., (2014). The structure of a typical zwitterionic polymer synthesized by free radical polymerization is shown in Figure 4.

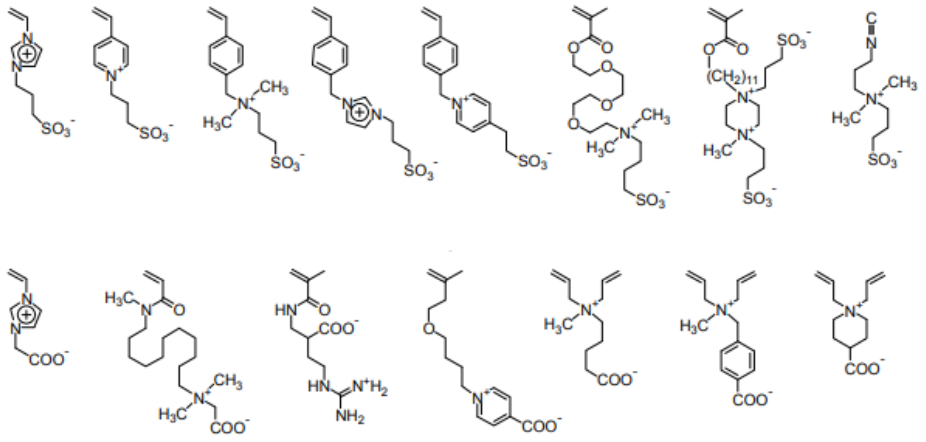

Figure 4. The structure of sulfonated and carboxylated zwitterionic polymers. (Li et al., (2014)

Acrylic acid and the associated tertiary amine-oriented monomers can be used to produce the carboxylic betaine type zwitterionic polymer. When acrylic acid reacts with tertiary amine monomers, an internal neutralization reaction occurs, producing a stable betaine structure that carries both a quaternary ammonium cation and a carboxylate anion within the same monomer unit. These interactions focus on overcoming the limitations of conventional polymer solutions in high-salinity, high-temperature conditions. Conventional polymers such as HPAM lose viscosity in the presence of high concentrations of Na^{+}, Ca^{2+}, and Mg^{2+} due to electrostatic screening of the negatively charged carboxylate groups, which causes polymer chains to collapse. In contrast, zwitterionic carboxybetaine units maintain a balanced internal charge that prevents the chain from collapsing even at elevated salinity. The interaction of a tertiary amine with acrylic acid could be performed either with or without the use of a solvent. The concentration level of acrylic acid and amine in the surfactant matrix can range from 5 to 99% by mass, with a preferred range of 60-95%. In general, a somewhat high acid-to-amine ratio is desired to encourage the swing of stability to the synthesis of betaine. For operational applications, the acid-to-amine proportion should be between 0.1:1 and 10:1, preferably between 1:1 and 5:1. For instance, 2:1 to 3:1 mole proportion could give equilibrium rates of an amine into betaine as much as 80-90%. According to Li et al., (2014), pure betaine monomer can be achieved through further refining. As the starting materials for this purification procedure, either the reaction mixture or the isolated betaine, acid can be used. Using an inorganic base, organic base, or base ion exchange filler, the acid can be eliminated from the process medium or the betaine. Any form of base resin could be applied as long as it can absorb the acids from the zwitterionic monomer.

The modified composition of partially HPAM with a zwitterionic unit has been extensively studied by Lu et al., (2021). The example of the incorporation of zwitterionic monomer [2-(methacryloyloxy)ethyl]dimethyl-(3-sulfopropyl) into HPAM is shown in Figure 5.

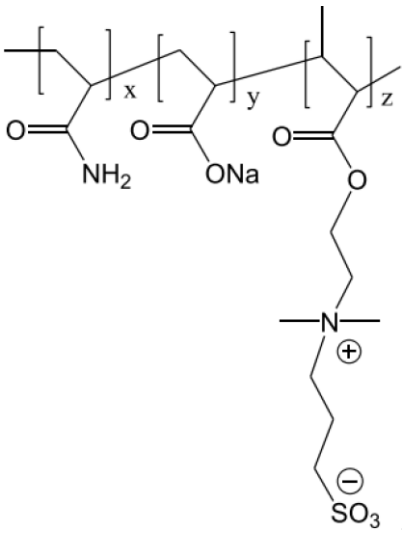

Figure 5. Zwitterion-modified HPAM polymer(Lu et al., 2021).

2.6 Current applications and studies of zwitterionic polymers for polymer flooding

The unique feature of zwitterionic polymers allows to provide the effect of surfactant and polymer interchangeably to increase the oil recovery. For instance, as surfactants, they are able to decrease the interfacial tension between raw oil and water to an extremely minimal value in order to extract trapped oil from the reservoir (R. Zhang et al., 2015). According to Gupta & Mohanty, (2008), the capability of surfactants to convert the wetting ability of a reservoir to a water-wet state is also another essential consideration when considering a surfactant for EOR applications. Simultaneously, containing a polymer main backbone chain, zwitterionic polymers are able to control the mobility ratio, increasing the viscosity of displacing fluid.

Lu et al., (2021) investigated and compared the viscoelastic properties of conventional HPAM and modified HPAM with the zwitterionic unit. The increase in salinity has a detrimental effect on conventional HPAM. However, the viscosity of modified HPAM steadily increased with the increase of salinity from 10 000ppm up to 200 000 ppm due to “salting-in” and electrostatic crosslinking within zwitterionic units. Also, modified HPAM showed better temperature resistance in terms of viscosity with respect to

salinity at different temperatures compared to the conventional HPAM. The results of the solution viscosity change are shown in Figure 6 below.

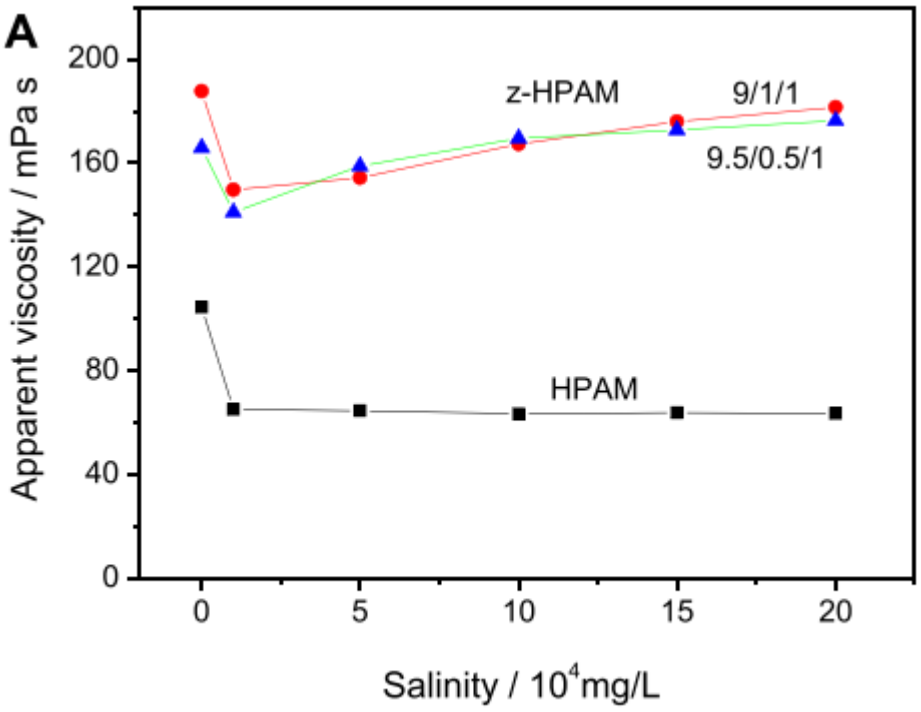

Figure 6. Viscosity change for z-HPAM and HPAM under different salinity ranges (Lu et al., 2021).

Gou et al., (2015) synthesized water-soluble copolymers of acryl amide (AM), acrylic acid (AA), and 2-((2-(acryloyloxy) ethyl)dimethylammonio)ethyl sulfite (ADMES) using oxidation-reduction initiation system. The synthesis route is shown in Figure 7.

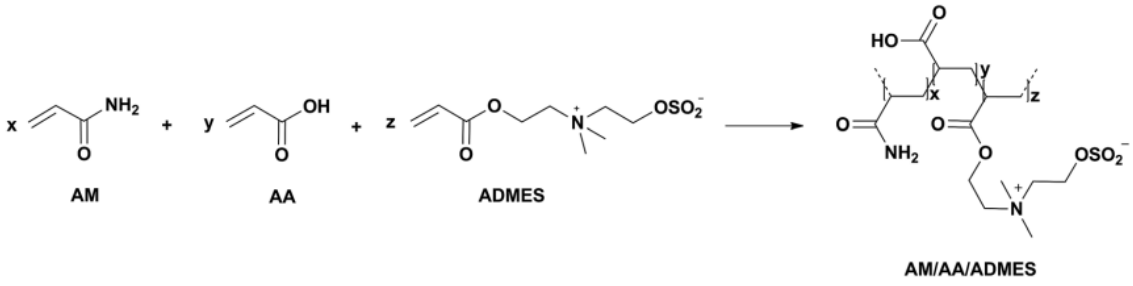

Figure 7. Synthesis route for AM/AA/ADMES (Gou et al., 2015).

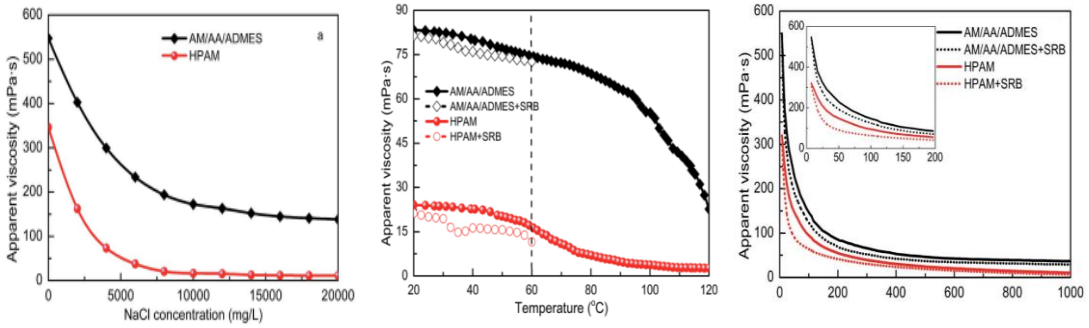

Figure 8. Rheological experiments are based on the effect of a) salinity (ppm) b) temperature (°C) c) shear rate (s^{-1}) (Gou et al., 2015).

Additionally, the effect of sulfate reducing bacteria (SRB) has been investigated to observe the impact on polymer viscosity. SRB plays an essential role in oilfield operations as it became a major contributing factor to microbiological-induced corrosions of pipelines. Overall, according to obtained results, the incorporation of zwitterionic monomers into the structure helped to increase its tolerance towards salinity, temperature, and high shear rate conditions, as shown in Figure 8.

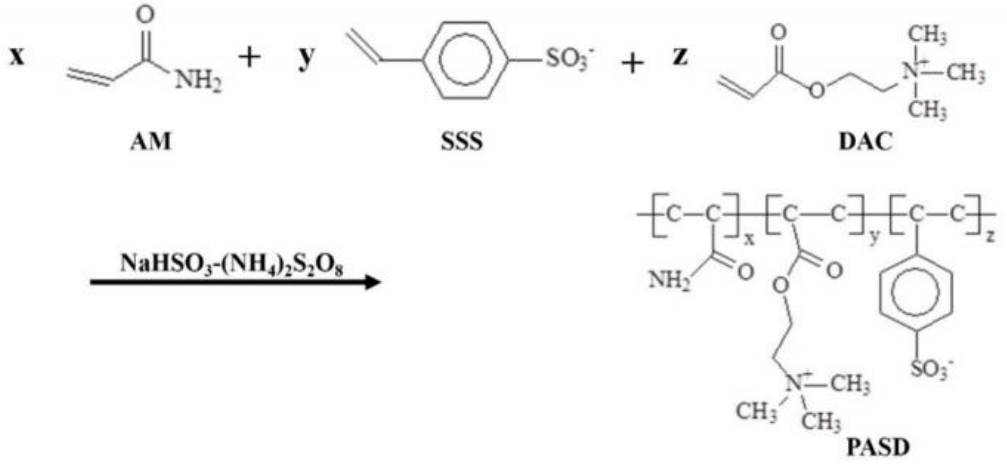

Figure 9. Synthesis of zwitterion-modified HPAM (Dai et al., 2017).

Another thermal-resistant and shear-stable zwitterionic polymer has been extensively studied by (Dai et al., 2017). In their research, they investigated zwitterionic polymer with the scattered arrangement of the ionic groups at different monomers sites. Acrylamide, sodium styrene sulfonate (SSS), and acryloxyethyl trimethylammonium chloride (DAC) monomers were reacting using free-radical polymerization reactions under high salinity conditions. The reaction route is shown in more details in Figure 9. In the first step, the monomer mixture containing AM, SSS, and DAC is dissolved in water

under controlled pH and temperature conditions. Free-radical polymerization was initiated followed by the propagation of radical to the vinyl groups of AM, SSS, and DAC. Because all three monomers contain C=C bonds,

they readily undergo chain-growth copolymerization. Based on the experiments, as expected, amphoteric polyacrylamide (PASD) polymer exhibited temperature stability, salt tolerance, and shear resistance. In addition, they obtained the same trend of increasing viscosity with the salinity level due to the "salt-in" effect as in previous studies, as shown in Figure 10.

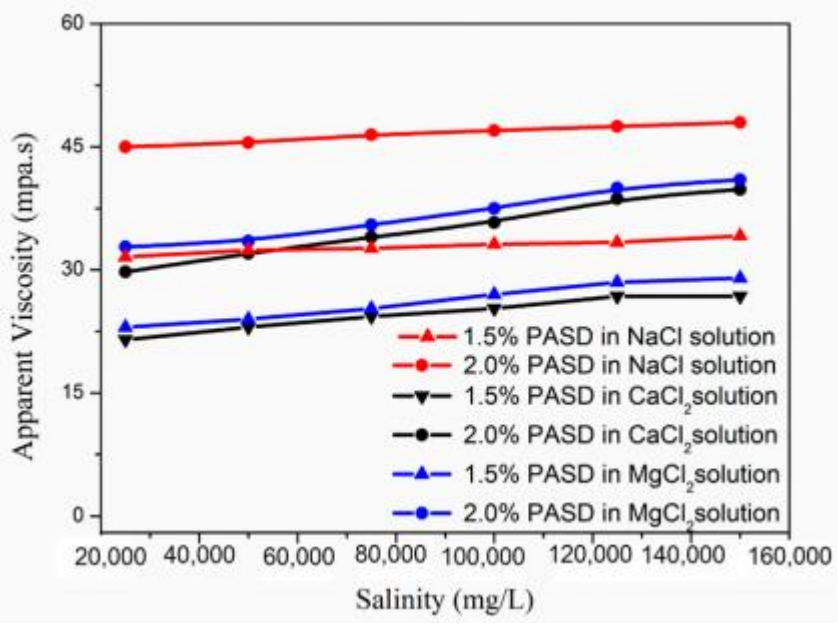

Figure 10. Viscosity change of PASD solution at different salt concentrations (Dai et al., 2017)

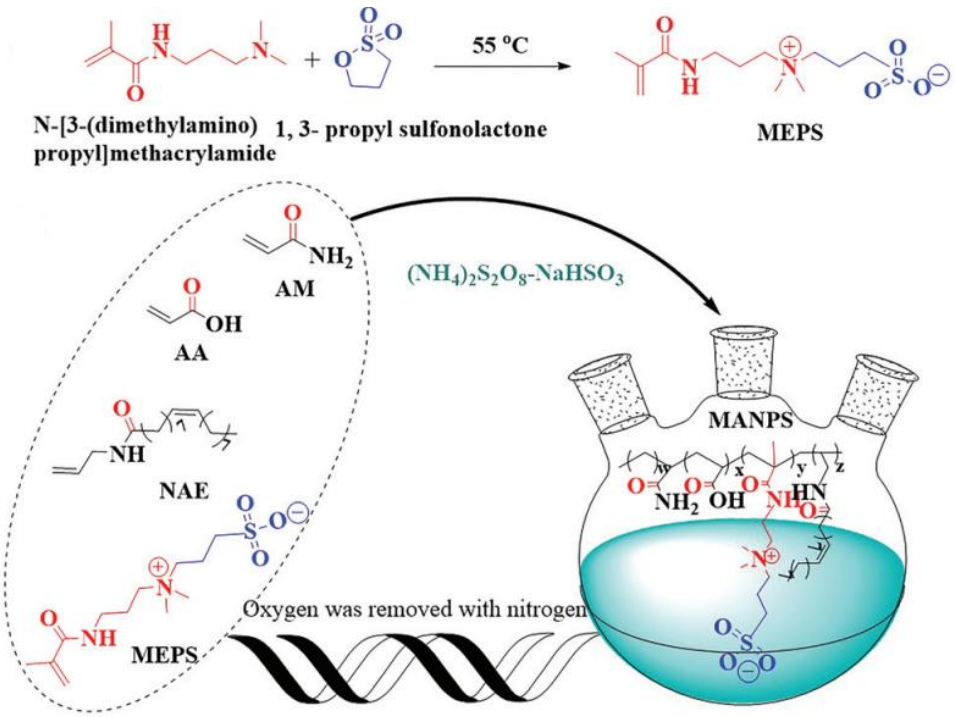

Figure 11. Synthetic route for MEPS and MANPS (L. Liu et al., 2020)

A comprehensive analysis of zwitterionic polymer containing a hydrophobic group has been also proven in previous studies on the enhanced rheological performance and injectivity analysis (L. Liu et al., 2020). This zwitterionic polymer, called MANPS, integrated a hydrophobic monomer, octadec-9-enoic acid allylamide (NAE), and a zwitterionic monomer, 3-(3-methylacrylamide propyl dimethylamino)-propyl-1-sulfonate (MEPS), into a conventional acrylamide-acrylic acid backbone. The obtained results have been also compared with HPAM, the most widely used polymer solution in the oilfield as a baseline. MANPS showed increased apparent viscosity, excellent viscoelasticity, strong shear thinning and shear recovery behavior, and notable thixotropy. These properties were attributed to the synergistic effects of hydrophobic interactions, molecular chain entanglement, and the unique anti-polyelectrolyte characteristics of zwitterionic groups, which enhance the formation of a robust physical crosslinked network in aqueous environments. In oil displacement experiments, MANPS achieved a 10.4% higher recovery rate compared to HPAM under identical conditions, indicating its

effectiveness in improving oil extraction efficiency. The synthetic route for the polymer preparation is shown in Figure 11.

The results obtained from scientific studies, on the viscoelastic characterizations of zwitterionic polymers showed good potential for the implementation of EOR projects. Their higher temperature resistance, shear sensitivity and salt tolerance compared to conventional HPAM indicate the advantages of using a zwitterion-modified structure within a polymer backbone chain. The studies conclude that zwitterionic polymers are promising candidates for next-generation polymer flooding applications in challenging oil reservoir environments, offering improved performance and environmental tolerance due to its zwitterionic and hydrophobic molecular design.

2.7 Coreflooding (injectivity) experiments related to polymer flooding

Today, research in the oil and gas industry heavily relies on laboratory coreflooding experiments, as it is the only way to predict in-situ the oil recovery process. Coreflooding system allows to imitate the flooding process starting from the surface injection equipment down to the oil reservoir. Over the last decades, the performance of coreflooding systems proved to be a critical and inevitable part of providing versatile and accurate results. The industry shows a particular interest in exploring new options and advancements in core flooding systems. As a result, starting from 1987, there are already more than 10 known modifications to the coreflooding system, which is summarized in Table 1 below.

Table 1. Summary of currently used coreflooding systems.

Author	Year	Upstream	Downstream	Used Fluids
Hornof and Morrow	1987	Metering pump	n/a	Isooctane, brine, water and oil
Chand and Grigg	1994	Syringe pumps with PA	Multiport rotary valve with vials	CO_2, brine, oil, and surfactant solution
Legowo and Pratomo	1999	Displacement pump "Quizix" with PA	Fraction collector and separator	Water, oil, and different microbial cultures
Bagci et al.	2001	Syringe pump	Fraction collector	Water, oil, and different microbial cultures
Sedaee	2004	Displacement pump with PA	Effluent condenser with collector	Steam, CH_4, and heavy oil
Nobakht et al.	2007	Syringe pump with PA	Oil sample collector with gas flow meter	Crude oil, and CO_2
Hadia et al.	2007	Dual piston syringe pump with PA	Fraction collector	Oil and water
Mandal et al.	2010	Syringe pump with PA	Fraction collector	Oil-in-water emulsion, oil, and water
Samanta et al.	2012	Syringe pump with PA	Fraction collector	Oil, brine, and chemical slug
Veerabhadrappa et al.	2013	Syringe pump with PA	Effluent sample collector	Oil, water, and polymer
Ko et al.	2014	Syringe pump with PA	Fraction collector with centrifuge tube	Brine, oil and surfactant

Conventional coreflooding system consists of three main components: the upstream, the core, and the downstream. The upstream system consists of displacement fluids and pumps to inject. The core system contains a porous core and holder to imitate the reservoir downhole conditions, which include an overburden pressure valve and temperature chamber. In the downstream, the effluent fluid is collected in the back end of the core system. The main constituents of the system are integrated using a data acquisition component for further visualization. The schematic of the coreflooding system that is commonly used nowadays is shown in Figure 12.

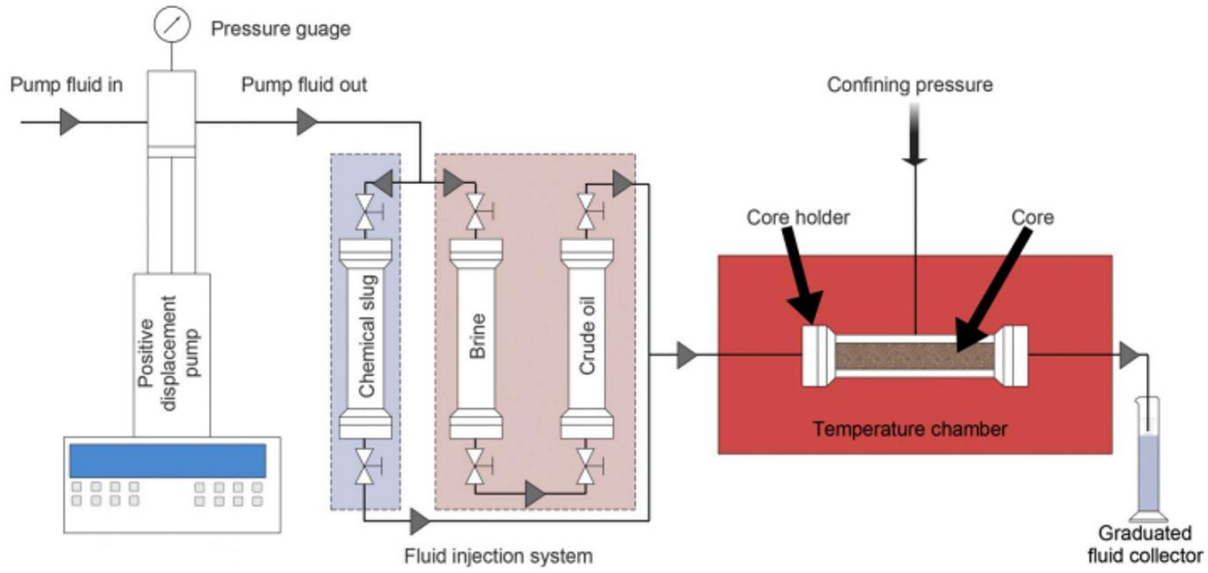

Figure 12. Schematic of coreflooding system.

Gou et al., (2015) investigated the injectivity experiments through a core flooding system when they studied the application of zwitterionic polymer for enhanced oil recovery. In the study, they presented the development and evaluation of a novel acrylamide-based copolymer (AM/AA/ADMES) designed for EOR, particularly under harsh reservoir conditions involving high salinity, temperature, and microbial contamination. In addition, they measured and compared flow characteristics for HPAM and zwitterion-modified polymer. The experimental setup included a stainless-steel core holder packed with quartz sand (80–100 mesh) to simulate porous rock, with a porosity of 22.8%. Based on the results from Figure 13, the injection pressure during polymer flooding and post-flushing for zwitterionic polymer were higher compared to conventional HPAM which indicated stronger mobility control and retention behavior. The pressure stabilized after the initial rise, reflecting steady polymer propagation through the porous medium. Following polymer flooding, post-water flooding was performed, and the residual resistance factor (RRF) was calculated based on the pressure during this stage. A high RRF value of 4.6 implies that the polymer retained its resistance characteristics, effectively reducing water mobility and sustaining flow control even after polymer breakthrough. Additionally, potential EOR implementation has been investigated to measure cumulative oil recovery for these polymers. Due to the stronger viscoelastic behavior of zwitterionic polymer, it showed an additional 11% of incremental oil recovery compared to 5.5% for HPAM after

3 PV of water injection, as it is shown in Figure 14. This result reflects the polymer's favorable viscoelastic behavior, which enhances microscopic sweep efficiency, and its resistance to microbial degradation, which maintains functionality over extended periods.

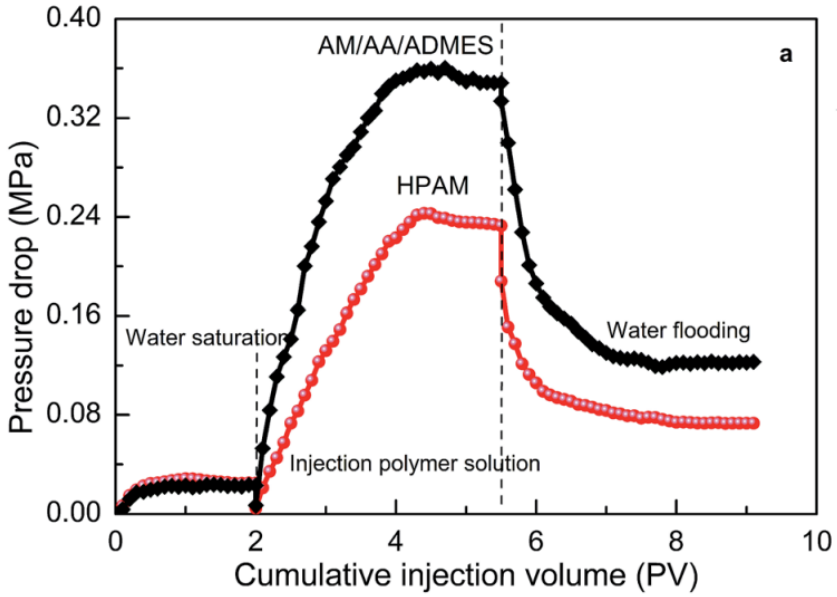

Figure 13. Flow characteristic graph of polymer injected volumes and pressure drop (Gou et al., 2015)

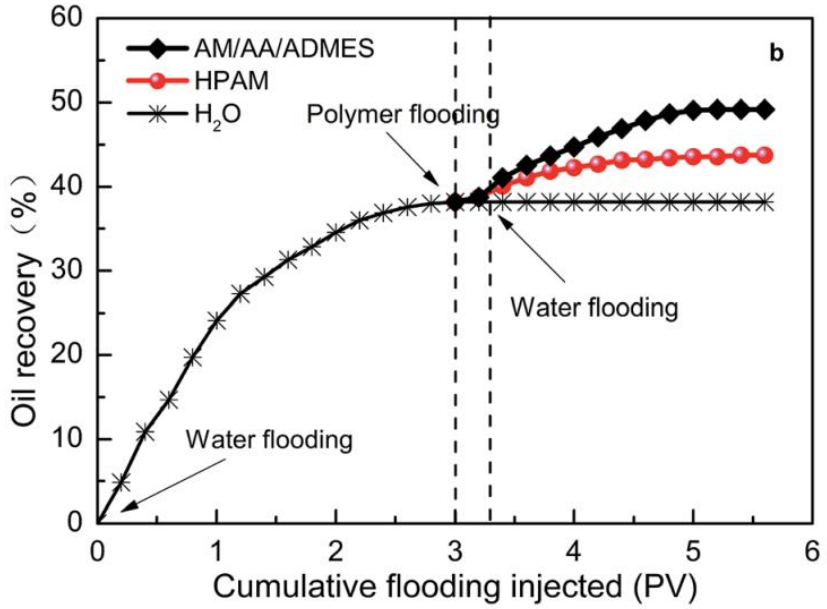

Figure 14. Cumulative oil recovery rate based on pore volume injected for different stages (Gou et al., 2015)

The displacement effect of zwitterion-modified polymer MANPS and conventional HPAM has been also analyzed using a coreflooding setup, and the results are shown in Figure 15 (L. Liu et al., 2020). Thus, as could be predicted, the pressure started to increase when the polymer started to inject, after the water flooding. The peak in pressure corresponds to the point when all polymer solutions have been injected and then gradually decreased during the post-flush process. As a result, an additional 13.4% of oil recovery has been observed for MANPS and 3.0% for HPAM, respectively.

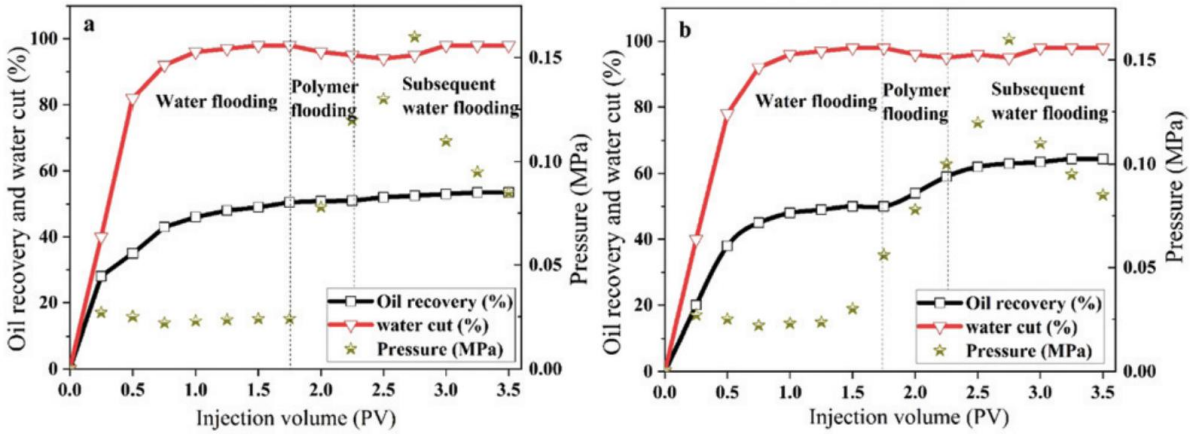

Figure 15. The coreflooding experiments of the polymer-based a flow characteristic and cumulative oil recovery for a) HPAM b) MANPS (L. Liu et al., 2020)

2.8 Conclusion

This chapter provided a detailed review of EOR methods with a specific focus on polymer flooding and the development of advanced zwitterionic polymers for chemical EOR. The literature clearly demonstrates that while conventional polymers such as HPAM remain widely used due to their cost-effectiveness and viscosity-enhancing capabilities, their performance is significantly constrained under high-salinity and high-temperature reservoir conditions. In such harsh environments, polymer chain contraction, thermal degradation, and interactions with divalent ions (Ca^{2+}, Mg^{2+}) cause rapid viscosity loss and reduced mobility control.

Zwitterionic polymers, particularly those incorporating sulfobetaine and carboxybetaine functional groups, have emerged as promising alternatives owing to their unique structural balance of positive and negative charges. This intrinsic charge neutrality

provides strong hydration and electrostatic shielding, resulting in exceptional tolerance to salinity, temperature, and shear. Numerous studies have reported that zwitterionic polymers exhibit the “salting-in” effect, where viscosity increases with salinity, contrasting with the “salting-out” behavior of anionic polymers like HPAM. Experimental results from previous works demonstrated enhanced viscosity pefrormance, superior shear stability, and incremental oil recovery improvements of up to 10–13% over HPAM during coreflooding under harsh conditions.

Despite significant progress in the development of zwitterionic polymers for enhanced oil recovery, several key research gaps remain and form the basis of the present PhD work. First, existing studies have not fully established quantitative links between polymer molecular structure and performance, particularly how zwitterionic architecture influences thermal stability, viscosity retention, and oil recovery. Second, most prior evaluations were conducted under mild conditions, leaving a lack of systematic experimental data for environments exceeding 200,000 ppm salinity and temperatures above 60 °C. Third, long-term thermal degradation and sustained viscosity values of zwitterionic polymers remain insufficiently explored, limiting understanding of their durability over extended reservoir residence times. Finally, few studies have validated laboratory findings through numerical reservoir-scale modeling, creating a gap in assessing the scalability and real-field applicability of these polymers. This PhD research addresses these gaps through integrated experimental and numerical approaches designed to bridge molecular design, rheological behavior, and reservoir performance.

CHAPTER 3. SYNTHESIS OF ZWITTERIONIC MONOMER AND COPOLYMERS

3.1 Introduction

In the context of EOR, polymer flooding is a widely used technique aimed at increasing the viscosity of the displacing water phase, thereby improving sweep efficiency and residual oil mobilization. However, one of the primary challenges in deploying conventional polymers such as polyacrylamide or its partially hydrolyzed derivatives lies in their poor rheological behaviour under high-temperature, high-salinity reservoir conditions. These polymers often suffer from thermal degradation, viscosity loss, hydrolysis, and precipitation in the presence of multivalent cations, severely limiting their field performance and lifespan.

To overcome these limitations, zwitterionic polymers have been proposed as robust alternatives. The presence of both cationic and anionic groups within the same side chain leads to the formation of strong intermolecular electrostatic interactions, promoting structural stability and chain rigidity. Moreover, the electrical neutrality of zwitterionic group minimizes their interaction with reservoir brine components, further enhancing their solubility and long-term performance.

In this study, three zwitterionic monomers, N,N-dimethyl-N-(3-methacrylamidopropyl)-N-(3-sulfopropyl)ammonium betaine (DMAPMAPS), sulfobetaine vinylimidazole (SBVI), and sulfobetaine 4-vinylpyridine (SBVP), were selected for copolymerization with acrylamide. The selection of these monomers was driven by their high glass transition temperatures (Tg), which are critical for maintaining polymer performance in thermally demanding EOR applications.

The copolymerization of these monomers with acrylamide was conducted via aqueous free-radical polymerization to produce three zwitterionic copolymers: zPAM 1, zPAM 2, and zPAM 3. These copolymers aim to combine the favorable rheological and water-soluble properties of acrylamide with the salt-tolerant, thermally stable characteristics of

zwitterionic functionalities. This chapter provides detailed information about the synthesis procedures, and polymer conversion behavior.

3.2 Materials and Methods

3.2.1 Materials

All chemical reagents used in the synthesis of zwitterionic copolymers were procured from Sigma-Aldrich to ensure high purity and consistency. These included N-(3-dimethylaminopropyl)methacrylamide (DMAPMA), 1,3-propane sultone (1,3-PS), acrylamide, ethanol (solvent), 1-vinylimidazole (1-VI), 4-vinylpyridine (4-VP).

Solvents such as acetonitrile and acetone were used in monomer synthesis, while ethanol served as the non-solvent for copolymer precipitation. Ammonium persulfate was used as a free-radical initiator in aqueous copolymerization reactions, and 2,2,6,6-tetramethylpiperidine 1-oxyl (TEMPO) was employed as a radical scavenger to minimize side reactions.

3.2.2 Synthesis of zwitterionic monomers

Three zwitterionic monomers were synthesized via nucleophilic ring-opening reactions between tertiary amines and 1,3-propane sultone. The general reaction mechanism involves the nucleophilic attack of a nitrogen atom on the sulfonate ring of 1,3-PS, resulting in the formation of a stable sulfobetaine structure.

Sulfobetaine vinylimidazole (SBVI) (5 mL) and sulfobetaine 4-vinylpyridine (SBVP) (5 mL) were synthesized through the nucleophilic ring opening of 1,3-propanesultone (5mL) with 1-vinylimidazole and 4-vinylpyridine, respectively. The reaction was performed using acetonitrile (50 mL) and TEMPO as the solvent, with a reaction temperature of 50°C and a duration of 22 hours. The synthetic conditions for the monomer synthesis are shown in Table 2. The precipitated monomers were white to yellowish-white powders that were subsequently washed three times with ethyl acetate. The purity of the compounds was confirmed by analyzing their ^{1}H NMR and FTIR spectra.

The synthesis of N,N-dimethyl-N-(3-methacrylamidopropyl)-N-(3-sulfopropyl) ammonium betaine (DMAPMAPS) monomer involved the reaction between DMAPMA (8.5 g) and 1,3-PS. A solution containing 1,3-PS (5 mL) and acetone (19 mL) was added dropwise to a three-neck round-bottom flask containing DMAPMA and acetone. The reaction mixture was stirred for 30 minutes and then left to stir at room temperature for 24 hours. The resulting product appeared as a white powdery substance, which was subsequently filtered, washed with acetone, and dried under vacuum conditions at 40°C for 24 hours. The synthesis pathway for DMAPMAPS is presented in Table 3, and the purity of the final product was confirmed through ^{1}H NMR and FTIR spectroscopic analysis.

3.2.3 Synthesis of zwitterionic copolymers

For the copolymer synthesis, a predetermined quantity of acryl amide (AM) (19.6 g) and zwitterionic monomers (0.4 g) were dissolved in water. Then, the copolymerization process was initiated by the slow addition of ammonium persulfate (10 mL) as the initiator into the reaction system. The copolymerization reaction was then carried out under a nitrogen atmosphere at a temperature of 40°C for a duration of 8 hours. The resulting copolymers were precipitated using ethanol and subsequently dried overnight at 45°C in a vacuum oven to obtain the final product. The described aqueous solution copolymerization method was employed for the synthesis of all zwitterionic copolymers, and the specific synthesis conditions and routes are summarized in Table 2 and 3. Product conversion was quantified by calculating the ratio of the mass of the dried polymer product to the initial total mass of monomers charged into the reaction mixture. This gravimetric approach provides a direct measure of polymerization efficiency and ensures comparability across different copolymer systems.

Table 2. Copolymerization synthesis conditions.

Copolymer	Initiator (wt %)	Temperature (°C)	Concentration (wt %)	Monomer (wt %)	
				AM	ZW
ZP + AM	0.2	40	20	98	2

Table 3. The synthesis routes for zwitterionic polymers.

Polymer	Monomer synthesis reaction	Copolymer synthesis reaction	Product conversion
DMAPMAPS + AM zPAM 1	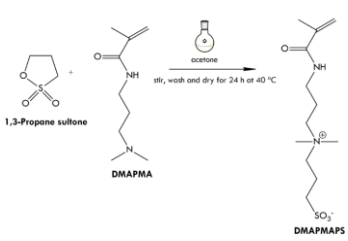	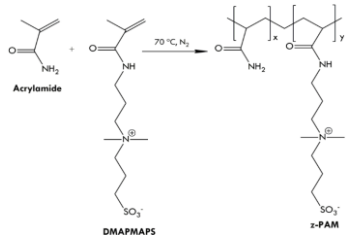	90 %
SBVI + AM zPAM 2	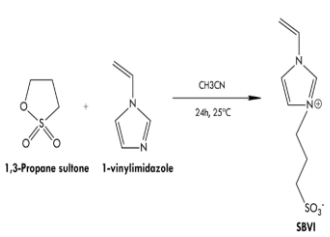	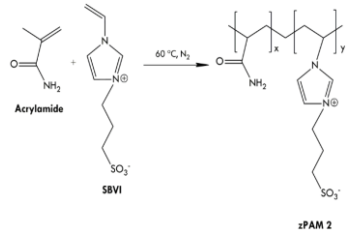	88%
SBVP + AM zPAM 3	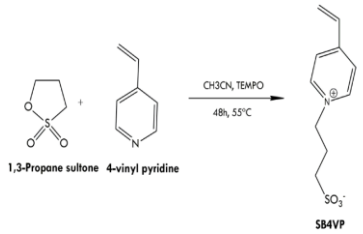	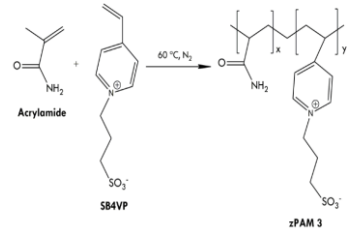	80%

3.3 Results & Discussion

The synthesis of three zwitterionic monomers was achieved using nucleophilic ring-opening reactions between 1,3-propane sultone and respective amine-containing

precursors. These monomers were specifically chosen for their well-documented high glass transition temperatures (Tg), a property critical for polymer performance in harsh thermal and saline environments in the oilfield conditions. The high Tg values of these monomers reflect their structural rigidity, which arises from either aliphatic (in the case of DMAPMAPS) or aromatic (in SBVI and SBVP) moieties. Aromatic rings, such as those found in imidazole and pyridine groups, introduce chain stiffness and enhance cohesive interactions within the polymer matrix. These thermal characteristics are essential to ensure that the copolymers maintain mechanical integrity, resist thermal degradation, and retain viscosity at high temperatures.

Following monomer synthesis, free-radical aqueous copolymerization with acrylamide was performed using ammonium persulfate as an initiator under inert nitrogen conditions. After precipitation and drying, all copolymers appeared as fine, white powders with no visible impurities or discoloration. Each material demonstrated excellent solubility in deionized water, forming clear and homogeneous viscous solutions at room temperature. This high aqueous solubility is particularly relevant for field applications in EOR, where polymers must dissolve easily for injection into porous rock formations. The physical appearance and dissolution behavior further suggest that no cross-linking or phase separation occurred during synthesis and that the zwitterionic groups were successfully incorporated into the polymer backbone in a controlled and compatible manner.

The observed conversion efficiencies, in Table 3, indicate that the polymerization proceeded effectively for all cases. zPAM 1, based on the aliphatic monomer, exhibited the highest conversion. This is likely due to the reduced steric hindrance and better copolymerization compatibility of the methacrylamide backbone with acrylamide (Pan & Ouchi, 2023).

In contrast, zPAM 2 and zPAM 3, containing aromatic groups, showed slightly lower conversions. This can be attributed to both steric and electronic effects from the imidazole and pyridine rings, which may reduce the propagation rate or lead to less favorable radical reactivity during the copolymerization process (Van Guyse et al., 2019).

Despite this, all three systems achieved conversion values above 80%, which is considered acceptable for aqueous copolymerization processes and suitable for practical application development.

3.4 Conclusion

In this chapter, three zwitterionic monomers, DMAPMAPS, SBVI, and SBVP, were synthesized via nucleophilic ring-opening reactions with 1,3-propane sultone. The subsequent copolymerization of each monomer with acrylamide was successfully carried out using aqueous free-radical polymerization, resulting in three zwitterionic copolymers: zPAM 1, zPAM 2, and zPAM 3. The reactions exhibited high conversion efficiencies ranging from 80% to 90%, with all copolymers obtained as fine, water-soluble powders. The observed variations in polymer yield reflect differences in monomer reactivity influenced by steric and electronic factors inherent to the monomer structures. While the synthetic procedures yielded products consistent with the expected zwitterionic structures, the full confirmation of successful monomer and polymer formation is presented in the next chapter chapter.

From a scalability perspective, the synthetic routes used for DMAPMAPS, SBVI, SBVP, and their corresponding copolymers offer practical advantages for larger-scale production. Both reaction pathways rely on readily available reagents, mild reaction temperatures, and solvent systems (water, acetone, acetonitrile) that are compatible with industrial polymerization processes. The high monomer-to-polymer conversion efficiencies (80–90%) further indicate low material loss and efficient utilization of reactants, which are essential for economically viable scale-up. In addition, the precipitation and purification steps used in this work are standard unit operations in industrial polymer manufacturing and can be readily adapted to continuous or semi-continuous processing. Overall, the simplicity of the reaction mechanisms, high yields, and absence of side products suggest that the synthesis routes developed for zPAM 1, zPAM 2, and zPAM 3 have strong potential for scale-up, supporting their feasibility for future field-level EOR applications.

In the next chapter, to further understand and validate the structural and morphological characteristics of these zwitterionic copolymers, comprehensive analyses are conducted using various analytical techniques. Fourier-transform infrared spectroscopy and proton nuclear magnetic resonance are employed to confirm the chemical structures and functional groups present in the polymers. Dynamic light scattering is utilized to assess the molecular weight for each polymers. Scanning electron microscopy is used to examine the surface morphology and microstructural features of the copolymers.

These characterization techniques provide a deeper understanding of the copolymers' properties, required for specific applications in EOR with high thermal and saline resistance.

CHAPTER 4. PHYSICOCHEMICAL AND STRUCTURAL CHARACTERIZATION OF ZWITTERIONIC COPOLYMERS

4.1 Introduction

Comprehensive physicochemical and structural characterization is essential for validating the successful synthesis of zwitterionic copolymers and understanding their structure–property relationships. As it was found in the previous chapter, three zwitterionic copolymers were synthesized via aqueous free-radical copolymerization using zwitterionic monomers (DMAPMAPS, SBVI, and SBVP, respectively) and acrylamide.

In this chapter, the structural, compositional, and morphological features of the synthesized zwitterionic copolymers are systematically investigated using different analytical techniques. Fourier-transform infrared spectroscopy (FTIR) is employed to identify key functional groups and verify successful copolymerization by identifying the presence and disappearance of characteristic vibrational peaks. Proton nuclear magnetic resonance was utilized to confirm the incorporation of zwitterionic monomer units into the acrylamide backbone and assess the purity and structural integrity of the copolymers. Dynamic light scattering provided insights into the molecular weight of the polymers in solution, a key determinant of their viscoelastic behavior and injectivity in porous media. Finally, scanning electron microscopy offered a detailed view of the surface morphology and internal structural organization of the copolymers, revealing how zwitterionic structural network influence polymer behavior.

Together, these characterization methods form a comprehensive basis for correlating the chemical structure and physical morphology of the zwitterionic copolymers with their functional performance in EOR applications.

4.2 Materials & Methods

4.2.1 FTIR

The FTIR spectra of the samples were acquired using a Nicolet iS10 FT-IR Spectrometer, covering the spectral range of 500-4000 cm^{-1}. This spectrometer, as depicted in Figure

16**,** was sourced from ThermoFisher. FTIR spectroscopy was performed using a Nicolet iS10 FT-IR spectrometer operating over the wavenumber range of 4000–500 cm^{-1}. FTIR is based on the principle that molecular bonds absorb infrared radiation at characteristic frequencies corresponding to vibrational transitions. These absorbsion features generate a molecular fingerprint that enables identification of functional groups and verification of monomer and polymer structures. For the zwitterionic copolymers, FTIR was particularly valuable for confirming the presence of amide bonds, sulfonate groups, and quaternary ammonium functionalities, as well as ensuring the complete disappearance of vinyl C=C stretching bands following polymerization. Prior to FTIR analysis, polymer powders were dried to remove moisture and placed directly onto the ATR crystal. Each spectrum was baseline-corrected and normalized to ensure accurate comparison between samples.

Figure 16. Nicolet iS10 FT-IR Spectrometer

4.2.2 NMR

The ^{1}H NMR spectra were recorded on a JNM-ECA 500 MHz NMR spectrometer, utilizing deuterium oxide (D_2O) as the solvent. Figure 17 illustrates the NMR spectrometer employed in this analysis. NMR spectroscopy provides insight into the chemical environment of hydrogen nuclei, allowing identification of proton signals associated with the polymer backbone and zwitterionic side chains. For the synthesized copolymers, the absence of vinyl proton resonances confirmed complete monomer conversion, while characteristic signals from amide protons, sulfonated methylene groups, and aromatic protons in SBVI and SBVP verified successful incorporation of the

zwitterionic monomers. The polymer samples were dissolved in D_2O, filtered to remove undissolved particulates, and transferred to NMR tubes, ensuring that solvent suppression and peak resolution were optimized for structural assignment.

Figure 17. JNM-ECA 500 MHz NMR spectrometer

4.2.3 Molecular Weight determination

The molecular weight distribution of the zwitterionic copolymers was determined using a Zetasizer Nano ZS instrument operating in backscatter mode. Dynamic light scattering is a non-destructive technique based on analysis of the time-dependent fluctuations in scattered laser light caused by the Brownian motion of polymer chains in solution. These fluctuations yield the diffusion coefficient, which is converted to the hydrodynamic radius through the Stokes–Einstein relationship. The molecular weight was subsequently estimated through the construction of a Debye plot using Rayleigh scattering theory. To ensure accuracy, polymer solutions of varying concentration were prepared sequentially, beginning with the lowest concentration to minimize interparticle interactions. A refractive index increment (dn/dc) of 0.132 was used, consistent with acrylamide-based systems. All measurements were performed at 25 °C to eliminate thermal effects on diffusion behavior. This technique allowed reliable estimation of molecular weight

despite the relatively high molar masses of the copolymers, as the instrument is calibrated for macromolecular systems up to 2×10^7 Da.

Figure 18. Zetasizer Nano ZS

4.2.4 SEM

The morphological features of the copolymers were examined using a ZEISS Crossbeam 540 scanning electron microscope. SEM provides detailed information on surface topology by scanning a focused electron beam across the sample and detecting emitted secondary electrons. Zwitterionic polymers often exhibit network-like or granular surface structures that influence their water uptake, hydration kinetics, and viscoelastic performance. The SEM analysis in this study enabled visualization of morphological differences between zPAM 1, zPAM 2, and zPAM 3, including the more ordered and interconnected network structure observed in zPAM 1. Prior to SEM imaging, the polymer samples were freeze-dried to preserve morphological integrity and coated with a 5 nm layer of gold to mitigate charging effects under the electron beam.

Figure 19. ZEISS Crossbeam 540 SEM

4.3 Results & Discussion

4.3.1 FTIR

The FTIR spectra of the zwitterionic monomers and copolymers were meticulously analyzed, with the results illustrated in Figure 20. These spectra exhibited distinct characteristic peaks that provided clear evidence of the molecular structures and confirmed the successful copolymerization process.

The FTIR spectra revealed several key vibrational modes that confirmed the presence of expected functional groups and the absence of unreacted monomers, validating the synthesis process. The stretching vibration of the N-H bond, characteristic of the amide groups in both the acrylamide units and the zwitterionic monomers, was prominently observed across all samples. Specific peaks for N-H stretching appeared at 3319, 3330, 3331, 3336, and 3338 cm^{-1}, with slight variations attributed to differences in hydrogen bonding environments and molecular packing among the monomers and copolymers (Nandiyanto et al., 2023). These peaks were consistently present in both monomers and copolymers, indicating the retention of amide functionalities post-polymerization.

For the zwitterionic monomers, absorption peaks associated with C-H stretching were identified at 3036, 3043, and 3112 cm^{-1} (Nandiyanto et al., 2023). These peaks correspond to the aliphatic and aromatic C-H bonds present in the monomer structures, particularly in the vinyl groups and heterocyclic rings. Additionally, the monomers exhibited distinct peaks for C=C stretching at 1612, 1615, 1621, and 1649 cm^{-1}, which are indicative of the vinyl double bonds critical for polymerization (Waly et al., 2021). The presence of these C=C peaks in the monomer spectra confirmed their chemical integrity prior to reaction. However, these peaks were notably absent in the FTIR spectra of the copolymers (zPAM 1, zPAM 2, zPAM 3), providing direct evidence of successful polymerization. The disappearance of the C=C stretching bands is a sign of successful free radical polymerization, as the vinyl double bonds are consumed during the formation of the polymer backbone, converting the monomers into a saturated polymer chain.

Further analysis of the copolymer spectra revealed characteristic peaks associated with the carbonyl (C=O) groups specifically to the acrylamide units and zwitterionic monomers. The C=O stretching vibrations were observed at 1662, 1639, 1649, 1656, 1662, and 1649 cm^{-1} across the copolymer samples. The slight variations in peak positions are attributed to differences in the electronic environment surrounding the carbonyl groups, influenced by the zwitterionic groups and hydrogen bonding interactions within the polymer structure (Smith, 2021). The consistency of these peaks across zPAM 1, zPAM 2, and zPAM 3 confirms the successful incorporation of acrylamide into the copolymer structures, as the amide carbonyl is a key structural feature of the polymer backbone.

A critical indicator of the zwitterionic nature of the copolymers was the presence of symmetric stretching vibrations of sulfonated groups (SO_3^-), which are integral to the zwitterionic functionality. These peaks were observed at 1113, 1189, 1177, 1182, 1189, and 1174 cm^{-1}, with minor shifts reflecting differences in the molecular environment of the sulfonate groups across the three copolymers (Kalak et al., 2021). zPAM 2 and zPAM 2 showed slightly stronger intensities at 1189 cm^{-1}, possibly due to enhanced ionic interactions, while zPAM 3 exhibited a peak at 1174 cm^{-1}, influenced by the pyridine ring's electronic effects. The presence of these sulfonate peaks in all copolymer spectra confirmed the incorporation of zwitterionic monomers into the polymer structure, highlighting the successful synthesis of the designed materials.

The FTIR analysis provided evidence of the successful synthesis of zPAM 1, zPAM 2, and zPAM 3 through free radical polymerization. The disappearance of the C=C stretching bands, combined with the retention of N-H, C=O, and SO_3^- vibrational modes, demonstrated the transformation of monomers into copolymers while preserving the zwitterionic functionality.

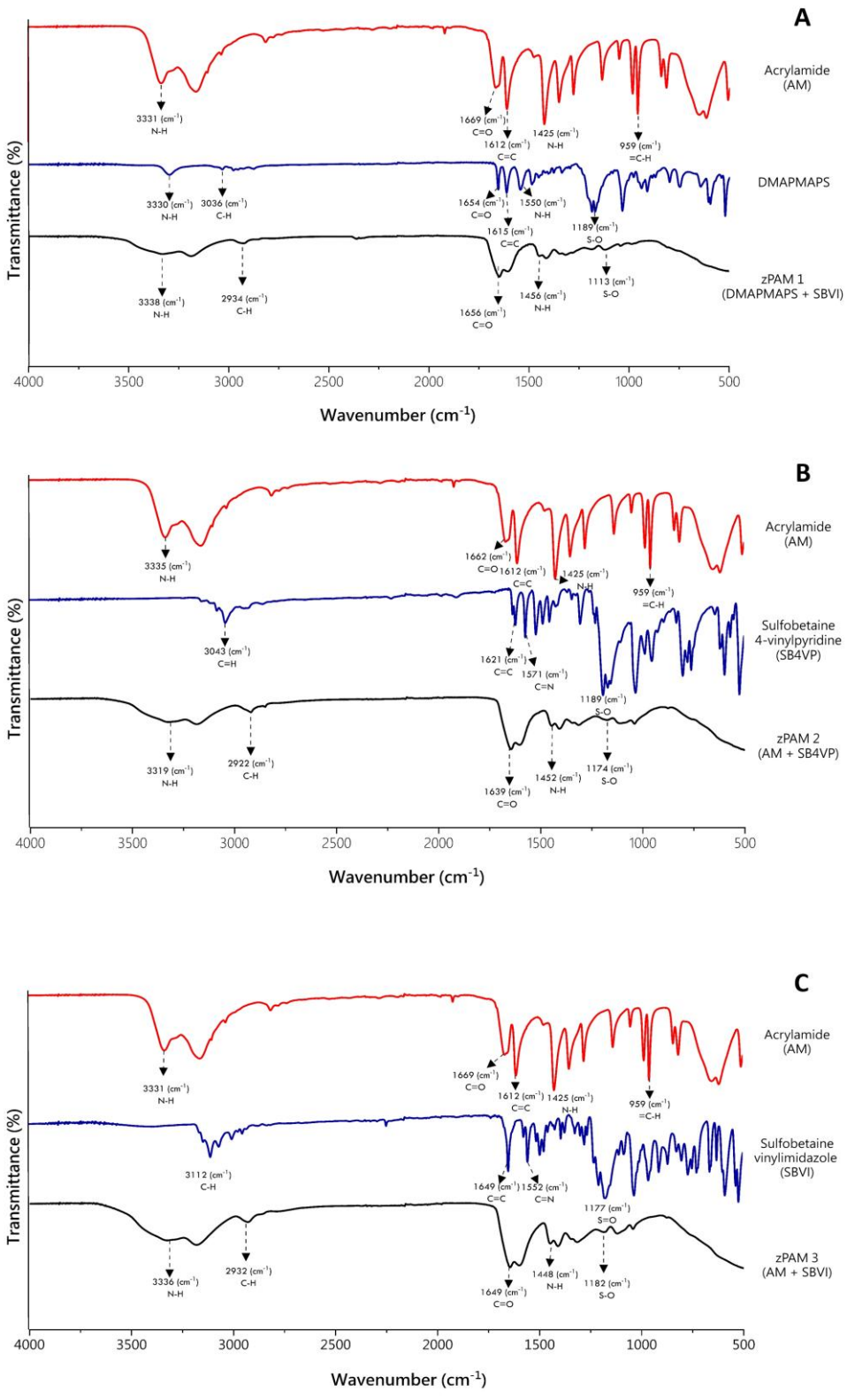

Figure 20. FT-IR spectra of zwitterionic copolymers: (a) zPAM 1; (b) zPAM 2; (c) zPAM 3

4.3.2 NMR

The structural characterization and purity assessment of the synthesized zwitterionic polymers were conducted through detailed ^{1}H Nuclear Magnetic Resonance spectroscopy. ^{1}H NMR provides precise information on the chemical connectivity and functional group distribution within the polymer chains, enabling confirmation of successful copolymerization and the incorporation of zwitterionic monomers into the acrylamide backbone. For sample preparation, approximately 10–15 mg of each polymer was dissolved in 0.6 mL of deuterium oxide (D_2O), which served as both the solvent and the internal lock signal for the spectrometer. D_2O was selected due to its compatibility with the hydrophilic nature of the zwitterionic polymers and its minimal interference with proton signals, as it lacks exchangeable protons that could overlap with the polymer signals. Chemical shifts (δ) were calibrated relative to the residual signal in D_2O at 4.79 ppm, providing a standardized reference for accurate peak assignment across all spectra.

The resulting ^{1}H NMR spectra for zPAM 1, zPAM 2, and zPAM 3 are presented in Figure 21 offering detailed insights into the chemical composition, structural configuration, and purity of each copolymer. These spectra were systematically analyzed to identify characteristic proton signals corresponding to the acrylamide backbone, zwitterionic side chains, and heterocyclic ring systems, ensuring the successful synthesis of the designed materials through free radical polymerization. The integration of peak areas was performed to confirm the monomer ratios (98:2 acrylamide:zwitterionic monomer) as per Table 2, and the absence of residual monomer signals was verified to assess the degree of polymerization and purity.

The ^{1}H NMR spectrum of zPAM 1 is shown in Figure 21A. The spectrum revealed a series of well-defined proton signals associated with the acrylamide polymer backbone, which forms the primary structural framework of the copolymer. Chemical shifts in the range of 0.91 to 1.08 ppm, 1.46 to 1.62 ppm, and 2.01 to 2.20 ppm were assigned to the $-CH_2-CH_3$ groups, corresponding to the methylene ($-CH_2-$) and methine (-CH-) protons along the polymer backbone (Melean Brito et al., 2024). These signals are characteristic

of the saturated carbon chain formed during polymerization, confirming the successful incorporation of acrylamide units. The zwitterionic sulfobetaine group of DMAPMAPS was evidenced by a distinct signal at 2.98 ppm, attributed to the -CH_2-CH_2-SO_3^- protons in the sulfonate-containing side chain. This peak reflects the aliphatic protons adjacent to the sulfonate group, a critical component of the zwitterionic functionality that enhances the polymer's salinity tolerance. Additionally, signals in the range of 3.46 to 3.52 ppm were assigned to the -CH_2-N^+-$(CH_3)_2$-CH_2 groups, corresponding to the quaternary ammonium protons in the zwitterionic side chain (Schonemann et al., 2021). The integration of these peaks relative to the backbone signals matched the expected 98:2 AM:DMAPMAPS ratio, indicating high monomer conversion and minimal residual monomer content. The absence of vinyl proton signals (typically at 5–6 ppm) further confirmed the complete polymerization of DMAPMAPS, aligning with the FTIR findings of C=C bond disappearance.

The ^{1}H NMR spectrum of zPAM 2, synthesized from sulfobetaine vinylpyridine and acrylamide, is presented in Figure 21B. The spectrum displayed characteristic signals associated with the aromatic pyridine ring of the SBVP monomer, alongside the acrylamide backbone. Aromatic protons in the pyridine ring were identified by peaks at 8.69 ppm and 7.84 ppm, assigned to the -CH-CH- groups within the ring structure (Bravetti et al., 2023).. These chemical shifts are consistent with the electron-deficient nature of the pyridine ring, influenced by the nitrogen atom and its conjugation with the zwitterionic side chain. Protons in the aliphatic linker region adjacent to the pyridine ring were observed at 3.59 ppm and 3.49 ppm, reflecting the -CH_2- protons connecting the pyridine to the quaternary ammonium group. The zwitterionic sulfobetaine functionality was confirmed by a signal at 3.31 ppm, corresponding to the -CH_2-CH_2-SO_3^- group, and an additional peak at 2.82 ppm assigned to the -CH_2-CH_2-SO_3^- protons closer to the sulfonate group (Amrenova et al., 2025). These signals indicate the successful incorporation of the SBVP monomer into the copolymer, with the sulfonate group maintaining its structural integrity post-polymerization. The acrylamide backbone signals were consistent with those observed in zPAM 1, appearing at 0.91 to 2.20 ppm, confirming the uniform polymerization of AM across all copolymers (Imekova et al.,

2024). The absence of residual vinyl protons (5–6 ppm) agree with the FTIR results, indicating complete monomer consumption and high purity of the synthesized zPAM 2.

The ^{1}H NMR spectrum of zPAM 3, derived from sulfobetaine vinylimidazole (SBVI) and acrylamide (AM), is shown in Figure 21C. Given the structural similarity between SBVI and SBVP, zPAM 3 was expected to exhibit comparable signals for the zwitterionic side chain, with additional peaks unique to the imidazole ring system. The spectrum confirmed these expectations, with aromatic proton signals at 7.69 ppm, 7.48 ppm, and 6.75 ppm assigned to the -CH-N- groups within the imidazole ring (Amrenova et al., 2025). These chemical shifts are characteristic of the imidazole ring's electronic environment, where the two nitrogen atoms contribute to distinct proton environments compared to the pyridine ring in zPAM 2. The zwitterionic sulfobetaine moiety was evidenced by signals at 3.31 ppm and 2.82 ppm, corresponding to the -CH_2-CH_2-SO_3^- protons, consistent with those observed in zPAM 2 and reflecting the sulfonate group's presence in the side chain. The acrylamide backbone signals appeared in the range of 0.91 to 2.20 ppm, mirroring those in zPAM 1 and zPAM 2, which confirmed the consistent incorporation of AM across all three copolymers (Imekova et al., 2024). The absence of vinyl proton signals (5–6 ppm) in the spectrum further validated the complete polymerization of SBVI, aligning with the FTIR evidence of C=C bond consumption.

The detailed ^{1}H NMR analysis of zPAM 1, zPAM 2, and zPAM 3 provided robust confirmation of their successful synthesis, with all expected structural features clearly identified in the spectra. The distinct chemical shifts associated with the acrylamide backbone, zwitterionic side chains, and aromatic rings offered comprehensive insights into the proton environments and molecular connectivity within the copolymers. The high conversion efficiencies (80–90%) and absence of residual monomer signals underscored the effectiveness of the free radical polymerization process, ensuring the purity and structural integrity of the materials.

A

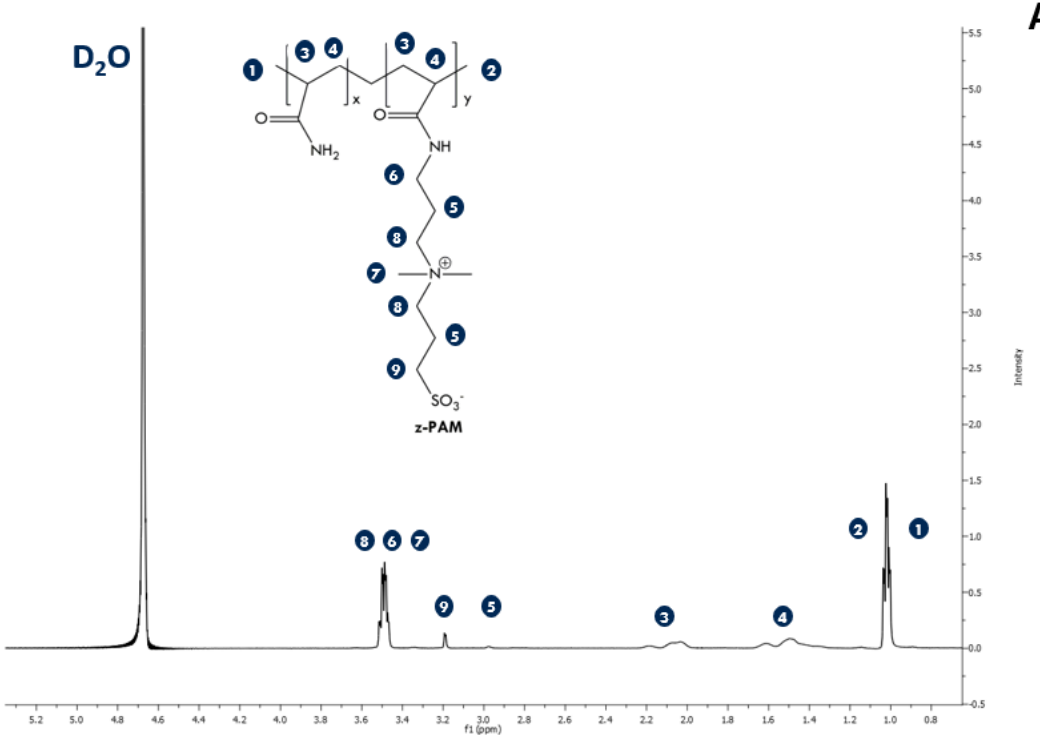

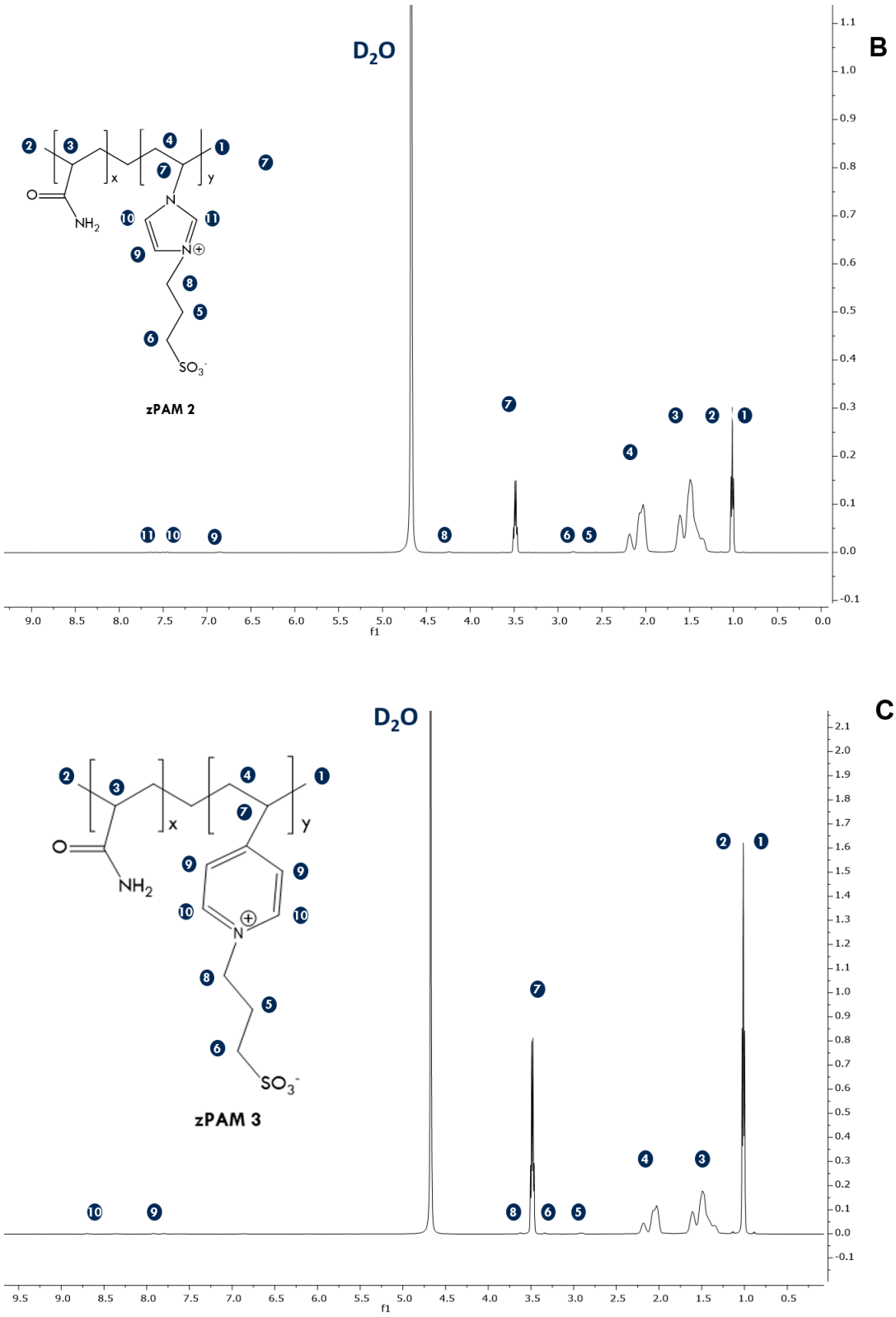

Figure 21. NMR Spectra of the zwitterionic polymers: (a) zPAM 1; (b) zPAM 2; (c) zPAM 3

4.3.3 Molecular weight determination

Dynamic Light Scattering (DLS), also known as photon correlation spectroscopy, was employed to determine the molecular weights of the synthesized zwitterionic polymers, providing critical insights into their hydrodynamic properties and size distributions in solution. DLS is a non-invasive technique that measures the time-dependent fluctuations in the intensity of scattered light caused by the Brownian motion of polymer molecules in a dilute solution. These fluctuations are analyzed through an autocorrelation function, which yields the diffusion coefficient (D) of the polymer molecules. The diffusion coefficient is subsequently used to estimate the hydrodynamic radius (Rh) via the Stokes-Einstein equation, and, in conjunction with mathematical models such as the Rayleigh equation, the molecular weight (Mw) of the polymer can be determined. This approach is particularly valuable for characterizing water-soluble polymers like zwitterionic copolymers, which exhibit complex interactions in high-salinity environments, as is the case in enhanced oil recovery (EOR) applications.

The Rayleigh equation allows for the determination of the intensity of light scattered by particles in solution and can be expressed as per Equation:

$$\frac{KC}{R_\theta} = \left(\frac{1}{M_w} + 2A_2C\right)P(\theta)$$

where, R(θ) represents the Rayleigh ratio, which denotes the ratio of scattered light to incident light in the sample. The equation incorporates the sample's molecular weight (M_w), concentration (C), the angular dependence of scattering intensity (P(θ)), the second virial coefficient (A_2), and the optical constant (K), which is defined using Equation 2:

$$K = \frac{4\pi^2}{\lambda_0^4 N_a}\left(n_0 \frac{dn}{dc}\right)^2$$

where N_a – Avoradro's constant, λ_0 is the laser wavelength, n_0 – solvent refractive index, $\frac{dn}{dc}$ is the differential refractive index.

The intensity versus concentration plot, often referred to as the Debye plot, is utilized alongside DLS analysis to determine the consistency of scattering behavior across different concentrations. This plot, generated by measuring the intensity at varying concentrations, facilitates the evaluation of concentration-dependent effects, such as changes in scattering efficiency or potential interactions between polymer molecules. This linear relationship suggests that the scattering efficiency remained relatively constant within the measured concentration range, with no significant aggregation or intermolecular interactions affecting the scattering behavior. Furthermore, the second virial coefficient can be determined by examining the gradient of the Debye plot.

According to Figure 22, there is a direct correlation between the concentration of the polymer solution and the intensity of scattered light. As the concentration increases, the intensity likewise increases proportionally, indicating that the scattering effect is directly influenced by the presence of polymer molecules in the solution. These findings suggest that the scattering efficiency remains relatively constant within the measured concentration range. However, it is important to emphasize that the direct determination of molecular weight relies on the rigorous analysis of DLS data and the application of appropriate models specific to the Zetasizer Nano ZS instrument. As a result, based on

the experimental data, the molecular weight of the zwitterionic polymer was estimated and is presented in Table 4.

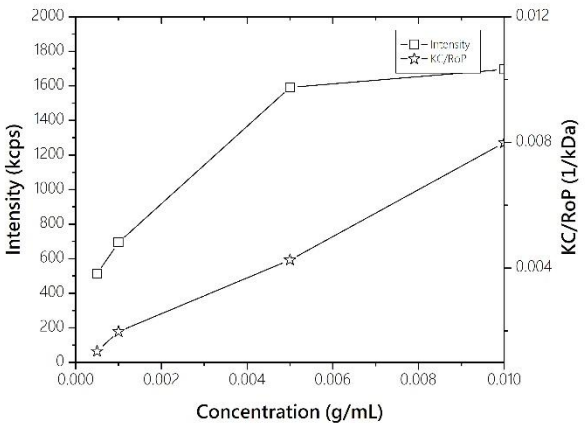

(a)

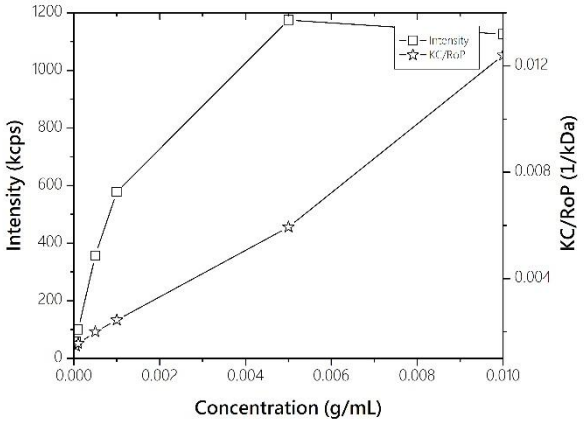

(b)

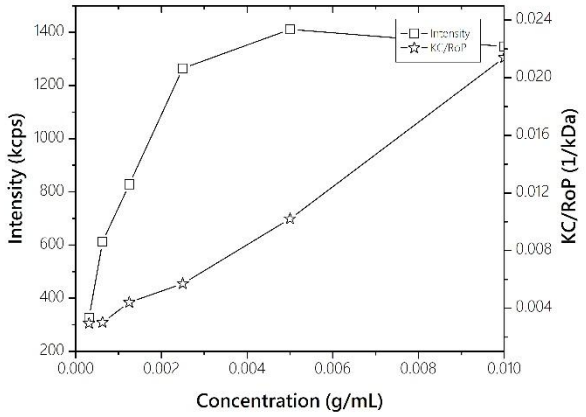

(c)

Figure 22. Debye plot: (a) zPAM 1; (b) zPAM 2; (c) zPAM 3

Table 4. Molecular weight determination of zwitterionic polymers.

Polymer	Molecular Weight (kDa)
zPAM 1	598 ± 110
zPAM 2	630 ± 78.5
zPAM 3	734 ± 165

The DLS analysis, supported by the Debye plot and Rayleigh scattering models, provided a robust method for determining the molecular weights of the zwitterionic polymers, offering valuable insights into their size and solution behavior. These molecular weight values are critical for understanding the polymers' rheological properties and performance in EOR applications, as higher molecular weights typically correlate with increased viscosity and improved mobility control in polymer flooding. The consistency of the scattering behavior across concentrations, combined with the detailed mathematical modeling, ensures the reliability of the molecular weight estimates for zwitterionic polymers. It is important to note that DLS provides an indirect estimation of molecular weight through hydrodynamic radius, derived from the diffusion coefficient. High-molecular-weight, flexible polymer coils such as zwitterionic copolymers exhibit broad size distributions, strong hydration shells, and non-spherical conformations, all of which increase the variability in DLS fitting models. Additionally, intensity-weighted analysis biases measurements toward larger species, contributing to higher uncertainty. For these reasons, DLS typically reports molecular weight values with ±15–25% variability for polymers in the 500–1000 kDA range, which is consistent with the observed error margins in this study (Birch & Schiffman, 2014).

4.3.4 SEM

Characterization of the zwitterionic polymers through scanning electron microscopy (SEM) revealed intriguing morphological features. The SEM images on Figure 23 provided valuable insights into the structural organization and surface topography of the polymers.

For zPAM 1 and zPAM 2, a highly ordered network structure with a compact pore size distribution was observed. This well-defined morphology suggests the presence of additional intermolecular electrostatic crosslinking, facilitated by the ion pairing of zwitterionic groups. The formation of such crosslinking interactions may contribute to the enhanced structural integrity and stability of the polymers. Furthermore, the observed hydrogen interactions within the zwitterionic groups likely facilitate the formation of the organized network structure, further enhancing the polymer's overall morphology.

The morphological analysis of zPAM 3 revealed a distinct absence of a well-defined cavity network structure. The presence of the imidazole ring in the polymer structure appears to hinder the formation of robust backbone connections, resulting in a reduced pore size network. This observation suggests that the incorporation of the imidazole ring affects the overall morphology and may impact the material's mechanical properties.

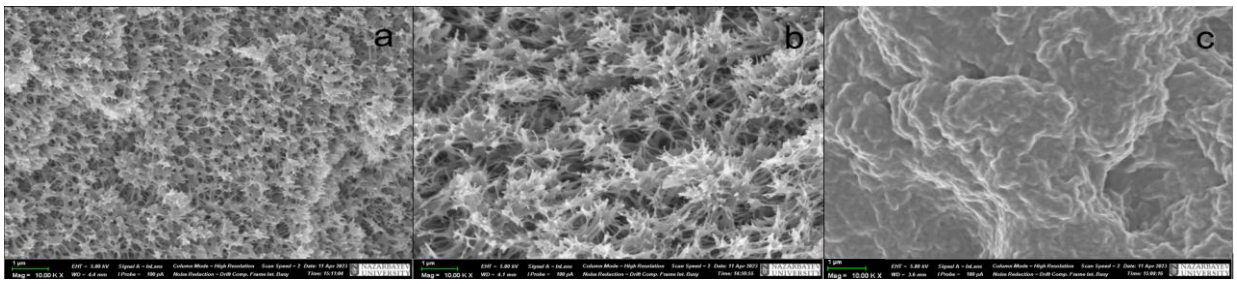

Figure 23. SEM analysis of the zwitterionic polymers at 10K X: (a) zPAM 1; (b) zPAM 2; (c) zPAM 3

The SEM characterization of the zwitterionic polymers provides valuable information about their structural organization and surface morphology. The observed variations in morphology among the different polymers indicate the influence of specific functional groups on the overall architecture of the materials. These insights into the morphological characteristics of the zwitterionic polymers pave the way for a deeper understanding of their potential applications and properties.

4.4 Conclusion

This chapter presented a comprehensive characterization of three zwitterionic copolymers through the application of FTIR, ^{1}H NMR, DLS, and SEM techniques. FTIR analysis confirmed the successful copolymerization by the disappearance of vinyl (C=C) groups and the retention of functional groups such as amide (N–H, C=O) and sulfonate (SO_3^-), characteristic of both acrylamide and the zwitterionic monomers. The ^{1}H NMR spectra provided complementary structural verification, demonstrating the successful incorporation of zwitterionic units and the absence of unreacted monomers, with chemical shifts and integrations aligning with the expected copolymer compositions.

DLS analysis yielded molecular weight estimates ranging from 598 to 734 kDa, with consistent scattering behavior across multiple concentrations, confirming the suitability of the polymers for EOR applications. These molecular weight values are in the desirable range for achieving high viscosity and effective mobility control in porous media. SEM analysis further revealed how the chemical composition of the zwitterionic moieties impacts the copolymer morphology. ZPAM 1 and zPAM 2 exhibited dense, organized pore networks, indicative of strong intermolecular interactions and possible electrostatic crosslinking. In contrast, zPAM 3 displayed a more disordered structure, influenced by the imidazole ring's effect on chain packing and hydrogen bonding.

Collectively, the results validate the successful synthesis and structural integration of zwitterionic group into acrylamide-based copolymers. The insights gained in this chapter form a crucial foundation for subsequent rheological experiments and coreflooding experiments under simulated reservoir conditions, which are discussed in the following chapters.

CHAPTER 5. RHEOLOGICAL PERFORMANCE OF ZWITTERIONIC COPOLYMERS

5.1 Introduction

The rheological behavior of polymers is a critical parameter in determining their suitability for EOR applications, particularly in challenging high-temperature, high-salinity environments. Building upon the synthesis and physicochemical characterization of the zwitterionic copolymers zPAM 1, zPAM 2, and zPAM 3, this chapter investigates their rheological performance in conditions simulating reservoir environments. The focus is on how polymer concentration, temperature, salinity, and long-term thermal exposure influence their apparent viscosity and structural integrity. These parameters are directly linked to polymer efficiency in controlling fluid mobility and improving sweep efficiency in porous media.

Typically, HPAM-based zwitterionic polymers exhibit Newtonian fluid behavior at low shear rates. Viscosity vs shear rate relationships were explored to assess flow behavior and non-Newtonian properties, while temperature ramp tests were conducted to understand viscosity sensitivity and degradation dynamics at high temperatures. Additionally, salt-tolerance experiments were designed to evaluate polymer performance in high salinity conditions, reflecting formation water compositions. Long-term thermal aging studies over a 60-day period provided further insights into polymer stability under sustained thermal stress, a key determinant of field applicability.

Collectively, this rheological assessment provides essential information on the flow characteristics, durability, and application potential of zwitterionic copolymers in oilfield polymer flooding operations.

5.2 Materials & Methods

The rheological characteristics of the zwitterionic polymers were evaluated using an Anton Paar MCR 301 Rheometer, as illustrated in Figure 24.

Figure 24. Anton Paar MCR 301 Rheometer

The polymer preparation followed the API guidelines to ensure consistency and adherence to the recommended standards. Detailed information on the preparation of the polymer solutions can be found in Figure 25. The precise amount of polymer required for each concentration was carefully weighed, as outlined in Table 5.

Table 5. Mass of polymer needed for polymer preparation.

Concentration of polymer	**1000ppm**	**2000ppm**	**3000pppm**
Mass of polymer	0.2g	0.4g	0.6g
Volume of water	200mL	200mL	200mL

A magnetic stirrer operating at a constant speed of 600 rpm was utilized to induce a vortex in the solution to ensure consistent and effective mixing. Careful attention was given to the addition of the polymer, as rapid introduction could lead to the formation of undesired large slugs or "fish-eyes." Fish-eyes are characterized as unhydrated particle granules that hinder the complete hydration process of polymers. Therefore, a gradual and controlled addition of the polymer, followed by stirring at a lower speed of 80 rpm, was deemed crucial to achieve complete dissolution of the polymer in water. Initially, the polymer was

dissolved in distilled water. However, when investigating the influence of salinity on polymer performance, adjustments were made to the water's salinity level accordingly.

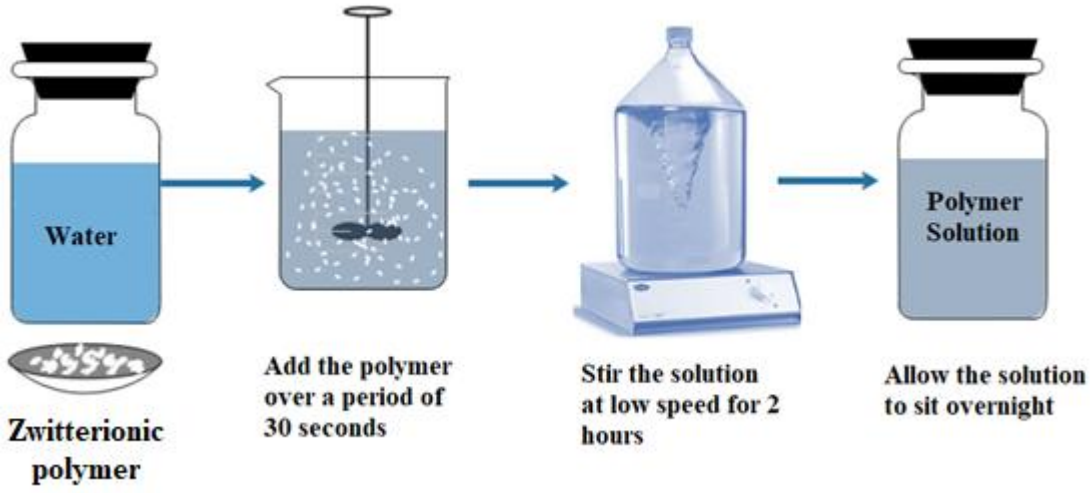

Figure 25. Polymer preparation process

Polymer solutions were initially dissolved in deionized water. However, for rheological tests involving salinity effects, the water salinity was adjusted precisely according to the required test conditions. Each polymer solution was prepared using the corresponding salt concentration prior to rheological measurement, ensuring accurate evaluation of polymer behavior under the intended test conditions.

5.3 Results & Discussion

5.3.1 Effect of concentration

Concentration plays a significant role in determining the viscosity of polymer solutions. In dilute solutions, where the polymer concentration is low, the viscosity is primarily governed by the interactions between the polymer chains and the solvent molecules. At low concentrations, the polymer chains are well-separated and experience minimal entanglement, resulting in lower viscosity. As the polymer concentration increases, the polymer chains start to interact with each other, leading to chain entanglements. This entanglement effect significantly increases the solution viscosity.

At even higher concentrations, the polymer chains can undergo further interactions, such as intermolecular interactions or physical cross-linking, leading to additional increases in

viscosity. In such cases, viscosity behavior can be influenced by other factors, such as the degree of polymerization, the flexibility of the polymer chains, and the presence of specific interactions, such as hydrogen bonding or electrostatic interactions, which are present in zwitterionic groups.

Each of the three zwitterionic copolymers displayed strong non-Newtonian flow properties, demonstrating evident shear thinning behavior at the specified concentration. Figure 26 presents a direct correlation between viscosity, concentration, and shear rate. In all instances, as the concentration increased, the viscosity of the polymer also increased, indicating that zPAM 2 exhibited the highest viscosity as both concentration and shear rate increased, surpassing the other two polymers.

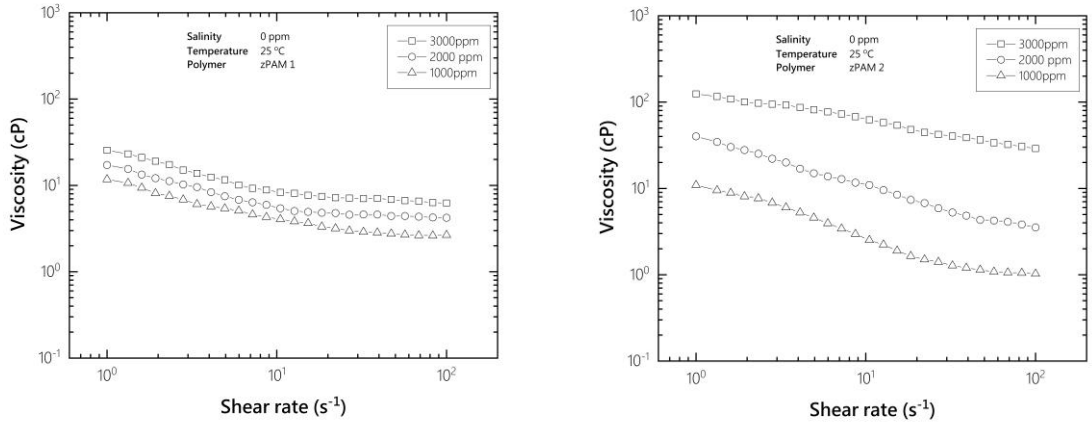

(a) (b)

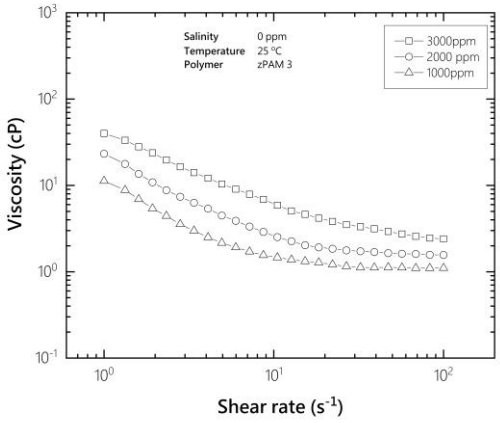

(c)

Figure 26. Viscosity vs shear rate for different polymer concentrations (a) zPAM 1; (b) zPAM 2; (c) zPAM 3

The differences observed among the three copolymers can be directly attributed to the chemical structure of their zwitterionic monomers. zPAM 2 exhibited the highest viscosity across all concentrations and shear rates, which may be explained by the presence of the aromatic pyridine ring in its zwitterionic moiety. Aromatic rings introduce additional rigidity to the polymer backbone and increase intermolecular interactions, resulting in more pronounced chain expansion (Song et al., 2024). The lower viscosity of zPAM 1 relative to aromatic zwitterionic polymer can be explained by fundamental differences in their molecular architecture and the nature of intermolecular interactions generated by their zwitterionic monomers. zPAM 1 contains the aliphatic sulfobetaine monomer DMAPMAPS, which is more flexible and mobile with weaker intermolecular associations. As a result, flexible polymer chains adopt more compact coil structures with lower hydrodynamic radius, which reduces solution viscosity (Israr et al., 2025).

Increasing polymer concentration enhances chain entanglement and zwitterionic interactions, while structural features of the zwitterionic monomers, including aromaticity, rigidity, and charge distribution, influence the magnitude of viscosity enhancement. These structure relationships help explain why zPAM 2 demonstrated superior viscosity performance across the tested conditions, affirming the importance of monomer selection in designing advanced polymers for high-salinity EOR applications.

5.3.2 Effect of temperature

Temperature is a critical parameter influencing the rheological properties of polymers, particularly their viscosity, which directly affects their flow behavior and performance. The viscosity of a polymer solution is governed by a complex interplay of factors, including the polymer's molecular structure and intermolecular interactions. In general, an increase in temperature leads to a decrease in polymer viscosity, a phenomenon driven by the enhanced thermal energy. This thermal energy disrupts intermolecular forces, such as van der Waals interactions and hydrogen bonds that maintain the polymer's coiled or entangled structure in solution. As a result, the polymer chains gain increased mobility, reducing the resistance to flow and thereby lowering the solution's viscosity. This behavior is particularly evident in water-soluble polymers like zwitterionic copolymers, where the solvent-polymer interactions are heavily influenced by temperature-induced changes in chain conformation and solvation dynamics (Jing et al., 2025).

In the context of the presented study, the viscosity measurements of three zwitterionic copolymers were conducted under different temperature conditions. Notably, the viscosity of all the polymers exhibited a significant decrease as temperature was elevated, from 25 to 80 degC, as shown in Figure 27. To evaluate and compare the polymers' performance under high-temperature conditions, the degradation factor was employed as a reliable measure of polymer stability. It is calculated using the equation below, by comparing the testing viscosity (μ_{test}) with the initial viscosity (μ_{ref}) in the solution:

$$Degradation\ factor = \left|\frac{\mu_{test} - \mu_{ref}}{\mu_{ref}}\right| * 100\%$$

The measurements were specifically conducted at a shear rate of approximately $10s^{-1}$, which closely corresponds to $7.3s^{-1}$ (Ilyasov et al., 2021) This shear-rate range is representative of the hydrodynamic environment experienced by polymer solutions through injection pipelines and within reservoir porous media. Selecting this shear rate ensures that the measured viscosities accurately reflect field-relevant conditions while minimizing mechanical degradation effects, thereby enabling direct comparison with the coreflooding experiments and reliable incorporation into numerical simulations

Based on the degradation factor analysis, as depicted in Figure 28, it was observed that zPAM 1 exhibited the highest temperature stability, demonstrating the least decrease in viscosity compared to the other polymers. In contrast, zPAM 2 and 3 demonstrated the highest level of thermal degradation, with a substantial decline in viscosity beyond 40°C.

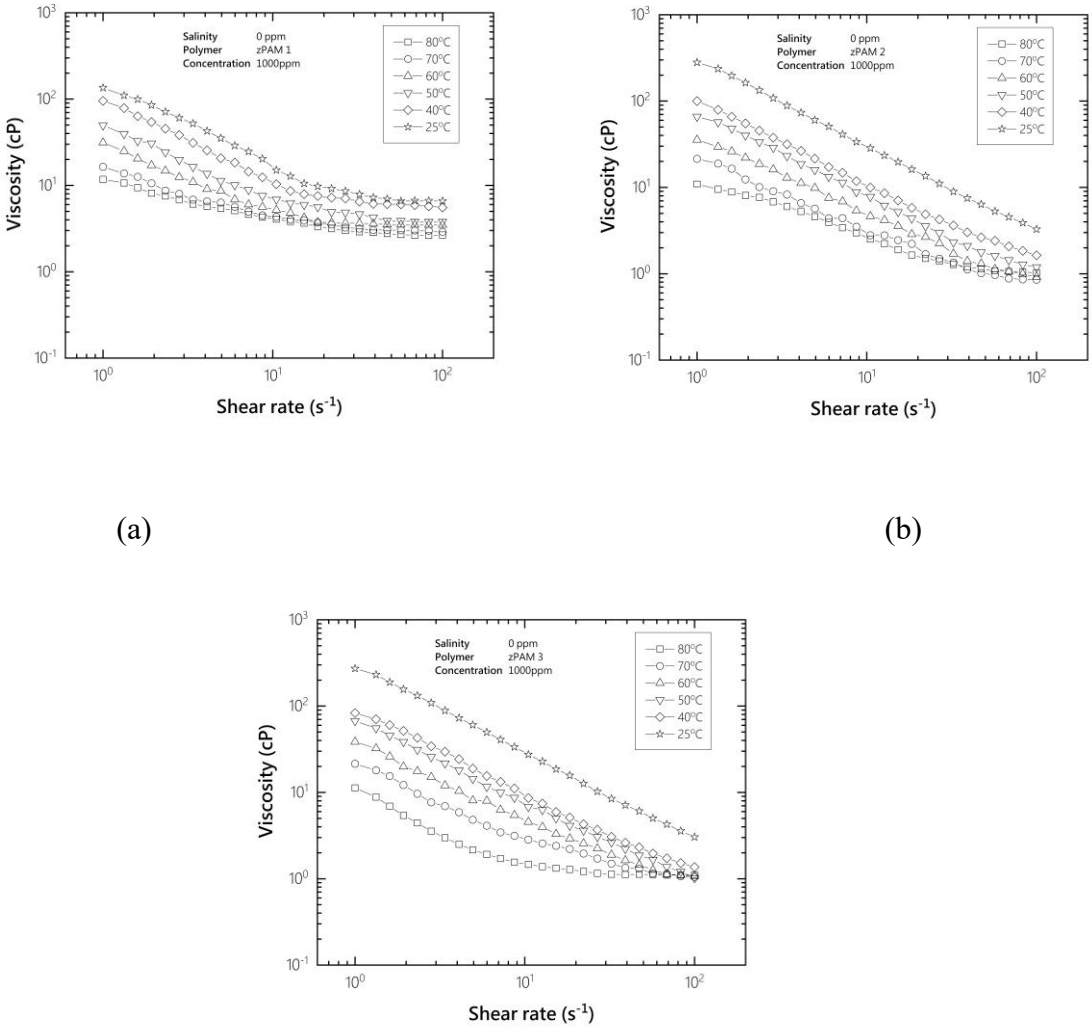

(a) (b)

(c)

Figure 27. Viscosity vs shear rate for different temperature conditions (a) zPAM 1; (b) zPAM 2; (c) zPAM 3

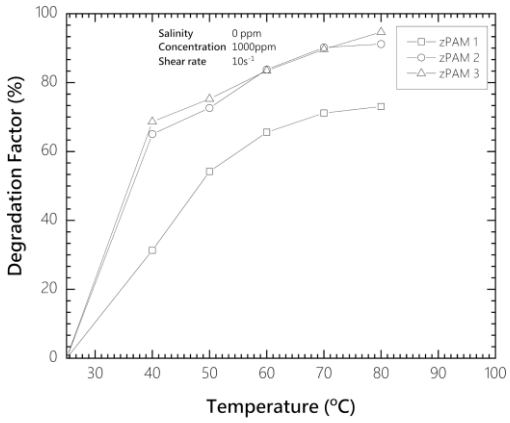

Figure 28. Thermal degradation factor estimation for zwitterionic polymers

The thermal degradation trends further clarify the relative thermal robustness of zPAM 1, zPAM 2, and zPAM 3. Although zPAM 2 consistently exhibits the highest viscosity across all temperatures, its viscosity loss with increasing temperature is the most pronounced among the three materials. Between 25°C and 80°C, zPAM 2 undergoes more than 70% viscosity degradation, indicating that despite its highly interconnected microstructure and strong electrostatic interactions, the polymer network becomes substantially destabilized under high thermal stress. In contrast, zPAM 1 shows a comparatively lower degradation of about 65% over the same temperature interval, even though its absolute viscosity values remain lower than those of zPAM 2. This suggests that the aliphatic zwitterionic unit in zPAM 1, while forming a less viscous network at ambient conditions, may maintain a relatively more stable chain configuration at elevated temperatures (Du et al., 2024).

Overall, these results demonstrate that viscosity magnitude alone is not sufficient for selecting polymers for enhanced oil recovery. Instead, the ability of a polymer to retain viscosity under reservoir-relevant temperatures is a more reliable predictor of field performance

5.3.3 Effect of salinity

Zwitterionic polymers possess a distinctive molecular architecture characterized by the coexistence of positively and negatively charged functional groups. As a consequence of

this unique feature, these polymers exhibit remarkable sensitivity to variations in the ionic environment, particularly concerning changes in the salinity of the surrounding solution. The electrostatic interactions between the charged groups and the surrounding ions play a fundamental role in shaping the conformation and interactions of the zwitterionic polymers within the solution.

Thus, to understand the effect of salinity and in the pursuit of replicating the formation conditions observed in oil-bearing reservoirs, an extensive series of rheological experiments were meticulously performed on three distinct zwitterionic copolymers. The experiments involved subjecting these polymers to varying salinity levels to imitate the diverse conditions encountered in reservoir environments. A stock solution of synthetic brine with an initial salinity of 203 * 10^4 ppm was prepared, followed by the dilutions to attain salinity levels of 101.5 * 10^4 ppm, respectively to represent the condition of Uzen oilfield formation water (Sokolova et al., 2021). The ion composition of synthetic brine is shown in Table 6.

Table 6. Synthetic Brine Composition.

Salts	Formation water (FW) (g/L)	0.5 * FW (g/L)
NaCl	106.76	53.38
$CaCl_2 * 2H_2O$	128.35	64.18
Total Salinity	203	101.5

Figure 29 illustrates a comprehensive investigation into the apparent viscosity variations for different zwitterionic polymers at varying salinity levels. The experimental conditions include a fixed polymer concentration of 1000 ppm and a temperature of 60°C. It should be noted that all studied zwitterionic copolymers showed a consistent and noteworthy trend of higher viscosity with increasing salinity.

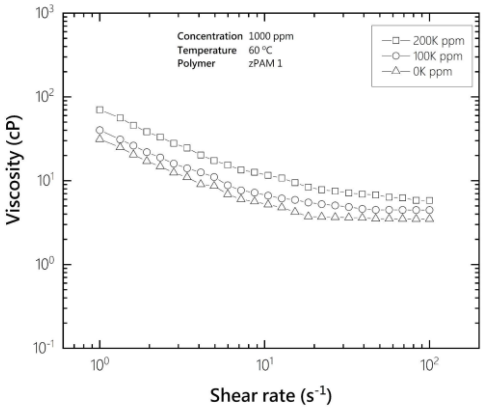

(a)

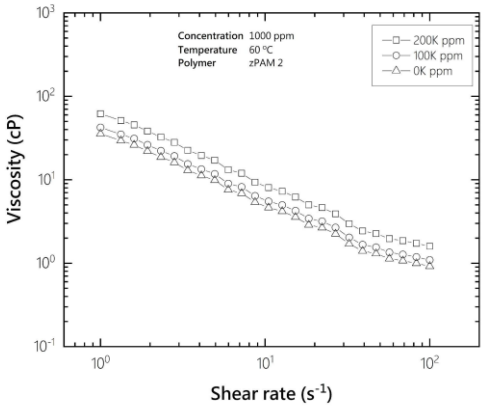

(b)

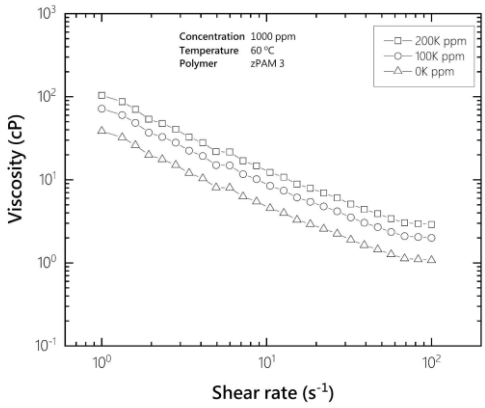

(c)

Figure 29. Zwitterionic polymer viscosity change with the salinity (a) zPAM 1; (b) zPAM 2; (c) zPAM 3

The observed salinity-driven effects on zwitterionic polymer viscosity are governed by different mechanisms. These encompass the intricate interplay of ion-polymer interactions, consequential conformational changes in the polymer chains, as well as the complex "salting-in" and "salting-out" phenomena (Lu et al., 2021). Such intricate processes collectively influence the polymer's overall conformation and behavior in response to varying salinity conditions, thus significantly affecting their viscosity profiles.

Upon an increase in salinity, the presence of ions in the solution serves to screen the charges on the zwitterionic polymer, leading to competitive interactions between ions and water molecules for association with the charged groups. This, in turn, exerts a profound influence on the polymer's solvation and conformation. The nature and charge density of the ions significantly dictate the extent and character of these interactions. Furthermore, the shielding effect of ions diminishes the repulsive forces between charged groups, resulting in a more extended conformation adopted by the polymer chains. Subsequently, this extended conformation fosters increased chain entanglements, resulting in reduced chain mobility and an elevation in solution viscosity.

In addition, depending on the specific nature of the zwitterionic polymer and the particular ionic environment, an escalation in salinity may elicit either a "salting-in" effect or a "salting-out" effect. The "salting-in" effect manifests when the added ions strengthen the interactions between the polymer and water molecules, consequently promoting improved solvation and a reduction in viscosity. Conversely, the "salting-out" effect arises when ions weaken the interactions between the polymer and water, instigating polymer aggregation and precipitation, thereby leading to an increase in the solution's viscosity (Lu et al., 2021).

5.3.4 Long term thermal degradation

The thermal stability of the zwitterionic polymers was evaluated through a long-term thermal degradation test to assess their durability under conditions mimicking reservoir environments, a critical factor for their application in enhanced oil recovery. In EOR, polymers are used to increase the viscosity of injected water, thereby improving sweep efficiency and enhancing oil displacement within the reservoir. However, prolonged exposure to elevated temperatures, as often encountered in reservoir conditions, can lead to thermal degradation, resulting in viscosity loss and diminished performance. Thus, long term thermal degradation test was designed to replicate the thermal stresses experienced in a reservoir, providing valuable insights into the long-term viability and stability of the synthesized zwitterionic copolymers under field-relevant conditions. The

test has been performed for 60 days, allowing for a comprehensive analysis of degradation trends over an extended period. The prepared polyme solutions were transferred into sealed glass vials to prevent evaporation and oxidative contamination, as both factors can influence polymer stability. These vials were subsequently placed inside a temperature-controlled oven set to the predetermined reservoir temperature of 63 °C, which corresponds to the characteristic temperature of the Uzen oilfield. The oven provided a stable thermal environment with minimal fluctuations, allowing the polymer solutions to experience continuous thermal exposure comparable to in-situ reservoir conditions. Throughout the 60-day degradation period, the vials were periodically withdrawn at scheduled intervals to assess the extent of viscosity loss.

Figure 30 illustrates the viscosity profiles of the zwitterionic copolymers over the 60-day aging period. All three polymers exhibited a noticeable decline in viscosity, with the most significant reduction occurring within the first 10 days of aging. By day 10, zPAM 1's viscosity decreased to approximately 40% for zPAM 1, and 60% for zPAM 2 and 3, respectively, from their initial values. This rapid initial decline is attributed to the thermal cleavage of weaker intermolecular interactions, such as hydrogen bonds between the amide groups and water molecules, as well as potential hydrolysis of the acrylamide backbone under prolonged thermal stress. After the initial 10 days, the viscosity loss rate slowed, and by day 60, the viscosities stabilized. The final viscosity reductions were 43%, 61%, and 62%, respectively, highlighting zPAM 1's superior resistance to thermal degradation compared to zPAM 2 and zPAM 3. The superior performance of zPAM 1 is likely due to its DMAPMAPS-based zwitterionic structure, which facilitates stronger electrostatic crosslinking and chain rigidity, mitigating the effects of thermal degradation. In contrast, the pyridine (SBVP in zPAM 2) and imidazole (SBVI in zPAM 3) rings may introduce steric hindrance or electronic effects that make the polymer chains more susceptible to thermal breakdown, despite their higher molecular weights (Du et al., 2024).

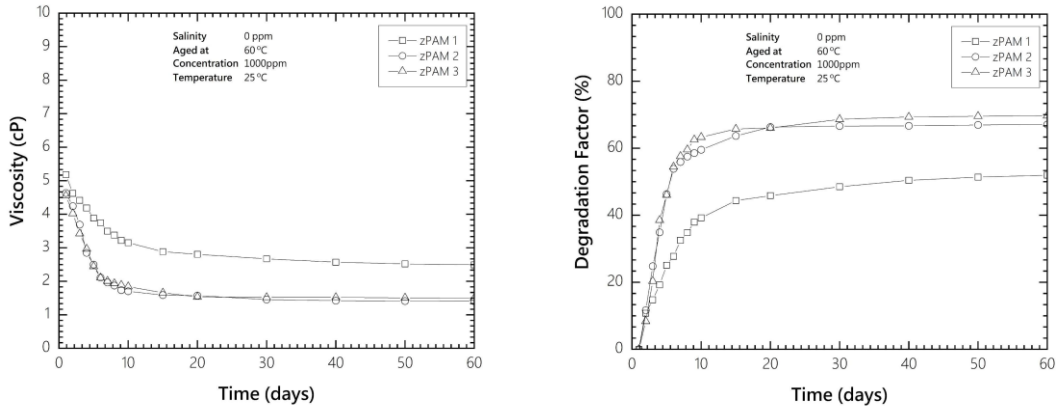

(a) (b)

Figure 30. Long term thermal degradation for zwitterionic polymers (a) relative viscosity degradation (b) degradation factor

The long-term thermal degradation test provided critical insights into the stability of zPAM 1, zPAM 2, and zPAM 3 under moderate-temperature conditions, with zPAM 1 emerging as the most thermally stable candidate, retaining 57% of its initial viscosity after 60 days at 60°C. This stability is particularly advantageous for EOR applications in low-salinity, moderate-temperature reservoirs, where maintaining viscosity over extended periods is essential for effective mobility control and sweep efficiency. The rapid initial degradation observed across all polymers highlights the need for careful consideration of aging effects during field implementation, potentially necessitating the use of thermal stabilizers or optimized injection strategies to mitigate early viscosity loss. The plateau in degradation after 10 days suggests that the zwitterionic copolymers reach a stable conformation under prolonged thermal stress.

5.4 Conclusions

This chapter comprehensively examined the rheological performance of zwitterionic copolymers, zPAM 1, zPAM 2, and zPAM 3, under conditions relevant to enhanced oil recovery. The findings highlight key differences in viscosity response and thermal behavior among the three copolymers, shedding light on how polymer structure influences field performance. Following a thorough rheological experiments covering concentration, temperature, and salinity, it was found that among the three zwitterionic

polymers studied, zPAM 1 performed the best in enhancing viscosity under harsh conditions. This performance is attributed to its extended zwitterionic linear chain structure, which leads to enhanced interactions and entanglements, resulting in significant viscosity enhancement even under challenging environmental conditions. These findings highlight the importance of molecular design and chain structure in influencing the rheological behavior of zwitterionic polymers, especially for EOR applications. This underscores the critical role of the zwitterionic copolymer's structural composition and charge distribution in determining its viscosity response to the ionic environment. The insights gained from rheological experiments contribute to a better understanding of zwitterionic polymers' behavior under varying salinity conditions, with potential implications for enhanced oil recovery applications. Based on rheological screening experiments, zPAM 1 has been selected for further investigation in coreflooding analysis.

CHAPTER 6. EVALUATION OF ZWITTERIONIC POLYMER PERFORMANCE THROUGH COREFLOODING EXPERIMENT

6.1 Introduction

This chapter presents a comprehensive evaluation of the EOR performance of the newly developed zwitterionic copolymer zPAM 1, comparing with conventional HPAM under Uzen oilfield conditions (63°C, 200,000 ppm salinity) (Sokolova et al., 2021) . Conducted using a state-of-the-art CFS-700 coreflooding apparatus, these experiments aimed to quantify oil recovery efficiency, assess mobility control, and analyze pressure dynamics, providing critical insights into the polymers' applicability for EOR in challenging high-salinity, high-temperature environments. The experimental procedure was organized to ensure precision, reproducibility, and alignment with industry-standard practices, encompassing a series of preparatory steps, waterflooding, polymer flooding, and postflush phases.

Key performance indicators such as recovery factor**,** pressure drop behavior**,** resistance factor**,** and residual resistance factor were measured and compared. These experiments aimed not only to quantify incremental oil recovery but also to understand the dynamic interactions between polymer solutions and the porous rock matrix, thereby providing insight into the mechanisms driving improved sweep efficiency and mobility control.

6.2 Materials & Methods

For coreflooding experiments, crude oil sourced from the Uzen oilfield was utilized, characterized by a viscosity of 8 cP and a density of 787.05 kg/m^3 at the reservoir temperature of 63°C. This crude oil, classified as heavy oil due to its high asphaltene (13 wt.%) and paraffin (20 wt.%) content, was filtered prior to testing to remove mineral and rock particulates, ensuring experimental accuracy. Before filtration, the crude oil was preheated to 60 °C to reduce its viscosity and facilitate flow. Oil was then passed through a vacuum filtration unit equipped with a Büchner funnel and membrane filter. Fresh filters were used whenever a noticeable reduction in filtration rate was observed to ensure consistent removal of suspended solids. The filtrate was collected in clean, dry glass bottles, allowed to equilibrate to ambient temperature, and then stored in tightly sealed,

nitrogen-blanketed containers until use in coreflooding experiments. This procedure ensured that the crude oil used for flooding was free of visible particulates and suitable for reproducible displacement tests.

Berea sandstone core samples were employed for the coreflooding experiments, selected for their representative petrophysical properties. The core dimensions (length and diameter) were measured using a calibrated digital Vernier caliper with a precision of ±0.01 mm. Porosity was calculated using the measured pore volume and bulk volume (determined from core dimensions). Absolute permeability was measured using a steady-state flow test conducted on a coreflooding system, using Darcy's law. The physical characteristics of the core samples are detailed in Table 7, including length, diameter, pore volume (PV), porosity, and permeability, which were critical for simulating reservoir conditions and evaluating polymer flooding performance.

Table 7. Physical properties of the core samples used for coreflooding experiment.

	Sample ID	Length (cm)	Diameter (cm)	PV (cm3)	Porosity (%)	Permeability (mD)
Core #1	1	7.70	3.81	18.75	21.47	55.1
Core #2	2	7.80	3.81	18.75	21.19	53.5

Coreflooding experiments were conducted to validate the ability to enhance oil recovery under simulated reservoir conditions. CFS-700 core flooding apparatus by Vinci Technologies was used to perform experiments. The schematic of CFS-700 is shown in Figure 31.

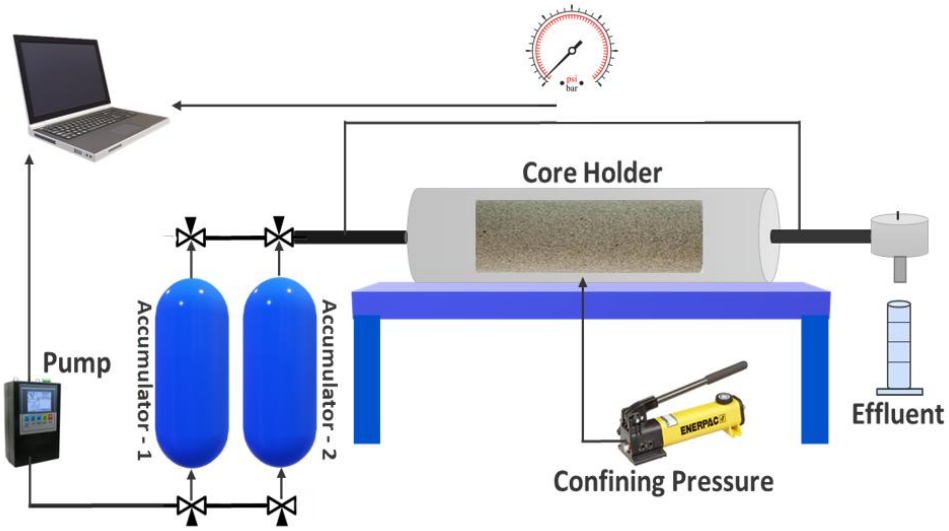

Figure 31. The schematic of coreflooding apparatus CFS-700.

Preceding the coreflooding experiments, the cores were saturated manually with the formation water using a vacuum saturator. Subsequently, the pore volume was determined using the equation below:

$$PV = \frac{W_{wet} - W_{dry}}{\rho_{FW}}$$

where W_{dry} is the dry weight of the core, W_{wet} is the wet weight of the core after saturation, and ρ_{FW} is the density of the formation water.

Following this, the absolute permeability of the cores was calculated by injecting formation water at various rates. To simulate a field condition, the coreflooding system was adjusted to reservoir conditions, maintaining the temperature of 63°C and a confining pressure of 1000 psi. Oil saturation was then achieved by the injection of oil into the cores at different flow rates, ranging from 1.0 cm^3/min to 2.0 cm^3/min, until the effluent oil cut reached 99% and stabilized pressured drop across the core sample was obtained. Increasing injection rates facilitated the mitigation of capillary end effects and helped to obtain initial water saturation (Swi) in the core. The effluent produced water was used to calculate Swi as per Equation:

$$S_{wi} = \frac{PV - V_w}{PV} \times 100$$

where V_w is the water volume collected in effluents, PV is the pore volume of the core.

Prior to conducting the experiments, polymer solutions (1000 ppm) were prepared using simulated formation water as per API guidelines. Subsequently, waterflooding was carried out at different rates (1.0 cm^3/min, 1.5 cm^3/min and 2 cm^3/min). The water flooding was preceded by polymer flooding and the same procedure has been implemented with two pore volumes for each flow rate. The volume of oil produced during both waterflooding, and polymer flooding was used to calculate the total recovery factor and EOR ability using Equations:

$$Recovery\ factor = \frac{V_{oi} - V_o}{V_{oi}} * 100$$

where V_{oi} is the original oil in place (OOIP) and V_o is the volume of oil produced by waterflooding and polymer flooding.

$$EOR\ Ability = RF_{pf} - RF_{wf}$$

where RF_{pf} is oil recovery after the polymer flooding and RF_{wf} is the oil recovery after the waterflooding.

The mobility control ability of the polymers is characterized by the resistance factor (RF) and the residual resistance factor (RRF). Following the end of polymer flooding, core samples were postflushed with the formation water to obtain pressure drop after each flow rate, employing the same procedures as for displacement experiments. The RF and RFF were calculated using Equations:

$$Resistance\ Factor\ (RF) = \frac{\Delta p_{PF}/Q_{PF}}{\Delta p_{WF}/Q_{WF}}$$

$$Residual\ Resistance\ Factor\ (RRF) = \frac{\Delta p_{WF}/Q_{WF}}{\Delta p_{postflush}/Q_{postflush}}$$

where Δp_{PF}, Δp_{WF} $\Delta p_{postflush}$ are the pressure drop during polymer flooding, waterflooding, and postflush; $Q_{PF}, Q_{WF}, Q_{postflush}$ are the injecting rates during each stage.

6.3 Results & Discussion

Initially, Berea sandstone core samples, characterized by consistent petrophysical properties mentioned in Table 7, were first saturated with synthetic formation water. This

saturation was achieved using a vacuum saturator to ensure complete pore space saturation. Absolute permeability was determined by injecting formation water at incrementally increasing flow rates (0.5, 1.0, 1.5, and 2.0 cm^3/min) while monitoring the pressure drop across the core using high-precision differential pressure transducers. Permeability was calculated using Darcy's law, establishing a robust baseline for the cores' hydraulic properties and ensuring their suitability for subsequent flooding experiments:

$$k = \frac{Q * \mu * L}{A * \Delta P}$$

where k is absolute permeability (mD), Q is the volumetric flow rate of injected fluid (cm^3/min), μ is viscosity of the injected fluid (cP), L is the core length (cm), A is the cross-section area of the core (cm^2), ΔP is the stabilized pressure drop across the core (psi).

Following water saturation, the cores were saturated with filtered crude oil from the Uzen oilfield, which was pretreated to remove mineral and rock particulates to prevent clogging or interference during testing. Oil injection was performed at flow rates ranging from 1.0 to 2.0 cm^3/min, incrementally increased to mitigate capillary end effects, until the effluent oil cut reached 99% and a stable pressure drop was recorded, indicating near-complete oil saturation. The volume of water displaced during this process was collected and measured to calculate residual water saturation. This step ensured the cores accurately replicated reservoir conditions with established initial oil saturation, critical for evaluating subsequent recovery processes.

The waterflooding phase simulated primary recovery and aimed to establish residual oil saturation after waterflooding. Two pore volumes of formation water were injected at three distinct flow rates (1.0, 1.5, and 2.0 cm^3/min) to ensure thorough displacement and minimize capillary end effects, which can affect recovery measurements on a core-scale level. Each of these flow rates corresponds to a characteristic shear rate within the porous medium. These values closely match the shear rates (~10 s^{-1}) used in the rheological measurements, ensuring consistency between rheology testing and in-core hydrodynamic

conditions. Therefore, the polymer flow behavior observed in the coreflooding experiments is representative of the shear environment expected under reservoir injection scenario. The injection was performed under a confining pressure of 1000 psi to replicate reservoir stress conditions, with the system maintained at 63°C using a temperature-controlled oven. The volume of oil produced was carefully quantified using graduated tubes, and the recovery factor was calculated relative to the original oil in place (OOIP). Pressure drop data were continuously recorded to monitor flow dynamics and ensure stable displacement behavior.

Polymer flooding was conducted to assess the EOR potential of zPAM 1 and HPAM. Two pore volumes of polymer solution were injected at the same flow rates as waterflooding (1.0, 1.5, and 2.0 cm^3/min) to evaluate the polymers' ability to displace residual oil trapped after waterflooding. The oil recovered during this phase was measured to determine the incremental recovery factor and total EOR performance. Pressure drop data were recorded to analyze the polymers' mobility control, with higher pressure drops indicating stronger interactions with the porous medium and enhanced sweep efficiency.

Following these stages, a postflush with formation water was performed to remove residual polymer from the core and collect additional pressure drop data, enabling the calculation of the resistance factor and residual resistance factor, which quantify the polymers' ability to reduce water mobility and enhance oil displacement.

The results of the coreflooding experiments revealed significant performance differences between zPAM 1 and HPAM. During the waterflooding phase, zPAM 1 achieved a recovery factor of 43.2% of OOIP, surpassing HPAM's 41%, indicating zPAM 1's superior initial displacement efficiency, likely due to its enhanced viscosity and interaction with the core matrix. In the polymer flooding phase, zPAM 1 recovered an additional 13.3% of oil, resulting in a total recovery factor of 56.5%, compared to HPAM's additional 11.3% and total recovery of 52.3%. Although the present study did not include replicate corefloods for statistical averaging, the experimental setup,

measurement precision, and equipment calibration allow for a reasonable assessment of the expected error range based on standard industry practice. All main operational parameters, such as injection rate, pressure, and temperature, were controlled using calibrated coreflooding equipment. Given these controls, the most realistic source of experimental error arises from the use of graduated glassware for quantifying produced oil and water volumes. The collection cylinders employed in this study have a resolution of 0.1 mL, which introduces a small but unavoidable margin of error when reading liquid levels, particularly during late-stage production when incremental oil volumes become very small. Based on the obtained results, shown in Table 8, zPAM 1 mobilized a greater volume of residual oil, attributed to its robust rheological properties and salinity tolerance, as confirmed by prior rheological experiments.

Based on Figure 32, during the initial waterflooding stage, both curves demonstrate a rapid increase in recovery factor at early PV injection, corresponding to the displacement of easily mobilized oil. HPAM, on Figure 32A, exhibits an early recovery of approximately 20% OOIP within the first PV, after which the slope progressively decreases, indicating the transition toward residual oil conditions. zPAM 1, on Figure 32B, follows a similar trend but yields a slightly higher recovery during waterflooding stage (43.2% vs. 41.0% for HPAM). The pressure drop profiles further clarify these behaviours. During waterflooding, both HPAM and zPAM 1 maintain relatively low pressure drops, consistent with low-viscosity brine injection.

Polymer flooding shows the most distinct contrast between the two polymers. In both experiments, injection begins at 1.0 cm^3/min, subsequently increasing to 1.5 and 2.0 cm^3/min. The pressure drop rises sharply in both cases due to the substitution of low-viscosity water with significantly more viscous polymer solutions. For HPAM, this pressure rise is moderate and stabilizes relatively quickly, consistent with HPAM's lower viscosity under high salinity and temperature. In contrast, zPAM 1 produces a substantially higher and more sustained pressure drop, reflecting superior viscosity and stronger resistance to flow, which directly enhances mobility control. This enhanced pressure is consistent with the zwitterionic structure of zPAM 1, which maintains chain

expansion and shear stability in high salinity. Correspondingly, the incremental oil recovery during polymer flooding reflects this contrast. HPAM mobilizes an additional 11.3% OOIP, whereas zPAM 1 mobilizes 13.3%, resulting in a markedly higher total recovery for zPAM 1 (56.5% vs. 52.3%). The higher incremental recovery indicates better sweep efficiency and reduced viscous fingering, driven by the higher viscosity and improved viscoelastic properties of zPAM 1.

A detailed comparative analysis, as depicted in Figure 32, highlighted zPAM 1's superior performance across all phases. The higher recovery factors in both waterflooding and polymer flooding demonstrated zPAM 1's enhanced oil displacement capabilities, driven by its molecular design, which facilitates stronger chain entanglement and viscosity retention under high-salinity conditions. Notably, zPAM 1 exhibited significantly higher pressure drops during the postflush phase, indicating stronger mobility control and more effective interaction with the porous medium. This elevated pressure drop resulted into improved sweep efficiency, enabling zPAM 1 to contact a larger portion of the oil-bearing zones within the core, thereby enhancing overall oil recovery. The pressure drop data further revealed that zPAM 1's interaction with the core matrix resulted in a more uniform displacement front, reducing viscous fingering and bypassing, which are common challenges in HPAM flooding.

The superior performance of zPAM 1 can be attributed to its zwitterionic structure, which leverages the "salting-in" effect and electrostatic crosslinking to maintain viscosity and structural integrity in the presence of high salinity and divalent ions (Ca^{2+}, Mg^{2+}). In contrast, HPAM's sensitivity to salinity and thermal degradation limited its effectiveness, as evidenced by its lower recovery factors and reduced pressure drops. These findings validate zPAM 1's potential as a next-generation polymer for EOR, particularly in harsh reservoir environments where conventional polymers falter.

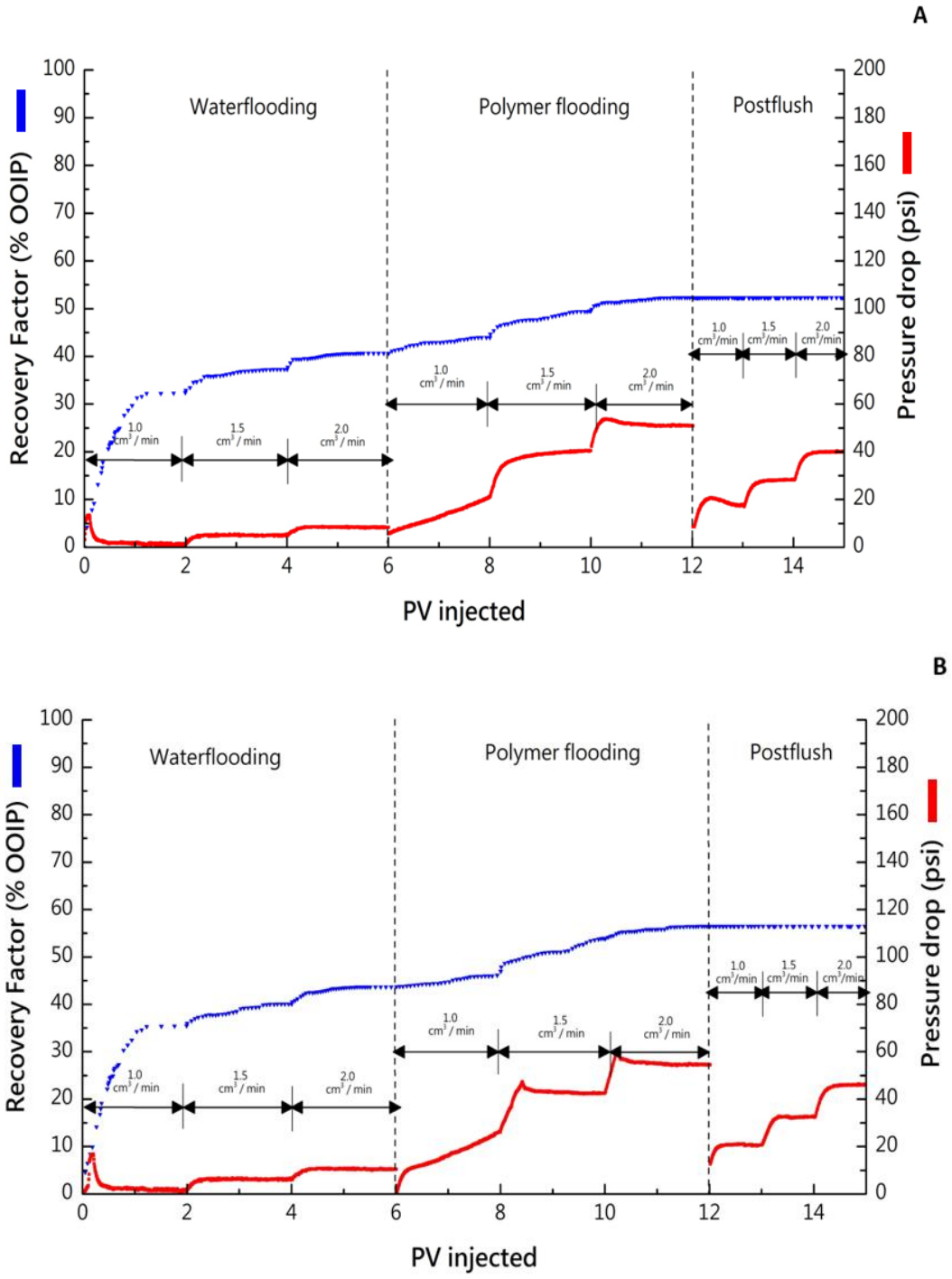

Figure 32. Recovery factor and pressure drop during coreflooding experiment (a) HPAM; (b) zPAM 1

Table 8. Summary of coreflooding experiment for HPAM and zPAM 1

Polymer	Recovery Factor (%OOIP)		Total Recovery Factor (%OOIP)	Resistance Factor	Residual Resistance Factor
	Waterflooding	Polymer flooding			
HPAM	41.0	11.3	52.3	6.0	0.21
zPAM 1	43.2	13.3	56.5	5.2	0.23

It is important to note that the capillary number, which quantifies the balance between viscous and capillary forces and is often used to interpret microscopic displacement efficiency, was not evaluated within the scope of this study. The primary focus of the present work was on macroscopic recovery behavior, specifically, oil displacement efficiency, pressure response, and mobility control under high-salinity conditions. Future work may incorporate capillary number calculations to further interpret the microscopic displacement mechanisms associated with zwitterionic polymer flooding.

6.4 Conclusion

The coreflooding experiments presented in this chapter clearly demonstrate the superior performance of the zwitterionic copolymer zPAM 1 over conventional HPAM in high-temperature, high-salinity conditions representative of the Uzen oilfield. zPAM 1 consistently outperformed HPAM during polymer flooding phases, yielding higher recovery factors and more favorable pressure responses.

During the waterflooding phase, zPAM 1 achieved a recovery factor of 43.2% of OOIP, slightly surpassing HPAM's 41.0%, suggesting improved initial displacement behavior possibly due to better core–polymer interaction. More significantly, during the polymer flooding phase, zPAM 1 recovered an additional 13.3% of oil, bringing the total to 56.5%,

while HPAM added only 11.3%, resulting in a lower total recovery of 52.3%. These results underscore zPAM 1's enhanced ability to mobilize residual oil post waterflooding.

The pressure drop and postflush data further confirmed zPAM 1's enhanced mobility control capabilities. Its higher resistance factor and residual resistance factor values indicate stronger interactions with the porous media and a more uniform displacement front, effectively reducing viscous fingering and bypassing. These outcomes are attributed to the unique zwitterionic structure of zPAM 1, which promotes better viscosity retention and sweep efficiency under harsh salinity conditions.

Moreover, zPAM 1 exhibited greater pressure buildup and sustained flow resistance during the postflush phase, reinforcing its role in improving areal and vertical conformance during EOR. In contrast, HPAM's performance was constrained by its known sensitivity to salinity and temperature, which led to lower displacement efficiency and weaker flow resistance.

In conclusion, the coreflooding results validate the practical advantages of zwitterionic polymers like zPAM 1 for field-scale polymer flooding applications in high-salinity, high-temperature reservoirs. To further validate and generalize the coreflooding findings**,** the next chapter presents a numerical simulation study, integrating the experimental results into a reservoir modeling framework. The simulation compares the displacement efficiency, sweep profile, and oil recovery behavior of zPAM 1 and HPAM under reservoir-scale conditions. This combined experimental and computational approach enhances the predictive reliability of polymer flooding performance and supports the scaling-up of zwitterionic polymers for field applications.

CHAPTER 7. COMPARATIVE ANALYSIS OF COREFLOODING AND NUMERICAL SIMULATION FOR POLYMER FLOODING

7.1 Introduction

In this chapter, to evaluate the scalability and practical applicability of the zwitterionic copolymer zPAM 1 in EOR, a comparative analysis was conducted between physical coreflooding experiments and numerical simulations. The numerical simulations were performed using the Computer Modelling Group (CMG) software, a widely recognized reservoir simulation tool in the oil and gas industry, known for its advanced capabilities in modeling complex fluid flow, phase behavior, and displacement dynamics in porous media. This comparison aimed to validate the reliability of the simulation model against experimental data, ensuring its suitability for predicting EOR performance in larger-scale reservoir management scenarios under conditions replicating the Uzen oilfield.

CMG, developed by the Computer Modelling Group Ltd., is a suite of reservoir simulation tools that include modules such as STARS (Steam, Thermal, and Advanced Processes Reservoir Simulator), which was utilized in this study for its robust handling of chemical EOR processes, including polymer flooding. The software employs finite difference methods to solve mass and energy balance equations, incorporating detailed fluid and rock properties to predict recovery performance with high accuracy. Its ability to model polymer rheology, adsorption, and mobility control effects was particularly critical for this study, given zPAM 1's unique shear-thinning behavior and salinity-driven viscosity enhancement.

7.2 Materials & Methods

The simulation model was constructed using a one-dimensional grid with 11 blocks, representing a linear displacement scenario between one injector and one production well, as specified in the simulation parameters. The model was built using a one-dimensional Cartesian grid representing the geometry of the Berea sandstone core. Eleven uniformly spaced gridblocks were used to discretize the 7.7–7.8 cm core length, while the cross-sectional area was calculated from the measured diameter of 3.81 cm. The reservoir properties were carefully defined to align with experimental conditions: porosity was set

at 18.75%, permeability at 55.1 mD, and temperature at 63°C, mirroring the coreflooding setup with Berea sandstone cores and Uzen oilfield conditions. Water and oil properties were represented as incompressible single-phase fluids. Water viscosity was set to 1 cP and oil viscosity to 8 cP, consistent with laboratory measurements of Uzen crude oil at 63 °C. The density of water was defined as 1000 kg/m³ and crude oil at 787 kg/m³. No fluid compressibility was included, as the coreflooding experiment operated under constant confining stress and the fluid system was effectively incompressible over the pressure range observed. The two-phase flow behaviour was modelled using Corey-type relative permeability functions. These curves were calibrated to match the experimental waterflood recovery trend up to 6 PV injection by adjusting end-point relative permeabilities until the simulated waterflood produced approximately 43% OOIP, consistent with the zPAM 1 coreflood result.

The polymer model for zPAM 1 incorporated experimentally measured shear-dependent viscosity data. The rheological input consisted of viscosity values tabulated as a function of concentration (1000 ppm) and shear rate ranging from 1 to 100 s^{-1}. The in-core shear rate was estimated at ~7.3–10 s^{-1}, and the polymer viscosity corresponding to this regime was directly implemented. Viscosity reduction with temperature was included using the experimentally derived degradation curve, ensuring that the input viscosity at 63 °C accurately represented the performance of zPAM 1 under reservoir-analogous thermal stress.

Polymer adsorption onto the rock surface was modelled using a Langmuir isotherm, which describes the adsorption mass as a function of polymer concentration. The maximum adsorption capacity was set to 150 µg/g-rock, and the Langmuir affinity coefficient to 0.012 L/mg. These values were selected to reflect the measured polymer retention during postflush analysis and are consistent with the significant but reversible adsorption behaviour typical of acrylamide-based polymers in sandstone. Polymer adsorption-induced permeability reduction (residual resistance factor) was captured using an empirical permeability reduction coefficient of 1.35, calibrated from the pressure increase observed during postflush injection.

The operational schedule was constructed to replicate the experimental injection sequence. The initial condition of the core was established at irreducible water saturation, equivalent to the endpoint achieved after oil flooding in the laboratory. Waterflooding was simulated by injecting two pore volumes of formation water at sequentially increasing flow rates of 1.0, 1.5, and 2.0 cm^3/min. After waterflooding, two pore volumes of polymer solution were injected at the same three flow rates. A final postflush with formation water was injected at identical rates to restore formation water mobility and quantify polymer retention effects.

The grid block size, shown in Figure 33, was optimized to ensure numerical stability and accurate representation of fluid displacement, with finer grids near the injector and producer to capture steep saturation gradients.

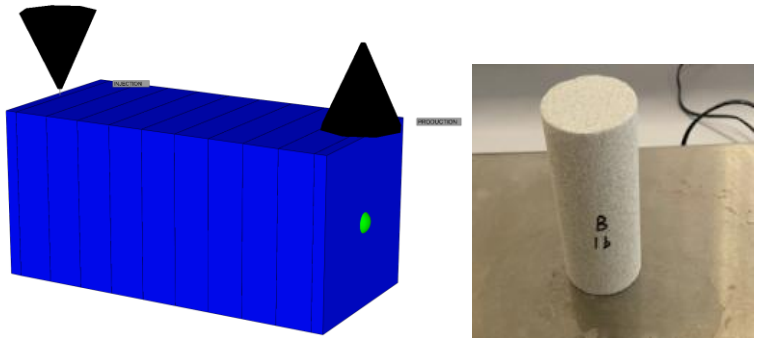

Figure 33. Grid blocks replicating the core used in CMG software

7.3 Results & Discussion

The construction and interpretation of relative permeability curves are essential for understanding two-phase flow behaviour during waterflooding and polymer flooding processes. The relative permeability plot, as shown in Figure 34, were constructed using the experimentally measured saturation endpoints, the irreducible water saturation (Swi = 0.317) and the residual oil saturation after waterflooding (Sorw = 0.3636). These values define the actual saturation interval over which two-phase flow occurs in the Berea sandstone cores. Accordingly, effective water saturation was normalized using the equation below:

$$S_{wn} = \frac{S_w - S_{wi}}{1 - S_{wi} - S_{orw}}$$

ensuring that $S_{wn} = 0$ corresponds to $S_w = S_{wi} = 0.317$ and $S_{wn} = 1$ corresponds to $S_w = 1 - S_{orw} = 0.6364$.

Then, the Corey-type correlations were applied to generate relative permeability curves within this constrained saturation window:

$$k_{rw} = k_{rw0}\,(S_{wn})^{N_w}$$
$$k_{ro} = k_{ro0}\,(1 - S_{wn})^{N_o}$$

Corey exponents of $N_w = 2$and $N_o = 3$ were selected because they are widely validated for consolidated, water-wet sandstones. Specifically, $N_w = 2$ produces the gradual increase in water mobility typically observed in Berea sandstone, where water initially occupies small, disconnected pore regions and only becomes mobile once continuous pathways form. The oil exponent $N_o = 3$ reflects the rapid loss of oil-phase continuity as water saturation increases, consistent with the experimental observation that oil production declines sharply once saturation moves beyond the mid-range.

The resulting curves begin at zero at the measured saturation endpoints because, physically, there is no water flow at $S_w \leq S_{wi}$, and no oil flow at $S_w \geq 1 - S_{orw}$. Therefore, the curves operate strictly in the region of 0.317 and 0.6364 dictated by experimental measurements.

The constructed relative permeability curve shows that oil maintains high relative permeability over the lower portion of the saturation range, which is consistent with the initial displacement observed during waterflooding. As water saturation increases, k_{ro} declines steeply due to the higher Corey exponent, matching the experimentally observed transition toward residual oil saturation. Meanwhile, k_{rw} rises slowly at first, consistent with the strongly water-wet nature of Berea sandstone and then increases as water forms continuous flow channels. Because k_{rw} increases slowly, water mobility remains low in

the early stages of waterflooding, delaying breakthrough but allowing efficient frontal displacement of oil. This behavior aligns well with the experimental waterflooding data, where the recovery curve shows steady oil production until approximately 6 PV injection. Incorporating these functions into CMG-STARS resulted in a model that accurately reproduced the experimental recovery during waterflooding. The agreement arises because the relative permeability functions govern the saturation-dependent fluid mobilities and therefore determine the shape of the fractional-flow curve. Since the experimental core is homogeneous and nearly ideal in terms of pore-size distribution, the Corey-type curves correctly represent its flow behaviour.

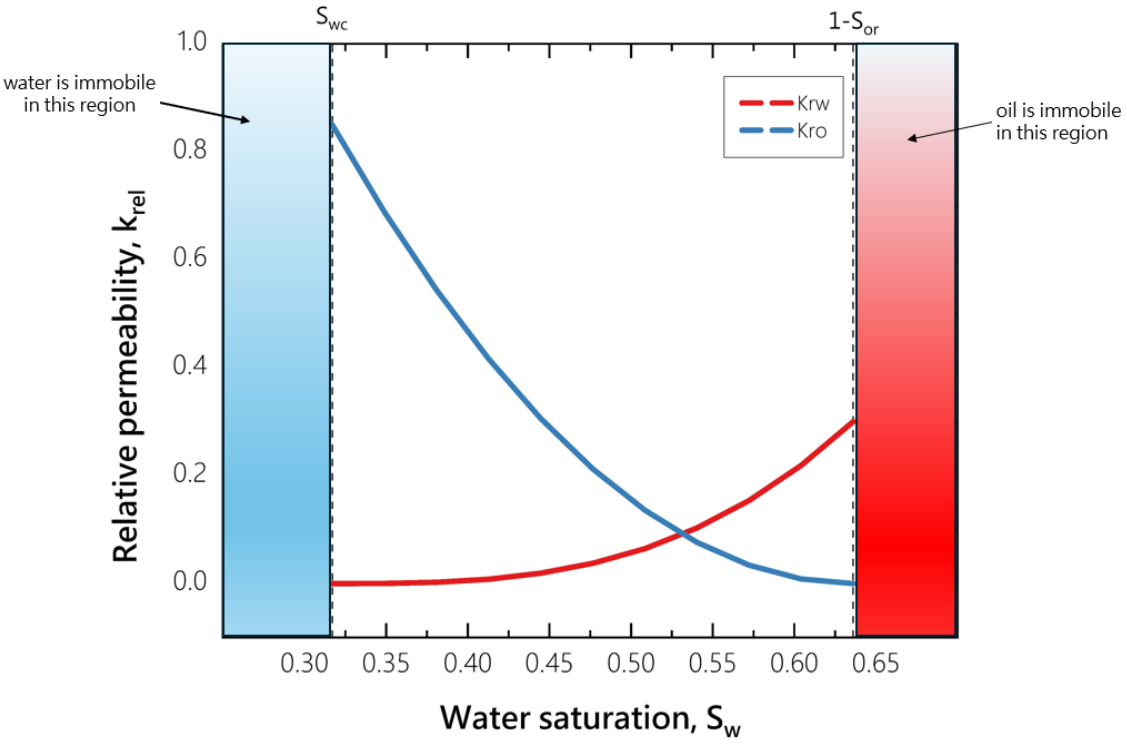

Figure 34. Relative permeability curve

The recovery factor as a function of injected pore volume (PV) for both the coreflooding experiment and CMG simulation is illustrated in Figure 35. During the waterflooding phase, both methods exhibited a comparable increase in recovery, reaching approximately 43% of the original oil in place (OOIP) after 6 PV injected. This alignment reflects the accuracy of the CMG model in capturing the initial displacement dynamics driven by waterflooding, where viscous forces dominate, and the reservoir's

homogeneous properties (porosity 18.75%, permeability 55.1 mD) minimize variability between the experimental and simulated setups.

The transition to polymer flooding revealed a slight difference in recovery trends at the beginning of injection. The CMG simulation initially overestimated the recovery rate, due to its idealized assumptions of fluid flow and displacement dynamics, which assume a homogeneous reservoir with uniform permeability and porosity distributions. In contrast, the coreflooding experiment, conducted on a small-scale Berea sandstone core was influenced by realistic challenges such as reservoir heterogeneity, viscous fingering, and polymer adsorption onto the rock surface. These factors can reduce sweep efficiency and lead to trapped residual oil. Additionally, the simulation did not fully account for microscale phenomena like polymer retention in pore throats or the impact of asphaltenes (13 wt.%) and paraffin (20 wt.%) on flow behavior, which may have contributed to the initial discrepancy.

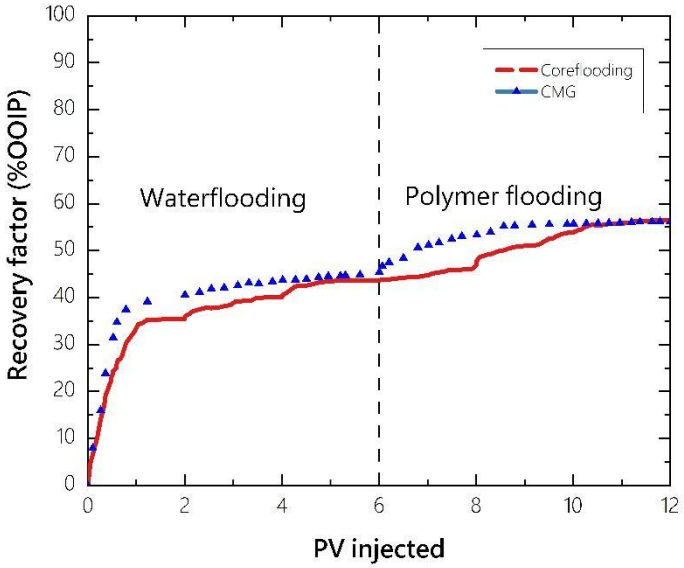

Figure 35. Comparison of recovery factors as a function of injected pore volume for coreflooding and CMG simulation

Despite this initial difference, both methods converged to a similar ultimate recovery factor of 56.5 % at the end of polymer flooding, demonstrating zPAM 1's robust

performance in enhancing oil recovery. The coreflooding experiment recovered an additional 13.3% of oil during polymer flooding, while the CMG simulation closely matched this trend, achieving a total recovery within 1% of the experimental value. The alignment in ultimate recovery underscores the CMG model's ability to accurately capture the essential physical and chemical processes governing oil recovery, including zPAM 1's viscosity enhancement, mobility control, and interaction with the porous medium under high-salinity and high-temperature conditions.

The strong correlation between the experimental and simulated recovery trends validates the robustness of the CMG-STARS model for predicting EOR performance. The model's ability to incorporate detailed fluid properties, and polymer behavior ensures its applicability for larger-scale reservoir management strategies. However, the initial discrepancy highlights the importance of refining the simulation to account for microscale heterogeneities and polymer-rock interactions, which could be addressed in future work by integrating more detailed core characterization data or advanced adsorption models.

7.4 Conclusion

This chapter presented a comparative study between coreflooding experiments and numerical simulation using CMG-STARS to evaluate the EOR performance of the zwitterionic copolymer zPAM 1 under Uzen oilfield conditions. The simulation closely replicated the experimental trends in both waterflooding and polymer flooding phases, ultimately confirming 56.5% OOIP total oil recovery and validating the robustness of the simulation framework.

The CMG model successfully captured the key rheological and transport properties of zPAM 1, including shear-thinning, viscosity enhancement with salinity, and incremental recovery potential. While slight discrepancies were noted in the early stages of polymer injection, primarily due to idealized assumptions and omission of pore-scale retention, the model's convergence with experimental results confirms its utility for scaling up polymer EOR strategies to reservoir-level applications.

The findings underscore the importance of integrating experimental data into numerical models to ensure accuracy and realism in predicting polymer flooding performance. The CMG model's predictive accuracy supports its use as a reliable tool for optimizing injection strategies, such as adjusting polymer concentration, injection rates, or slug sizes, to maximize recovery in field-scale applications. Moreover, the simulation's scalability allows for the extrapolation of zPAM 1's performance to larger reservoir systems, providing a foundation for designing cost-effective and efficient EOR operations in mature fields like the Uzen oilfield. This comparative analysis not only bridges the gap between laboratory-scale experiments but also highlights the critical role of numerical modeling in advancing EOR technologies, offering a pathway for further optimization of zwitterionic polymer flooding in challenging reservoir conditions.

CHAPTER 8. CONCLUSION AND FUTURE WORK

8.1 Conclusion, main results and significance of research

This research delivers an in-depth exploration of the synthesis, characterization, and performance evaluation of novel zwitterionic copolymers, zPAM 1, zPAM 2, and zPAM 3, for enhanced oil recovery applications in challenging high-salinity, high-temperature reservoir environments, such as those of the Uzen oilfield. Through a systematic approach, the study successfully synthesized three zwitterionic copolymers via free radical polymerization, integrating zwitterionic monomers with acrylamide to develop polymers with enhanced thermal stability, viscosity retention, and oil displacement capabilities. Different characterization techniques provided a comprehensive understanding of the copolymers' molecular, structural, and rheological properties, while core-scale experiments and simulations validated their practical efficacy in EOR, offering a robust foundation for future development.

The synthesis of zPAM 1, zPAM 2, and zPAM 3 was rigorously confirmed through Fourier Transform Infrared (FTIR) spectroscopy, which revealed characteristic peaks for N-H (3319–3338 cm^{-1}), C=O (1639–1662 cm^{-1}), and sulfonate groups (1113–1189 cm^{-1}), alongside the absence of C=C stretching bands (1612–1649 cm^{-1}), indicating complete polymerization of the monomers. In addition, 1H NMR spectroscopy investigated the molecular structures, identifying proton signals from the acrylamide backbone (0.91–2.20 ppm), zwitterionic side chains (e.g., $-CH_2-CH_2-SO_3^-$ at 2.82–3.31 ppm), and aromatic rings (e.g., pyridine at 7.84–8.69 ppm in zPAM 2, imidazole at 6.75–7.69 ppm in zPAM 3). The high conversion efficiencies (80–90%) and absence of residual vinyl signals affirmed the purity and structural integrity of the copolymers. Molecular weight determination via Dynamic Light Scattering (DLS) yielded values of 598 ± 110 kDa, 630 ± 78.5 kDa, and 734 ± 165 kDa for zPAM 1, zPAM 2, and zPAM 3, respectively, highlighting their high molecular weights, which are critical for effective viscosity enhancement in EOR applications.

SEM analysis showed distinct morphological differences among the copolymers, with zPAM 1 exhibiting a more ordered, interconnected network structure, likely due to

enhanced electrostatic crosslinking from its DMAPMAPS-based zwitterionic part. In contrast, zPAM 2 and zPAM 3 displayed greater surface roughness and porosity, influenced by the steric and electronic effects of their pyridine and imidazole rings, respectively, which impact chain packing and intermolecular interactions.

Rheological experiments further revealed the copolymers' flow behavior under varying conditions of concentration, temperature, and salinity. zPAM 1 demonstrated the most pronounced shear-thinning behavior and superior viscosity values. Long-term thermal degradation tests at 60°C underscored zPAM 1's exceptional stability, positioning it as the most resilient candidate for EOR applications.

Core-scale experiments and numerical simulations provided critical insights into the EOR performance of the zwitterionic copolymers. Coreflooding experiments, conducted using Berea sandstone cores under Uzen oilfield conditions, demonstrated zPAM 1's superior efficacy, achieving a total oil recovery of 56.5%. The improved sweep efficiency and oil displacement were attributed to zPAM 1's higher viscosity and stronger interaction with the porous medium, facilitating more uniform displacement fronts and reducing viscous fingering. Core-scale numerical simulations using CMG-STARS verified these findings, achieving a comparable recovery factor of 56% and validating the experimental results by accurately modeling zPAM 1's viscosity enhancement and mobility control. The slight initial discrepancy in recovery trends between the simulation and experiment, attributed to idealized assumptions in CMG (e.g., homogeneous core properties), was mitigated by the alignment in ultimate recovery, affirming the reliability of the simulation model for predicting EOR performance.

This research significantly advances the understanding of zwitterionic polymers in EOR, highlighting the pivotal role of molecular design, charge distribution, and zwitterionic functionality in enhancing polymer performance under harsh conditions. zPAM 1 emerges as a good candidate, offering superior thermal stability, viscosity, and oil recovery efficiency compared to both its zwitterionic counterparts and commercial HPAM.

8.2 Future Work

Despite these promising results, several challenges, including polymer adsorption, thermal degradation at elevated temperatures, and the need for field-scale validation, highlight the necessity for further research to fully realize the potential of zwitterionic polymers in practical EOR applications. The following recommendations outline a pathway to enhance the performance, durability, and economic viability of these copolymers, ensuring their successful transition from laboratory-scale success to field-scale implementation in mature reservoirs.

To begin, the thermal and chemical stability of zwitterionic copolymers must be further improved to withstand the extreme conditions often encountered in reservoirs exceeding 80°C. While zPAM 1 exhibited a degradation factor of 43% after 60 days at 60°C (0 ppm salinity), it indicates that additional modifications are required. Future research should focus on tailoring the molecular structure by incorporating thermally resistant monomers into the copolymer backbone to mitigate the viscosity loss under prolonged thermal stress.

The transition from core-scale to field-scale applications introduces additional complexities, such as reservoir heterogeneity, variable salinity, and prolonged exposure to thermal and shear stresses, requiring field-scale pilot testing to evaluate zPAM 1's long-term performance and economic feasibility. Such tests should be conducted in a reservoir with conditions imitating the Uzen oilfield, monitoring key parameters like oil recovery, pressure drop, polymer retention, and degradation over extended periods to assess durability and optimize injection strategies.

Furthermore, the slight discrepancies observed in core-scale numerical simulations using CMG-STARS, attributed to idealized assumptions like homogeneous core properties, highlight the need for advanced rheological modeling to improve predictive accuracy. Future research should develop models that account for microscale phenomena, including polymer adsorption in pore throats, viscoelastic effects, and the influence of asphaltenes on flow behavior. These models should be integrated into simulation tools to better predict performance in reservoirs with extreme conditions. In addition, while the present

work establishes a robust experimental–numerical foundation at the core scale, future research should extend these simulations to full-reservoir geometries to comprehensively assess the performance of zwitterionic polymers under realistic field conditions and to guide the design of optimized injection strategies for large-scale deployment.

From an economic perspective, the synthesis of zwitterionic polymers involves specialized monomers which may increase production costs despite their superior performance. A detailed cost-benefit analysis should be conducted to compare the economic viability of zwitterionic polymers against conventional polymers like HPAM, considering synthesis costs, required polymer dosage, and incremental oil recovery.

To further boost oil recovery, hybrid EOR strategies combining zwitterionic polymer flooding with techniques like surfactant flooding or alkali-surfactant-polymer (ASP) flooding should be investigated. The zwitterionic nature of zPAM 1, with its balanced charge distribution, may synergize with surfactants to reduce interfacial tension while maintaining viscosity, potentially achieving higher recoveries. Coreflooding experiments should evaluate the compatibility of zPAM 1 with common EOR surfactants and alkalis, focusing on emulsion stability, phase behavior, and incremental recovery, particularly in reservoirs with heavy oils or high asphaltene content where interfacial effects are significant.

By pursuing these research directions, the potential of zwitterionic polymers in EOR can be fully deployed, offering a pathway toward more efficient, and economically viable oil recovery operations. The core-scale success of zPAM 1 provides a strong foundation for these advancements, and continued innovation in molecular design, field implementation, and hybrid strategies will further establish zwitterionic polymers as a transformative solution in chemical EOR, contributing to the maximization of recovery from oil reservoirs.

REFERENCES

Abbas, S., Sanders, A. W., & Donovan, J. C. (2013). Applicability of hydroxyethylcellulose polymers for chemical EOR. *Society of Petroleum Engineers - SPE Enhanced Oil Recovery Conference, EORC 2013: Delivering the Promise NOW!*, *Odian 2004*, 981–989. https://doi.org/10.2118/165311-ms

Ahmed, I. M., & Tunio, S. Q. (2025). Comprehensive Review of Enhanced Oil Recovery as Thermal and Non-thermal Techniques. *Improved Oil and Gas Recovery*, *9*.

Al Lawati, H., S. Al Hashmi, N. Al Harthi, H. Salimi, I. Al Shaqsi, T. Divers, J. Nesbit, and G. Dupuis. "Polymer Flooding in Gharif Reservoirs: From Concept to Pilot." In *SPE EOR Conference at Oil and Gas West Asia*, p. D021S019R003. SPE, 2025.

Al Shakry, B. (2021). Polymer Injectivity: Experimental Studies of Flow in Porous Media for EOR Polymers.

Al-Kindi, S., Al-Bahry, S., Al-Wahaibi, Y., Taura, U., & Joshi, S. (2022). Partially hydrolyzed polyacrylamide: enhanced oil recovery applications, oil-field produced water pollution, and possible solutions. *Environmental Monitoring and Assessment*, *194*(12), 875.

Alagorni, A. H., Yaacob, Z. Bin, & Nour, A. H. (2015). An Overview of Oil Production Stages: Enhanced Oil Recovery Techniques and Nitrogen Injection. *International Journal of Environmental Science and Development*, *6*(9), 693–701. https://doi.org/10.7763/ijesd.2015.v6.682

Alsawafi, M. (2015). *Simulation of Enhanced Heavy Oil Recovery : History Match of Waterflooding and Polymer injection at Adverse Mobility Ratio*. *June*.

Amrenova, Y., Zhengis, A., Yergesheva, A., Abutalip, M., & Nuraje, N. (2025). Preparation of Zwitterionic Sulfobetaines and Study of Their Thermal Properties and Nanostructured Self-Assembling Features. *Nanomaterials*, *15*(1). https://doi.org/10.3390/nano15010058

Banerjee, I., Pangule, R. C., & Kane, R. S. (2011). Antifouling coatings: Recent developments in the design of surfaces that prevent fouling by proteins, bacteria, and marine organisms. *Advanced Materials*, *23*(6), 690–718. https://doi.org/10.1002/adma.201001215

Behera, U. S., Sangwai, J. S., Baskaran, D., & Byun, H. S. (2024). A Comprehensive Review on Low Salinity Water Injection for Enhanced Oil Recovery: Fundamental Insights, Laboratory and Field Studies, and Economic Aspects. *Energy & Fuels*, *39*(1), 72-103.

Benson, I., Nghiem, L. X., Group, C. M., Bryant, S. L., Sharma, M. M., & Huh, C. (2007). Development and Use of a Simulation Model for Mobility Conformance Control Using a pH-Sensitive Polymer. *SPE Annual Technical Conference and Exhibition*.

Birch, N. P., & Schiffman, J. D. (2014). Characterization of self-assembled polyelectrolyte complex nanoparticles formed from chitosan and pectin. *Langmuir*, *30*(12), 3441-3447.

Borhani, A. J., Ghazi, F., Akbari, A., Ranjbar, A., & Kazemzadeh, Y. (2025). A comprehensive review of advanced polymer gel technologies in enhanced oil recovery and water production control. *Ore and Energy Resource Geology*, 100109.

Bourdarot, G., & Ghedan, S. (2011). Modified EOR screening criteria as applied to a group of offshore carbonate oil reservoirs. *Society of Petroleum Engineers - SPE Reservoir Characterisation and Simulation Conference and Exhibition 2011, RCSC 2011*, 837–857. https://doi.org/10.2118/148323-ms

Bravetti, F., Russo, R. E., Bordignon, S., Gallo, A., Rossi, F., Nervi, C., ... & Chierotti, M. R. (2023). Zwitterionic or not? fast and reliable structure determination by combining crystal structure prediction and solid-state NMR. *Molecules*, *28*(4), 1876.

Brown, M. U., Seong, H. G., Margossian, K. O., Bishop, L., Russell, T. P., Muthukumar, M., & Emrick, T. (2022). Zwitterionic ammonium Sulfonate polymers: Synthesis and properties in Fluids. *Macromolecular Rapid Communications*, *43*(12), 2100678.

Brown, M. U., Triozzi, A., & Emrick, T. (2021). Polymer zwitterions with phosphonium cations. *Journal of the American Chemical Society*, *143*(17), 6528-6532.

Cancela, B. R., Palermo, L. C. M., de Oliveira, P. F., & Mansur, C. R. (2022).

Rheological study of polymeric fluids based on HPAM and fillers for application in EOR. *Fuel*, *330*, 125647.

Cao, B., Tang, Q., Li, L., Humble, J., Wu, H., Liu, L., & Cheng, G. (2013). Switchable antimicrobial and antifouling hydrogels with enhanced mechanical properties. *Advanced Healthcare Materials*, *2*(8), 1096–1102. https://doi.org/10.1002/adhm.201200359

Cao, D., Han, M., Leng, Z., & Wang, J. (2023). Study on polymer mechanical degradation in core plugs versus in capillary tubes. *Journal of Petroleum Exploration and Production Technology*, *13*(1), 111–121. https://doi.org/10.1007/s13202-022-01539-5

Chang, H. L. (1978). *Polymer flooding technology - yesterday, today and tomorrow.*

Chang, Y. (2022). *Designs of zwitterionic polymers. Journal of Polymer Research, 29(7), 286.*

Chatterji, J., & Borchardt, J. K. (1981). Applications of Water-Soluble Polymers in the Oil Field. *JPT, Journal of Petroleum Technology*, *33*(11), 2042–2056. https://doi.org/10.2118/9288-PA

Chen, Z. (2022). Surface hydration and antifouling activity of zwitterionic polymers. *Langmuir*, *38*(15), 4483-4489.

Chen, H. xing, Tang, H. ming, Gong, X. ping, Wang, J. jie, Liu, Y. gang, Duan, M., & Zhao, F. (2015). Effect of partially hydrolyzed polyacrylamide on emulsification stability of wastewater produced from polymer flooding. *Journal of Petroleum Science and Engineering*, *133*, 431–439. https://doi.org/10.1016/j.petrol.2015.06.031

Chen, S., Li, X., Lei, Q., Han, Y., Zhou, X., & Zhang, J. (2023). Synthesis, characterization and performance of lignin carboxyl betaine zwitterionic surfactants for application in enhanced oil recovery. *RSC advances*, *13*(24), 16352-16362.

Chiappa, L., Mennella, A., Lockhart, T. P., & Burrafato, G. (1999). Polymer adsorption at the brine/rock interface: The role of electrostatic interactions and wettability. *Journal of Petroleum Science and Engineering*, *24*(2–4), 113–122. https://doi.org/10.1016/S0920-4105(99)00035-2

Choi, B., Yu, K., & Lee, K. (2016). Modelling of polymer retention during low concentrated HPAM polymer flooding in the heterogeneous reservoirs. *International Journal of Oil, Gas and Coal Technology*, *11*(3), 249–263.

Choi, S. K., Sharma, M., Bryant, S., & Huh, C. (2009). p H Sensitive Polymers for Novel Conformance Control and Polymer Flooding Applications. *SPE International Conference on Oilfield Chemistry*.

Cui, Z. G., Du, X. R., Pei, X. M., Jiang, J. Z., & Wang, F. (2012). Synthesis of didodecylmethylcarboxyl betaine and its application in surfactant-polymer flooding. *Journal of Surfactants and Detergents*, *15*(6), 685–694. https://doi.org/10.1007/s11743-012-1396-2

Da Tan, J., Ramalingam, B., Wong, S.L., Cheng, J., Lim, Y.F., Chellappan, V., Khan, S.A., Kumar, J. and Hippalgaonkar, K. (2022). Machine learning predicts conversion and molecular weight distributions in computer controlled polymerization.

Dai, C., You, Q., Zhao, M., Zhao, G., & Zhao, F. (2023). Gas Miscible Flooding. In *Principles of Enhanced Oil Recovery* (pp. 193-226). Singapore: Springer Nature Singapore.

Dai, C., Xu, Z., Wu, Y., Zou, C., Wu, X., Wang, T., Guo, X., & Zhao, M. (2017). Design and study of a novel thermal-resistant and shear-stable amphoteric polyacrylamide in high-salinity solution. *Polymers*, *9*(7). https://doi.org/10.3390/polym9070296

Daripa, P., & Mishra, R. (2023). Modeling shear thinning polymer flooding using a dynamic viscosity model. *Physics of Fluids*, *35*(4).

Das Prasanta, Sumit Konale, R. K. (2014). No Title. *Effect of Salt Concentration on Base-Gel Viscosity of Different Polymers Used in Stimulation Fluid Systems*. https://doi.org/https://doi.org/10.2118/167786-MS

Delamaide, E., Let, K. M., Bhoendie, K., Paidin, W. R., & Jong-A-Pin, S. (2016, September). Interpretation of the Performance Results of a Polymer Flood Pilot in the Tambaredjo Oil Field, Suriname. In *SPE Annual Technical Conference and Exhibition?* (p. D021S035R007). SPE.

Du, J., Lv, C., Lan, X., Song, J., Liu, P., Chen, X., ... & Guo, G. (2024). A review on

viscosity retention of PAM solution for polymer flooding technology. *Petroleum Science and Technology*, *42*(3), 372-405.

Dupas, A., Hénaut, I., Argillier, J.-F., & Aubry, T. (2012). Mechanical Degradation Onset of Polyethylene Oxide Used as a Hydrosoluble Model Polymer for Enhanced Oil Recovery. *Oil & Gas Science and Technology – Revue d'IFP Energies Nouvelles*, *67*(6), 931–940. https://doi.org/10.2516/ogst/2012028

Ezeh, O., Ikiensikimama, S. S., & Akaranta, O. (2021). Critical review of polymer flooding in daqing field and pelican field: case studies of the world's largest polymer flooding in light and heavy oil reservoirs, respectively. *J. Eng. Res. Rep*, *21*, 25-40.

Ganat, T., & Ali, I. (2024). Mobility Control Requirement in EOR Processes. In *Advancements in Chemical Enhanced Oil Recovery* (pp. 225-244). Apple Academic Press.

Gao, C., Shi, J., & Zhao, F. (2014). Successful polymer flooding and surfactant-polymer flooding projects at Shengli Oilfield from 1992 to 2012. *Journal of Petroleum Exploration and Production Technology*, *4*(1), 1–8. https://doi.org/10.1007/s13202-013-0069-7

Gbadamosi, A., Patil, S., Kamal, M. S., Adewunmi, A. A., Yusuff, A. S., Agi, A., & Oseh, J. (2022). Application of polymers for chemical enhanced oil recovery: a review. *Polymers*, *14*(7), 1433.

Gou, S., He, Y., Ma, Y., Luo, S., Zhang, Q., Jing, D., & Guo, Q. (2015). A water-soluble antimicrobial acrylamide copolymer containing sulfitobetaine for enhanced oil recovery. *RSC Advances*, *5*(64), 51549–51558. https://doi.org/10.1039/c5ra07495a

Guo, H., Song, K., Liu, S., Zhao, F., Wang, Z., Xu, Y., Liu, J., Tang, E. and Yang, Z., 2021. Recent advances in polymer flooding in China: lessons learned and continuing development. *SPE Journal*, *26*(04), pp.2038-2052.

Gupta, R., & Mohanty, K. K. (2008). Wettability alteration of fractured carbonate reservoirs. *Proceedings - SPE Symposium on Improved Oil Recovery*, *2*(April), 709–721. https://doi.org/10.2118/113407-ms

Gutiérrez, M., Castro, R.H., Corredor, L.M., Fernández, F.R., Zapata, J., Jimenez, J.A.,

Reyes, J.D., Rojas, D.M., Jimenez, R., Acosta, T. and Dueñas, D.E., 2024, April. Chemical Enhanced Oil Recovery Experiences in Colombia: Field Pilots Review. In *SPE Improved Oil Recovery Conference?* (p. D031S019R003). SPE.

Han, M., Fuseni, A., Zahrani, B., & Wang, J. (2014). Laboratory study on polymers for chemical flooding in carbonate reservoirs. *Society of Petroleum Engineers - SPE EOR Conference at Oil and Gas West Asia 2014: Driving Integrated and Innovative EOR*, 655–670. https://doi.org/10.2118/169724-ms

Hassan, A. M., Al-Shalabi, E. W., & Ayoub, M. A. (2022). Updated perceptions on polymer-based enhanced oil recovery toward high-temperature high-salinity tolerance for successful field applications in carbonate reservoirs. *Polymers*, *14*(10), 2001.

Hassan, A.M., Mahboob, A., Khan, S.Z., Sebastian, A., Mushtaq, M., Al-Shalabi, E.W., Zeynalli, M. and Gowida, A. (2024). Experimental studies of polymer degradation in carbonates under challenging conditions. In *Offshore Technology Conference* (p. D011S007R008). OTC.

Hou, S., Liu, Y., Yan, J., Fang, Z., Gong, Y., Zhang, Q., & Yan, Y. (2025). Zwitterionic polymers: Structure design and emerging applications. *Macromolecular Chemistry and Physics*, e00106.

Ilyasov, I., Koltsov, I., Golub, P., Tretyakov, N., Cheban, A., & Thomas, A. (2021). Polymer retention determination in porous media for polymer flooding in unconsolidated reservoir. *Polymers*, *13*(16), 2737.

Imekova, G., Karimov, D., Nuraje, N., & Toktarbay, Z. (2024). Polymerization dynamics of zwitterionic monomers with polyacrylamide for enhanced oil recovery. *Engineered Science*, *31*, 1260.

Iravani, M., Simjoo, M., & Chahardowli, M. (2025). Screening key parameters affecting stability of graphene oxide and hydrolyzed polyacrylamide hybrid: Relevant for EOR application. *Heliyon*, *11*(4).

Israr, M., Mahboob, A., Hussain, S. M. S., Kamal, M. S., Solling, T., Alotaibi, M., & Fahmi, M. (2025). Synthesis, Characterization, and Effects of Aliphatic and Aromatic Amines on Thermal and Surface Properties of Zwitterionic Amphiphiles. ACS omega, 10(5), 4516-4525.

Jain, S., Pachisia, H., Sharma, A., Patel, S., Patel, S., & Ragunathan, B. (2022). A systematic review–Chemical EOR using surfactants and polymers. *Materials Today: Proceedings*, *62*, 7220-7223.

Jing, B., Zhu, Y., Zhao, W., Jiang, W., Zhang, S., Huang, B., & Du, G. (2025). A Zwitterionic Copolymer at High Temperature and High Salinity for Oilfield Fracturing Fluids. *Polymers*, *17*(20), 2733.

Kalak, T., Gąsior, K., Wieczorek, D., & Cierpiszewski, R. (2021). Improvement of washing properties of liquid laundry detergents by modification with N-hexadecyl-N, N-dimethyl-3-ammonio-1-propanesulfonate sulfobetaine. *Textile Research Journal*, *91*(1-2), 115-129.

Kalita, P., Sharma, V., Pandey, L., & Tiwari, P. (2021). Secondary and tertiary oil recovery processes. In *Microbial Enhanced Oil Recovery: Principles and Potential* (pp. 23-50). Singapore: Springer Singapore.

Kamal, M. S., Sultan, A. S., Al-Mubaiyedh, U. A., & Hussein, I. A. (2015). Review on polymer flooding: Rheology, adsorption, stability, and field applications of various polymer systems. *Polymer Reviews*, *55*(3), 491–530. https://doi.org/10.1080/15583724.2014.982821

Kaminsky; Wattenbarger; Szafranski; Coutee. (2007). No Title. *Guidelines for Polymer Flooding Evaluation and Development*. https://doi.org/https://doi.org/10.3997/2214-4609-pdb.147.iptc11200

Karimov, D. (2020). A comprehensive rheological characterization of HPAM-based polymers for the potential EOR implementation. In *SPE Annual Technical Conference and Exhibition?* (p. D023S100R012). SPE.

Karimov, D., & Toktarbay, Z. (2023). Enhanced oil recovery: Techniques, strategies, and advances. *ES Materials & Manufacturing*, *23*(2), 1005.

Khorsandi, S., Qiao, C., & Johns, R. T. (2017). Displacement Efficiency for Low-Salinity Polymer Flooding Including Wettability Alteration. *SPE Journal*. https://doi.org/10.2118/179695-PA

Kirschner, C., & Brenna, A. (2012). Bio-inspired antifouling strategies. *Annual Review of Materials Research*, *42*, 211–229.

Kozaki, C. (2012). *Efficiency of Low Salinity Polymer Flooding in Sandstone Cores*

(Doctoral Dissertation).

Laschewsky, A. (2014). Structures and synthesis of zwitterionic polymers. *Polymers*, *6*(5), 1544–1601. https://doi.org/10.3390/polym6051544

Lewandowska, K. (2007). Comparative studies of rheological properties of polyacrylamide and partially hydrolyzed polyacrylamide solutions. *Journal of Applied Polymer Science*, *103*(4), 2235–2241.

Li, Q., Wen, C., Yang, J., Zhou, X., Zhu, Y., Zheng, J., ... & Zhang, P. (2022). Zwitterionic biomaterials. *Chemical reviews*, *122*(23), 17073-17154.

Li, Y., Xue, H., Song, Y., & Zwitter Technology LLC. (2014). *Patent_Production_Purification_CB_Monomers*.

Liu, L., Gou, S., Gou, S., Zhang, H., Zhou, L., Tang, L., & Liu, L. (2020). A zwitterionic polymer containing a hydrophobic group: Enhanced rheological properties. *New Journal of Chemistry*, *44*(23), 9703–9711. https://doi.org/10.1039/d0nj01687j

Liu, S., Jia, H., Cao, Z., Fu, G., Liu, C., He, D., ... & Yu, Z. (2025). pH-Sensitive Polymer Gels for EOR in Fractured Tight Reservoirs: Mechanistic and Performance Analysis. *Journal of Applied Polymer Science*, e57470.

Lu, G., Zhao, J., Li, S., Chen, Y., Li, C., Wang, Y., & Li, D. (2021). Incorporation of Partially Hydrolyzed Polyacrylamide With Zwitterionic Units and Poly(Ethylene Glycol) Units Toward Enhanced Tolerances to High Salinity and High Temperature. *Frontiers in Materials*, *8*(December), 1–11. https://doi.org/10.3389/fmats.2021.788746

Mahajan, S., Yadav, H., Rellegadla, S., & Agrawal, A. (2021). Polymers for enhanced oil recovery: Fundamentals and selection criteria revisited. *Applied Microbiology and Biotechnology*, *105*(21), 8073-8090.

Malozyomov, B. V., Martyushev, N. V., Kukartsev, V. V., Tynchenko, V. S., Bukhtoyarov, V. V., Wu, X., ... & Kukartsev, V. A. (2023). Overview of methods for enhanced oil recovery from conventional and unconventional reservoirs. *Energies*, *16*(13), 4907.

Manichand, R., & Seright, R. S. (2014). *Field vs. Laboratory Polymer-Retention Values for a Polymer Flood in the Tambaredjo Field*. *April*, 12–16.

Martin, F. D., Hatch, M. J., Shepitka, J. S., & Ward, J. S. (1983). Improved Water-Soluble Polymers for Enhanced Recovery of Oil. *Society of Petroleum Engineers of AIME, (Paper) SPE*, 151–164. https://doi.org/10.2118/11786-ms

Meleán Brito, R. S., Iborra, A., Padró, J. M., Vega, I. N., Strumia, M. C., Milanesio, J. M., ... & Giussi, J. M. (2024). Hyperbranched Star Monomer: A New Strategy to Improve HPAM in Harsh Environments. *Industrial & Engineering Chemistry Research*, *64*(2), 948-958.

Mi, L., & Jiang, S. (2012). Synchronizing nonfouling and antimicrobial properties in a zwitterionic hydrogel. *Biomaterials*, *33*(35), 8928–8933. https://doi.org/10.1016/j.biomaterials.2012.09.011

Mirzaie Yegane, M., Boukany, P. E., & Zitha, P. (2022). Fundamentals and recent progress in the flow of water-soluble polymers in porous media for enhanced oil recovery. *Energies*, *15*(22), 8575.

Mohamed, M. H., & Mohyaldinn, M. E. (2025). Polyacrylamide-based solutions: A comprehensive review on nanomaterial integration, supramolecular design, and sustainable approaches for integrated reservoir management. *Polymers*, *17*(16), 2202.

Mohammadi, M. H., Kulakhmetovna, Y. A., & Joia, R. (2024). An overview of oil recovery techniques: from primary to enhanced oil recovery methods. *Journal for Research in Applied Sciences and Biotechnology*, *3*(1), 291-301.

Mohsenatabar Firozjaii, A., & Saghafi, H. R. (2020). Review on chemical enhanced oil recovery using polymer flooding: Fundamentals, experimental and numerical simulation. *Petroleum*, *6*(2), 115–122. https://doi.org/10.1016/j.petlm.2019.09.003

Morrow, N., & Buckley, J. (2011). Improved oil recovery by low-salinity waterflooding. *JPT, Journal of Petroleum Technology*, *63*(5), 106–113. https://doi.org/10.2118/129421-MS

Musa, M. S. M., Agi, A., Nwaichi, P. I., Ridzuan, N., & Mahat, S. Q. A. B. (2023). Simulation study of polymer flooding performance: Effect of salinity, polymer concentration in the Malay Basin. *Geoenergy Science and Engineering*, *228*, 211986.

Nandiyanto, A. B. D., Ragadhita, R., & Fiandini, M. (2023). Interpretation of Fourier

transform infrared spectra (FTIR): A practical approach in the polymer/plastic thermal decomposition. *Indonesian Journal of Science and Technology*, *8*(1), 113-126.

Navaie, F., Esmaeilnezhad, E., & Choi, H. J. (2022). Effect of rheological properties of polymer solution on polymer flooding characteristics. *Polymers*, *14*(24), 5555.

Nascimento, F. P., Pereira, V. D. J., Bastos, L. D. S., Costa, G. M. N., & Vieira de Melo, S. A. B. (2023). Low salinity water–polymer flooding in carbonate oil reservoirs: A critical review. *Macromolecular Reaction Engineering*, *17*(4), 2300007.

Pan, Y., & Ouchi, M. (2023). Stereospecific Radical Polymerization of a Side-Chain Transformable Bulky Acrylamide Monomer and Subsequent Post-Polymerization Modification for Syntheses of Isotactic Polyacrylate and Polyacrylamide. *Angewandte Chemie International Edition*, *62*(35), e202308855.

Perry, B. (1972). No Title. *Performance History on Use of Biopolymer in Springer Sand Waterflood in Southern Oklahoma*. https://doi.org/https://doi.org/10.2118/4085-MS

Puls, C., Clemens, T., Sledz, C., Kadnar, R., & Gumpenberger, T. (2016). Mechanical degradation of polymers during injection, reservoir propagation and production - Field test results 8 TH reservoir, Austria. *Society of Petroleum Engineers - SPE Europec Featured at 78th EAGE Conference and Exhibition*. https://doi.org/10.2118/180144-ms

Ragab, A., & Mansour, E. M. (2021). Enhanced oil recovery: chemical flooding. *Geophysics and Ocean Waves Studies*, *51*(1), 125-137.

Rogosic, M., Mencer, H. J., & Gomzi, Z. (1996). Polydispersity index and molecular weight distributions of polymers. *European Polymer Journal*, *32*(11), 1337–1344.

Romero-Zeron, L. (2016). *Chemical Enhanced Oil Recovery (cEOR): A Practical Overview*.

Sagandykova, D., Shakeel, M., & Pourafshary, P. (2024). Combining Thermal Effect and Mobility Control Mechanism to Reduce Water Cut in a Sandstone Reservoir in Kazakhstan. *Polymers*, *16*(12), 1651.

Sagandykova, D., Shakeel, M., & Pourafshary, P. (2025). Analyzing Polymer Flooding

Strategies for Enhanced Profitability in Water Cut Management: A Case Study of a Sandstone Field in Kazakhstan. In *International Petroleum Technology Conference* (p. D032S010R011). IPTC.

Sahuc, B., Engles, E., & Abirov, Z. (2024, November). An Alternative Approach of Polymer Flooding Implementation for the Fields of Kazakhstan. In *SPE Annual Caspian Technical Conference* (p. D011S005R001). SPE.

Salam, A.H., Alsaif, B., Hussain, S.M.S., Khan, S., Kamal, M.S., Patil, S., Al-Shalabi, E.W. and Hassan, A.M., 2024. Advances in Understanding Polymer Retention in Reservoir Rocks: A Comprehensive Review. *Polymer Reviews*, *64*(4), pp.1387-1413.

Schönemann, E., Koc, J., Karthäuser, J. F., Özcan, O., Schanzenbach, D., Schardt, L., ... & Laschewsky, A. (2021). Sulfobetaine methacrylate polymers of unconventional polyzwitterion architecture and their antifouling properties. *Biomacromolecules*, *22*(4), 1494-1508.

Sebastian, A. (2023). Effect of Water Chemistry on Polymer Retention in Carbonate Reservoirs under Harsh Conditions. *PhD dissertation*.

Seidy-Esfahlan, M., Tabatabaei-Nezhad, S. A., & Khodapanah, E. (2024). Comprehensive review of enhanced oil recovery strategies for heavy oil and bitumen reservoirs in various countries: Global perspectives, challenges, and solutions. *Heliyon*, *10*(18).

Seright, R. S., Fan, T., Wavrik, K., & De Carvaiho Balaban, R. (2011). New insights into polymer rheology in porous media. *SPE Journal*, *16*(1), 35–42. https://doi.org/10.2118/129200-PA

Seright, R. S., Jouenne, S., & Aften, C. (2025). Effect of Salinity and Hardness on HPAM Rheology in Sandstone. In *SPE International Conference on Oilfield Chemistry*. SPE.

Shakeel, M., Pourafshary, P., & Hashmet, M. R. (2022). Investigation of Brine pH Effect on the Rheological and Viscoelastic Properties of HPAM Polymer for an Optimized Enhanced Oil Recovery Design. *ACS omega*, *7*(17), 14961-14971.

Sheng, J. (2010). *Modern Chemical Enhanced Oil Recovery: Theory and Practice*. Gulf Professional Publishing.

Smith, B. C. (2021). The infrared spectra of polymers III: Hydrocarbon polymers. *Spectroscopy*, *36*(11), 22-25.

Sokolova, Diyana S., Ekaterina M. Semenova, Denis S. Grouzdev, Salimat K. Bidzhieva, Tamara L. Babich, Nataliya G. Loiko, Alexey P. Ershov et al. "Sulfidogenic microbial communities of the Uzen high-temperature oil field in Kazakhstan." *Microorganisms* 9, no. 9 (2021): 1818.

Song, H., Ghosh, P., Bowers, A., Niu, F., & Mohanty, K. (2024). Low-Salinity Polymer Flood for Enhanced Oil Recovery in Low-Permeability Carbonates. *SPE Journal*, *29*(01), 443-454.

Song, H., Ghosh, P., Mejia, M., & Mohanty, K. K. (2022). Polymer transport in low-permeability carbonate rocks. *SPE Reservoir Evaluation & Engineering*, *25*(04), 900-913.

Song, X., Man, J., Qiu, Y., Wang, J., Li, R., Zhang, Y., ... & Chen, Y. (2024). Study of hydration repulsion of zwitterionic polymer brushes resistant to protein adhesion through molecular simulations. *ACS Applied Materials & Interfaces*, *16*(14), 17145-17162.

Song, K., Tao, J., Lyu, X., Xu, Y., Liu, S., Wang, Z., Liu, H., Zhang, Y., Fu, H., Meng, E., & & Guo, H. (2022). Recent advances in polymer flooding in China. *Molecules*, *27*(20), 6978.

Sorbie, K. (1991). *Polymer-improved oil recovery*. Scotland: Blackie & Son.

Sosa-Fernandez, P. A., Post, J. W., Leermakers, F. A. M., Rijnaarts, H. H. M., & Bruning, H. (2019). Removal of divalent ions from viscous polymer-flooding produced water and seawater via electrodialysis. *Journal of Membrane Science*, *589*(July), 117251. https://doi.org/10.1016/j.memsci.2019.117251

Stavland, A., Åsen, S. M., Mebratu, A., & Gathier, F. (2021). Scaling of mechanical degradation of EOR polymers: From field-scale chokes to capillary tubes. *SPE Production & Operations*, *36*(01), 43-56.

Sun, H., Wang, H., Cao, X., Shu, Q., Fan, Z., Wu, G., Yang, Y., & Wu, Y. (2024). Innovations and applications of the thermal recovery techniques for heavy oil. *Energy Geoscience*, *5*(4), 100332.

Tileuberdi, N., Mashrapova, M., & Toktarbay, Z. (2023). A review on nitrogen flooding

for enhanced oil recovery. ES Materials & Manufacturing, 22, 968.

Unsal, E., ten Berge, A. B. G. M., & Wever, D. A. Z. (2018). Low salinity polymer flooding: Lower polymer retention and improved injectivity. *Journal of Petroleum Science and Engineering*. https://doi.org/10.1016/j.petrol.2017.10.069

Van Guyse, J. F., Verjans, J., Vandewalle, S., De Bruycker, K., Du Prez, F. E., & Hoogenboom, R. (2019). Full and partial amidation of poly (methyl acrylate) as basis for functional polyacrylamide (co) polymers. *Macromolecules*, *52*(14), 5102-5109.

Waly, A. L., Abdelghany, A. M., & Tarabiah, A. E. (2021). Study the structure of selenium modified polyethylene oxide/polyvinyl alcohol (PEO/PVA) polymer blend. *Journal of Materials Research and Technology*, *14*, 2962-2969.

Wang, G., Ma, X., Song, X., & Li, G. (2022). Modeling flow and heat transfer of fractured reservoir: Implications for a multi-fracture enhanced geothermal system. *Journal of Cleaner Production*, *365*, 132708.

Wever, D. A. Z., Picchioni, F., & Broekhuis, A. A. (2011). Polymers for enhanced oil recovery: a paradigm for structure–property relationship in aqueous solution. *Progress in polymer science*, *36*(11), 1558-1628.

Wu, Z., Mworia, M. R., Shu, K., Ren, Y., Gou, Q., Jiang, S., & Chen, Z. (2025). Steam injection pressures and rates, variable permeabilities systems, and wells alignments parameterization in SAGD: A simulation study. *Unconventional Resources*, 100232.

Yadali Jamaloei, B. (2022). Electromagnetic heating for heavy-oil and bitumen recovery: experimental, numerical, and pilot studies. *SPE Reservoir Evaluation & Engineering*, *25*(03), 433-454.

Yang, Y., Wang, Y., Liu, Y., & Liu, P. (2024). Enhancing oil recovery in Low-Permeability reservoirs using a Low-Molecular weight amphiphilic polymer. *Polymers*, *16*(8), 1036.

Yerniyazov, D., Yesmukhambet, M., Kenes, R., Bukayev, A., Shakeel, M., Pourafshary, P., & Musharova, D. (2023). Polymer screening for efficient water cut reduction in a sandstone oilfield in Kazakhstan. *Polymers*, *15*(8), 1969.

Yuan, R., Li, Y., Li, C., Fang, H., & Wang, W. (2013). Study about how the metal

cationic ions affect the properties of partially hydrolyzed hydrophobically modified polyacrylamide (HMHPAM) in aqueous solution. *Colloids and Surfaces A: Physicochemical and Engineering Aspects*, *434*, 16–24. https://doi.org/10.1016/j.colsurfa.2013.05.036

Zaitoun, A., Makakou, P., Blin, N., Al-Maamari, R. S., Al-Hashmi, A. R., Abdel-Goad, M., & Al-Sharji, H. H. (2012). Shear stability of EOR polymers. *SPE Journal*, *17*(2), 335–339. https://doi.org/10.2118/141113-PA

Zhang, L. (2024). Numerical Simulation Study on Flue Gas-Assisted Steam Huff and Puff in Heavy Oil Reservoirs. *ACS omega*, *9*(38), 39523-39532.

Zhang, D., Zhang, L., Wang, Y., Zhou, J., Sun, P., & Zhan, K. (2025). Experimental Study on the Mechanism of Steam Flooding for Heavy Oil in Pores of Different Sizes. *Processes*, *13*(10), 3083.

Zhang, G., & Seright, R. S. (2014). Effect of concentration on HPAM retention in porous media. *SPE Journal*, *19*(3), 373–380. https://doi.org/10.2118/166265-PA

Zhang, R., Shi, W., Yu, S., Wang, W., Zhang, Z., Zhang, B., Li, L., & Bao, X. (2015). Influence of salts, anion polyacrylamide and crude oil on nanofiltration membrane fouling during desalination process of polymer flooding produced water. *Desalination*, *373*, 27–37. https://doi.org/10.1016/j.desal.2015.07.006

Zhu, M. M., Fang, Y., Chen, Y. C., Lei, Y. Q., Fang, L. F., Zhu, B. K., & Matsuyama, H. (2021). Antifouling and antibacterial behavior of membranes containing quaternary ammonium and zwitterionic polymers. *Journal of Colloid and Interface Science*, *584*, 225-235.